INFRARED PHOTODISSOCIATION SPECTROSCOPY OF TRANSITION METAL CARBONYL AND METAL OXIDE CARBONYL CATIONS

By

ANTONIO DAVID BRATHWAITE

(Under the Direction of Michael A. Duncan)

ABSTRACT

Transition metal carbonyls and metal oxide carbonyls of the form $M(CO)_n^+$ and $MO_m(CO)_n^+$ are produced in a molecular beam via laser vaporization in a pulsed nozzle source. Size-selected ions are investigated using infrared laser photodissociation spectroscopy in the carbonyl stretching region (2000−2300 cm^{-1}) and in the metal oxide stretching region (800−1200 cm^{-1}). The number of infrared active bands, their relative intensities, and band positions provide insight into the bonding, coordination and geometries of these complexes. Density Functional Theory calculations are conducted in support of the experimental data. The $Y(CO)_8^+$ ion was produced and characterized. This complex is the first eight-coordinate homoleptic transition metal carbonyl observed in the gas phase. The group IV metal carbonyls ($M(CO)_n^+$, M = Ti, Zr, Hf) prefer an n = 6 coordination number, and a systematic decrease in the C−O stretching frequency was observed going from titanium to hafnium. $Cu(CO)_n^+$ complexes display non-classical carbonyl bonding and the n = 4 complex is the fully coordinated species, similar to isoelectronic $Ni(CO)_4$. All $VO_m(CO)_n^+$ complexes have a six coordinate core similar to pure vanadium carbonyl and oxidation causes the carbonyl frequencies to blue-shift.

INDEX WORDS: Laser Vaporization, Metal Carbonyls, Infrared Ion Spectroscopy

INFRARED PHOTODISSOCIATION SPECTROSCOPY OF TRANSITION METAL CARBONYL AND METAL OXIDE CARBONYL CATIONS

By

ANTONIO DAVID BRATHWAITE

B.S., Erskine College, 2009

A Dissertation Submitted to the Graduate Faculty of the University of Georgia

in Partial Fulfillment of the Requirements for the Degree

DOCTOR OF PHILOSOPHY

ATHENS, GEORGIA

2013

INFRARED PHOTODISSOCIATION SPECTROSCOPY OF TRANSITION METAL CARBONYL AND METAL OXIDE CARBONYL CATIONS

By

ANTONIO DAVID BRATHWAITE

Major Professor: Michael A. Duncan

Committee: Gary E. Douberly
Geoffrey D. Smith

Electronic Version Approved:

Maureen Grasso
Dean of the Graduate School
The University of Georgia
December 2013

DEDICATION

I dedicate this dissertation to my parents Annmarie and David Brathwaite. Thank you for sacrificing everything you had to facilitate this journey, and for instilling in me a spirit of power, love and a sound mind.

"To God be the glory, great things He hath done." − Fanny Crosby

ACKNOWLEDGEMENTS

Firstly, I would like to thank God for choosing me to demonstrate his wonder and for giving me the strength to endure when I was at my wits' end.

Whether he knew what he was getting himself into or if he blindly rolled the dice is still a mystery. Regardless, I would like to thank Professor Michael Duncan for giving me the opportunity to work in his lab. Your passion for science is unmistakable, and the ease with which you transform complex principles into simple ideas is beyond remarkable. I am truly grateful to have you as a mentor and advisor. Thank you for being patient with me and allowing me the time and space to grow.

I would like to thank Dr. Howard Thomas for admitting me to the chemistry program at Erskine College.

Soccer is undoubtedly the vehicle that got me to this point. As a result, I would like to thank my soccer coaches, Bertille St. Clair, Ralph Lundy, Ralph Polson and Warren Turner. Without their dedication to the sport and belief in me, this accomplishment would not be possible.

My time away from home has not been without its challenges. I would like to thank my teammates and friends for helping me cope with these trying times. Karl Phillips, Wes Knight, Keion Yearwood, Darren Toby, Rondell Honora, Kareem Yearwood, Sean Bateau, John Bello, Tyrell Dyson, Frantz Destin, Dr. Kyle Bennett, Deeley Hunt, Brady Johnson, Caley Kropp and family, Drew Annas and family, Taylor Craft-Middleton, Candice Charles, Rebecca Babot, Amanda Griffith, Mary Ann Langford, Hannah Howerton Cuozzo, Alex Tchangoue, Aleksi Reid, Sarah Stoddard, Theresa Henry, Nyasha Hazel, Dynell Adams, Dr. Avanelle Benoit,

Shauntelle Winchester, Alisha James, Omari Graham, Kemba Abdul-Hakim, Jeron Jordan, Khadija Holder, Javon Carrington, Cameron Miller, Khamisi Campbell, Aaron Singh, Tim Taylor, Ur Yu and the ever dependable Jaren Curry, thank you for transporting me and my belongings across the southeast, lending me your cars, feeding me, allowing me to spend holidays with your families, providing me with free lodging and entertaining me.

Thank you to the members of the Duncan Lab, past and present. I appreciate our lengthy lunch breaks and random conversations.

Lastly and most importantly, I would like to thank my family. To my wife, thank you for your unwavering support. I love you dearly. To my mother, thank you for being my rock and number one supporter. I am forever indebted to you for the sacrifices you made to get me to this point. To my father, thank you for engendering in me an unflinching belief in God and introducing me to his grace. To my sister Asante, you have motivated me to keep pushing when times were tough. I have regrettably missed out on several important milestones in your life. I promise to remedy this, starting with your law school graduation next year. To my uncle Curtis, thank you for the financial support. I hope I can continue to make you proud. To the rest of my extended family and in laws, thank you for believing in me. I appreciate your support. If I have forgotten to acknowledge anyone, charge it to my brain, not my heart.

"Trust in the Lord with all your heart and lean not on your own understanding. In all your ways acknowledge Him, and He shall direct your path." − Proverbs 3:5-6."

TABLE OF CONTENTS

Page

CHAPTER 1

INTRODUCTION

Transition metal-carbonyl complexes are pervasive in inorganic and organometallic chemistry, where they provide quintessential examples of metal-ligand bonding.[1-5] Metal carbonyls play a vital role in several catalytic processes[6] and carbon monoxide is the prototypical adsorbate in surface science for probing both pure metals and oxides.[7,8] The infrared spectroscopy of carbonyl ligands is a sensitive indicator of the bonding interactions, coordination number and geometry of metal carbonyl complexes.[1-5,9,10] Although the C-O stretching frequency occurs at 2143 cm^{-1} for free molecular CO,[11] interaction with a metal atom causes a systematic change in the frequency of this vibration. The magnitude and direction of the observed shifts in frequency depends on the charge, electronic structure and bonding configuration of the metal atom. In this work, IR spectroscopy of carbonyl vibrations and mass spectrometry are employed to investigate the bonding, coordination and structures of metal carbonyl and metal-oxide carbonyl cations in the gas phase.

The spectroscopy of the neutral transition metal carbonyls $Ni(CO)_4$, $Fe(CO)_5$, $Cr(CO)_6$, is well known[12-14] and their stability can be explained by the 18 electron rule.[1-4] This rule predicts stability for complexes in which the transition metal atom has 18 electrons occupying its valence orbitals ($s^2p^6d^{10}$).[2] Isoelectronic anions and cations should also follow this trend and display enhanced stability. However, compared to their neutral analogs, these ionized carbonyls have received far less attention. Metal carbonyl ions have been traditionally studied in the condensed phase, as salts stabilized with appropriate counterions.[15-18] In addition, unsaturated and saturated

ions have also been produced in cryogenic rare gas matrices and studied with infrared spectroscopy.[19-27] However, these condensed phase experiments preclude size selection, and the solvents and counter ions utilized may perturb the carbonyl vibrations of these small molecules.

Gas phase ion studies are important, as they reveal the intrinsic properties of metal carbonyls in an isolated environment and facilitate the investigation of mass-selected complexes. In addition, by studying small unsaturated metal-carbonyl systems, we can systematically investigate the effects of successive ligand coordination on the electronic structure of the central metal atom. Metal carbonyl ions have been studied extensively in the gas-phase using mass spectrometry.[28-39] Their structures and bonding have also been investigated with theory.[9,10,40-49] Reactions involving metal carbonyl ions have been well-characterized and the dissociation energies of numerous complexes have been determined.[31-39] However, there is significantly less data on the spectroscopy of these species. Photoelectron spectroscopy of mass-selected anions has provided information about the ground states of neutral carbonyls.[40-54] Multi-metal atom cluster carbonyls have been studied by photodissociation spectroscopy with infrared free electron lasers.[55-59] More recent work has employed infrared optical parametric oscillator (OPO) laser systems to study both clusters and monatomic complexes.[60-73]

The bonding in metal carbonyls is often explained using the Dewar-Chatt-Duncanson complexation model.[1-6] In this paradigm of metal-carbonyl bonding, two main interactions dominate the bonding landscape and influence the vibrational frequencies. These interactions are illustrated in Figure 1. In the first interaction, σ donation, the carbonyl ligand donates electron density from its HOMO along the metal-CO axis into empty metal *d* orbitals. Because the HOMO has partial antibonding character, the removal of electron density increases the bond order as well as the vibrational frequency. In agreement with this model, CO^+ has a greater

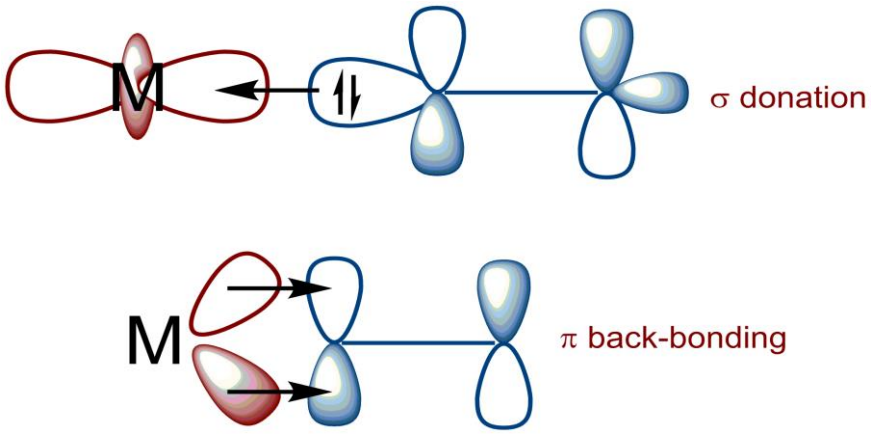

Figure 1.1. Illustration of σ donation and π back-bonding between orbitals on a carbonyl ligand and *d* orbitals on a metal atom.

vibrational frequency (2184 cm^{-1})[11] than that of neutral CO (2143 cm^{-1}). The second interaction is π back-bonding, in which partially filled metal *d* orbitals donate charge into the antibonding LUMO on CO. The addition of electron density to this orbital weakens the CO bond and reduces the vibrational frequency. In "classical" transition metal carbonyls, the effects of π back-bonding tend to outweigh those of σ donation. This results in a C-O stretch that is lower in frequency (i.e., red-shifted), compared to that of the free CO molecule (2143 cm^{-1}).[11] The importance of π back-bonding is highlighted in the vibrational frequencies of the isoelectronic analogs $Ni(CO)_4$, $Co(CO)_4^-$ and $Fe(CO)_4^{2-}$, which are 2094, 1946 and 1799 cm^{-1} respectively.[12,17,15] The anions in this series have greater electron density, thus they have more efficient π back-donation, and more significant red shifts. On the other hand, the neutral species only has a slightly red-shifted IR band (~50 cm^{-1}). The charge density available for π back-bonding in the cationic species in this series is expected to be less than in both the anions and neutrals. Investigation of the magnitude and direction of the shifts in vibrational frequency in these positive ions is therefore worthwile.

Most transition metal carbonyls follow the classical bonding model. However, some complexes exhibit "nonclassical" bonding. This occurs in systems where the *d* orbitals on the metal atom are filled and unable to accept or donate charge effectively.[60,61,47-49] A third type of interaction, electrostatic polarization, is thought to play a pivotal role in the metal-ligand bonding in these systems.[45,46] As shown in Figure 2, the carbon and oxygen atoms do not contribute equally to the formation of the C−O bond. The oxygen atom has a greater contribution to the bonding orbitals in the valence shell, hence the distribution of electron density is not uniformed. The attachment of an ion to the carbon end of CO causes a polarization that evenly redistributes the electron density on both atoms and strengthens their binding. Ab initio calculations have been used to study the role of metal charge in the polarization and subsequent redistribution of

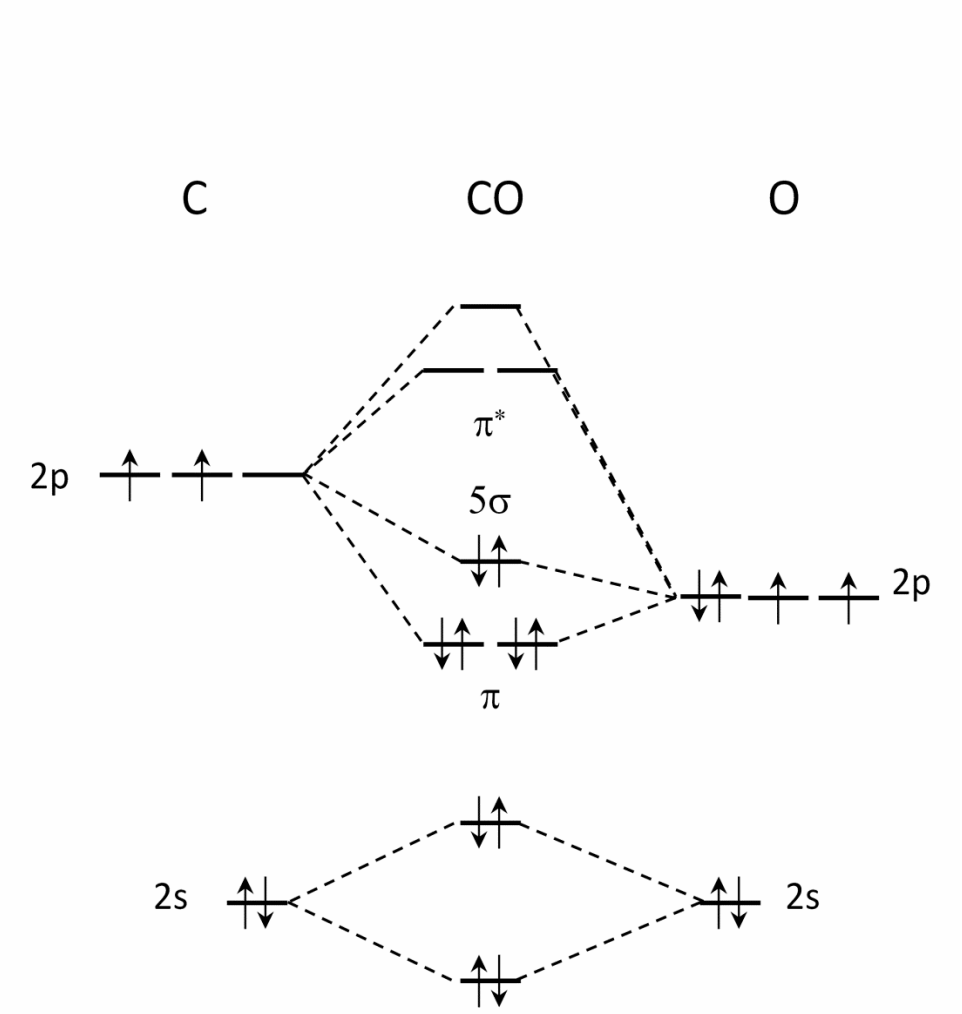

Figure 1.2. The molecular orbital diagram of CO.

electron density in the CO orbitals.[45] Frenking and coworkers conducted model studies using H^+−CO.[46] They suggest that electron density in the C-O bond is imbalanced, with greater charge density on oxygen. Polarization by the cation redistributes the electron density evenly, thus strengthening the C-O bond and causing a blue-shift in the CO frequency. This third type of interaction is convenient in explaining the blue shift observed for non-classical carbonyl cations. Metal carbonyl ions can be used to gain valuable insight into the intricacies of chemical bonding. Unfortunately, there are few spectroscopic studies of gas phase metal carbonyl cations in which these interactions can be explored.

Our research group has investigated numerous carbonyl systems. We have studied the late transition metal carbonyl cations of platinum and gold. C-O vibrations in both systems were observed to be blue shifted, consistent with "non-classical" carbonyl bonding. We have studied $Co(CO)_n^+$ and $Mn(CO)_n^+$ complexes[62,64] and compared them to their stable neutrals, $Fe(CO)_5$ and $Cr(CO)_6$. In both instances, the cationic species were observed to replicate the coordination and structure of their corresponding neutral analog. However, the frequencies of the cations were found to be less red-shifted than those of the neutral complexes. The carbonyls of group V facilitated the exploration coordination trends among congeners.[63] The coordination number of vanadium was found to be 6, although both theory[74] and binding energy studies[32] predict a 7C complex. Niobium formed both 6 and 7 coordinate complexes, while tantalum formed the 7 coordinate species exclusively. This trend lead us to conclude that both the size of the metal ion and the growth mechanism play an important role in this system. The carbonyl complexes of uranium and uranium oxide have also been studied.[65] An 8C complex with a square antiprism structure was found to be the fully coordinated $U(CO)_n^+$ species. In addition, the coordination of CO ligands to the main group element silicon has also been investigated.[66] It was also observed

that polarization of the occupied *s* orbitals leads to asymmetric carbonyl coordination. Although silicon cation does not have any occupied *d* orbitals, the red-shift induced by the *p* orbitals in these complexes is comparable to those observed for transition metal-carbonyls.

In this present work, infrared photodissociation spectroscopy, mass spectrometry and Density Function Theory (DFT) calculations are employed to test the limits of the 18 electron rule, by investigating the carbonyl cations of the early transition metals scandium and yttrium. This method is also utilized to investigate bonding and coordination trends among transition metal groups, by examining the carbonyls of titanium, zirconium and hafnium. The carbonyl complexes of copper are also studied. This system provides another example of nonclassical carbonyl bonding and also allows for the comparison of the isoelectronic pair, $Ni(CO)_4$ and $Cu(CO)_4^+$. Finally, the metal-oxide carbonyls of vanadium will be studied to ascertain the effect of oxidation on the carbonyl stretching frequency, as well as that of CO binding on the oxide stretches.

References

(1) Cotton, F. A. *Advanced Inorganic Chemistry*, 6th ed.; John Wiley and Sons, Inc.: New York, 1999.

(2) Huheey, J. E.; Keiter, E. A.; Keiter, R. L. *Inorganic Chemistry Principles of Structure and Reactivity*, Harper Collins: New York, 1993.

(3) Heck, R. F. *Organotransition Metal Chemistry*, Academic Press: New York, 1974.

(4) Nakamoto, K. *Infrared and Raman Spectra of Inorganic and Coordination Compounds*, John Wiley: New York, 1997.

(5) Bertini, I.; Gray, H. B.; Stiefel, E. I.; Valentine, J. S. *Biological Inorganic Chemistry Structure and Reactivity*, University Science Books: California, 2007.

(6) Hartwig, J. *Organotransition Metal Chemnistry*: *From Bonding to Catalysis*, University Science Books: California, 2010.

(7) Somorjai, G. A. *Introduction to Surface Chemistry and Catalysis*, John Wiley and Sons, Inc.: New York, 1994.

(8) Yates, J. T., Jr.; Madey, T. E. *Vibrational Spectroscopy of Molecules at Surfaces*; Plenum: New York, 1987.

(9) Frenking, G.; Fröhlich, N. The Nature of the Bonding in Transition-Metal Compounds. *Chem. Rev.* **2000**, *100*, 717−774.

(10) Zhou, M.; Andrews, L.; Bauschlicher, C. W., Jr. Spectroscopic and Theoretical Investigations of Vibrational Frequencies in Binary Unsaturated Transition-Metal Carbonyl Cations, Neutrals, and Anions. *Chem. Rev.* **2001**, *101*, 1931−1962.

(11) Huber, K. P.; Herzberg, G. *Molecular Spectra and Molecular Structure IV. Constants of Diatomic Molecules*, Van Nostrand Reinhold Co., 1979.

(12) Boquet, G.; Birgone, M. Infrared Spectra of $Ni(CO)_4$ in the Gas Phase. *Spectrochim. Acta* **1971**, *27*, 139−149.

(13) Jones, L. H.; McDowell, R. S.; Goldblatt, M.; Swanson, B. I. Potential Constants of Iron Pentacarbonyl from Vibrational Spectra of Isotopic Species. *J. Chem. Phys.* **1972**, *57*, 2050−2064.

(14) Jones, L. H.; McDowell, R. S.; Goldblatt, M. Force Constants of the Hexacarbonyls of Chromium, Molybdenum, and Tungsten from the Vibrational Spectra of Isotopic Species. *Inorg. Chem.* **1969**, *8*, 2349−2363.

(15) Stammerich, H.; Kawai, K.; Tavares, Y.; Krumholz, P.; Behmoiras, J.; Bril, S. Infrared Spectra of $Fe(CO)_4^{2-}$ in Aqueous Solution. *J. Chem. Phys.* **1960**, *32*, 1482−1487.

(16) Abel, E. W.; McLean, A. N.; Tyfield, S. P.; Braterman, P. S.; Walker, A. P.; Hendra, P. J. Infrared Spectra of $V(CO)_6^-$ and $Re(CO)_6^+$ in CH_3CN Solution. *J. Mol. Spec.* **1969**, *30*, 29−50.

(17) Edgell, W. F.; Lyford, J. I. Infrared Spectra of $Co(CO)_4^-$ in DMF Solution. *J. Chem. Phys.* **1970**, *52*, 4329−4333.

(18) McLean, R. A. N. Infrared and Raman Spectra of $Mn(CO)_6^+$ in CH_3CN Solutions and Solids. *Can. J. Chem.* **1974**, *52*, 213−215.

(19) Zhou, M.; Andrews, L. Infrared Spectra of $RhCO^+$, RhCO, and $RhCO^-$ in Solid Neon: A Scale for Charge Support in Catalyst Systems. *J. Am. Chem. Soc.* **1999**, *121*, 9171−9175.

(20) Zhou, M.; Andrews, L. Infrared Spectra and Density Functional Calculations of $CuCO_n^+$ (n=1-4),$CuCO_n$ (n=1-3), and $CuCO_n^-$ (n=1-3), in Solid Neon. *J. Chem. Phys.* **1999**, *111*, 4548−4557.

(21) Zhou, M.; Andrews, L. Infrared Spectra and Density Functional Calculations of $RuCO^+$, $OsCO^+$, $RuCO_x$, $OsCO_x$, $RuCO^-$, and $OsCO^-$ (x=1-4) in Solid Neon. *J. Phys. Chem. A* **1999**, *103*, 6956−6968.

(22) Zhou, M.; Andrews, L. Reactions of Laser-Ablated Iron Atoms and Cations with Carbon Monoxide: Infrared spectra of $FeCO^+$, $Fe(CO)_2^+$, $Fe(CO)_x$ and $Fe(CO)_x^-$ (x=1-4) in Solid Neon. *J. Chem. Phys.* **1999**, *110*, 10370−10379.

(23) Zhou, M.; Andrews, L. Matrix Infrared Spectra and Density Functional Calculations of ScCO, $ScCO^-$, and $ScCO^+$. *J. Phys. Chem. A* **1999**, *103*, 2964−2971.

(24) Zhou, M.; Andrews, L. Infrared Spectra and Density Functional Calculations of Small Vanadium and Titanium Carbonyl Molecules and Anions in Solid Neon. *J. Phys. Chem. A* **1999**, *103*, 5259−5268.

(25) Liang, B.; Zhou, M.; Andrews, L. Reactions of Laser-Ablated Ni, Pd, and Pt Atoms with Carbon Monoxide: Matrix Infrared Spectra and Density Functional Calculations on $M(CO)_n$ (n=1-4), $M(CO)^-$ (n=1-3), and $M(CO)^+$ (n=1-2), (M=Ni, Pd, Pt). *J. Phys. Chem. A* **2000**, *104*, 3905−3914.

(26) Liang, B.; Andrews, L. Reactions of Laser-Ablated Ag and Au Atoms with Carbon Monoxide: Matrix Infrared Spectra and Density Functional Calculations on $Au(CO)_n$ (n=2,3), $Au(CO)^-$ (n=1,2), and $M(CO)^+$ (n=1-4), (M=Ag, Au). *J. Phys. Chem. A* **2000**, *104*, 9156−9164.

(27) Zhou, M.; Andrews, L. Reactions of Zirconium and Hafnium Atoms with CO: Infrared Spectra and Density Functional Calculations of $M(CO)_x$, OMCCO, and $M(CO)_2^-$ (M = Zr, Hf; x = 1-4). *J. Am. Chem. Soc.* **2000**, *122*, 1531−1539.

(28) M. T. Bowers, ed., *Gas Phase Ion Chemistry*, Vol. 1-3, Academic Press, New York, 1979

(29) D. H. Russell, *Gas Phase Inorganic Chemistry*, Plenum, New York, 1989.

(30) B. S. Freiser, *Organometallic Ion Chemistry*, Kluwer, Dordrecht, The Netherlands, 1996.

(31) Khan, F. A.; Clemmer, D. E.; Schultz, R. H.; Armentrout, P. B. Sequential Bond Energies of Chromium Carbonyls ($Cr(CO)_x^+$, x=1-6). *J. Phys. Chem.* **1993**, *97*, 7978−7987.

(32) Sievers, M. R.; Armentrout, P. B. Collision-Induced Dissociation Studies of $V(CO)_x^+$, x=1-7: Sequential Bond Energies and the Heat of Formation of $V(CO)_6$. *J. Phys. Chem.* **1995**, *99*, 8135−8141.

(33) Meyer, F.; Chen, Y. M.; Armentrout, P.B. Sequential Bond Energies of $Cu(CO)_x^+$ and $Ag(CO)_x^+$ (x=1-4). *J. Am. Chem. Soc.* **1995**, *117*, 4071−4081.

(34) Goebel, S.; Haynes, C. L.; Khan, F. A.; Armentrout, P. B. Collision-Induced Dissociation Studies of $Co(CO)_x^+$, x=1-5: Sequential Bond Energies and Heats of Formation of $Co(CO)_4$. *J. Am. Chem. Soc.* **1995**, *117*, 6994−7002.

(35) Sievers, M. R.; Armentrout, P. B. Collision-Induced Dissociation Studies of $V(CO)_7^+$, x=1-7: Sequential Bond Energies and The Heat of Formation of $V(CO)_6$. *J. Phys. Chem.* **1995**, *99*, 8135−8141.

(36) Meyer, F.; Armentrout, P. B. Sequential Bond Energies of $Ti(CO)_x^+$, x= 1-7. *Mol. Phys.* **1996**, *88*, 187−197.

(37) Zhang, X. G.; Armentrout, P. B. Sequential Bond Energies of $Pt(CO)_x^+$ (x=1-4) Determined by Collision-Induced Dissociation. *Organometallics* **2001**, *20*, 4266−4273.

(38) Grushow, A.; Ervin, K. M. Ligand and Metal Binding Energies in Platinum Carbonyl Cluster Anions: Collision-Induced Dissociation of Pt_m^- and $Pt_m(CO)_n^-$. *J. Chem. Phys.* **1997**, *106*, 9580−9593.

(39) Spasov, V. A.; Ervin, K. M. Binding Energies of Palladium Carbonyl Cluster Anions: Collision-Induced Dissociation of $Pd_3(CO)_n^-$ (n = 0-6). *J. Chem. Phys*. **1998**, *109*, 5344−5350.

(40) Bauschlicher, C. W., Jr. Transition Metal-Ligand Bonding, II. *J. Chem. Phys*. **1986**, *84*, 260−267.

(41) Bauschlicher, C. W., Jr.; Bagus, P. S.; Nelin, C. J.; Roos, B. J. The Nature of Bonding in XCO for X=Fe, Ni and Cu. *J. Chem. Phys*. **1986**, *85*, 354−364.

(42) Bauschlicher, C. W., Jr.; Barnes, L. A. On the Dissociation Energies and Bonding in $NiC^{0/+}$ and $TiC^{0/+}$. *Chem. Phys. Lett.* **1988**, *124*, 383−394.

(43) Barnes, L. A.; Rosi, M.; Bauschlicher, C. W., Jr. Theoretical Studies of the First- and Second-Row Mono- and Di-Carbonyl Positive Ions. *J. Chem. Phys*. **1990**, *93*, 609−624.

(44) Sodupe, M.; Bauschlicher, C. W., Jr.; Lee, T. J. The Calculation of the Vibrational Frequencies of $CuC^{0/+}$, NiCO and $CuCH_3$. *Chem. Phys. Lett*. **1992**, *189*, 266−272.

(45) Goldman, A. S.; Krogh-Jespersen, K. Why do Cationic Carbon Monoxide Complexes Have High CO Stretching Force Constants and Short CO Bonds? Electrostatic Effects, Not σ bonding. *J. Am. Chem. Soc*. **1996**, *118*, 12159−12166.

(46) Lupinetti, A. J.; Fau, S.; Frenking, G.; Strauss, S. H. Theoretical Analysis of the Bonding Between CO and Positively Charged Atoms. *J. Phys. Chem.* **1997**, *101*, 9551−9559.

(47) Lupinetti, A. J.; Frenking, G.; Strauss, S. H. Nonclassical Metal Carbonyls. *Angew. Chem. Int. Ed.* **1998**, *37*, 2113−2116.

(48) Lupinetti, A. J.; Jonas , V.; Thiel, W.; Strauss, S. H.; Frenking, G. Trends in Molecular Geometries and Bond Strengths of the Homoleptic d^{10} Metal Carbonyl Cations: A Theoretical Study. *Chem. Eur. J.* **1999**, *5*, 2573−2583.

(49) Lupinetti, A. J.; Strauss, S. H.; Frenking, G. Non-Classical Metal Carbonyls. *Prog. Inorg. Chem.* **2001**, *49*, 1−112.

(50) Engelking, P. C.; Lineberger, W. C. Laser Photoelectron Spectrometry of the Negative Ions of Iron and Iron Carbonyls. Electron Affinity Determination for the Series $Fe(CO)_n$ n=0,1,2,3,4. *J. Am. Chem. Soc.* **1979**, *101*, 5569−5573.

(51) Villalta, P. W.; Leopold, D. G. A Study of $FeCO^-$ and the $^3\Sigma^-$ and $^5\Sigma^-$ States of FeCO by Negative Ion Photoelectron Spectroscopy. *J. Chem. Phys*. **1993**, *98*, 7730−7742.

(52) Bengali, A. A.; Casey, S. M.; Cheng, C. L.; Dick, J. P.; Fenn, P. T.; Villalta, P. W.; Leopold, D. G. Negative Ion Photoelectron Spectroscopy of the Coordinatively Unsaturated Group VI Metal Carbonyls of Chromium, Molybdenum and Tungsten. *J. Am. Chem. Soc*. **1992**, *114*, 5257−5268.

(53) Ganteför, G.; Schulze Icking-Konert, G.; Handschuh, H.; Eberhardt, W. CO Chemisorption on Ni_n, Pd_n and Pt_n Clusters. *Int. J. Mass Spectrom. Ion Processes* **1996**, *159*, 81−109.

(54) Butcher, C. P.; Johnson, B. F. G.; McIndoe, J. S.; Yang, X.; Wang, X. B.; Wang, L. S.; Collision-Induced Dissociation and Photodetachment of Singly and Doubly Charged Anionic Polynuclear Transition Metal Carbonyl Clusters $Ru_3CO(CO)_{13}^-$, $Ru_6CO(CO)_{16}^{2-}$, $Ru_6CO(CO)_{18}^{2-}$. *J. Chem. Phys*. **2002**, *116*, 6560−6566.

(55) Fielicke, A.; von Helden, G.; Meijer, G.; Pedersen, D. B.; Simard, B.; Rayner, D. M. Size and Charge Effects on Binding of CO to Small Isolated Rhodium Clusters. *J. Phys. Chem. B.* **2004**, *108*, 14591−14598.

(56) Moore, D. T.; Oomens, J.; Eyler, J. R.; Meijer, G.; von Helden, G.; Ridge, D. P. Gas-Phase IR Spectroscopy of Anionic Iron Carbonyl Clusters. *J. Am. Chem. Soc.* **2004**, *126*, 14726−14727.

(57) Fielicke, A.; von Helden, G.; Meijer, G.; Simard, B.; Rayner, D. M. Gold Cluster Carbonyls: Vibrational Spectroscopy of the Anions and the Effects of Cluster Size, Charge, and Coverage on the CO Stretching Frequency. *J. Phys. Chem. B.* **2005**, *109*, 23935−23940.

(58) Fielicke, A.; von Helden, G.; Meijer, G.; Pedersen, D. B.; Simard, B.; Rayner, D. M. Gold Cluster Carbonyls: Saturated Adsorption of CO on Gold Cluster Cations, Vibrational Spectroscopy, and Implications for Their Structures. *J. Am. Chem. Soc.* **2005**, *127*, 8416-8423.

(59) Fielicke, A.; von Helden, G.; Meijer, G.; Pedersen, D. B.; Simard, B.; Rayner, D. M. Size and Charge Effects on the Binding of CO to Late Transition Metal Clusters. *J. Chem. Phys.* **2006**, *124*, 194305/1-8.

(60) Velasquez III, J.; Njegic, B.; Gordon, M. S.; Duncan, M. A. IR Photodissociation Spectroscopy and Theory of $Au^+(CO)_n$ Complexes: Nonclassical Carbonyls in the Gas Phase. *J. Phys. Chem. A* **2008**, *112*, 1907–1913.

(61) Velasquez III, J.; Duncan, M. A. IR Photodissociation Spectroscopy of Gas Phase $Pt^+(CO)_n$ (n=4–6). *Chem. Phys. Lett.* **2008**, *461*, 28–32.

(62) Ricks, A. M.; Bakker, J. M.; Douberly, G. E.; Duncan, M. A. Infrared Spectroscopy and Structures of Cobalt Carbonyl Cations. *J. Phys. Chem. A* **2009**, *113*, 4701–4708.

(63) Ricks, A. M.; Reed, Z. D.; Duncan, M. A. Seven-Coordinate Homoleptic Metal Carbonyls in the Gas Phase. *J. Am. Chem. Soc*. **2009**, *131*, 9176–9177.

(64) Reed, Z. D.; Duncan, M. A. Infrared Spectroscopy and Structures of Manganese Carbonyl Cations, $Mn(CO)_n^+$ (n=1–9). *J. Am. Soc. Mass Spectrom.* **2010**, *21*, 739–749.

(65) Ricks, A. M.; Gagliardi, L.; Duncan, M. A. Infrared Spectroscopy of Extreme Coordination: The Carbonyls of U^+ and UO_2^+. *J. Am. Chem. Soc.* **2010**, *132*, 15905–15907.

(66) Brathwaite, A. D.; Duncan, M. A. Infrared Photodissociation Spectroscopy of $Si(CO)_n^+$ Complexes: Evidence for Asymmetric Coordination. *J. Phys. Chem. A* **2012**, *116*, 1375–1382.

(67) Ricks, A. M.; Brathwaite, A. D.; Duncan, M. A. Coordination and Spin States in Vanadium Carbonyl Complexes ($V(CO)_n^+$, n = 1–7) Revealed with IR Spectroscopy. *J. Phys. Chem. A* **2013**, *117*, 1001–1010.

(68) Wang, G.; Chi, C.; Cui, J.; Xing, X.; Zhou, M. Infrared Photodissociation Spectroscopy of Mononuclear Iron Carbonyl Anions. *J. Phys. Chem. A* **2012**, *116*, 2484–2489.

(69) Chi, C.; Cui, J.; Xing, X.; Wang, G.; Liu, Z.; Zhou, M. Infrared Photodissociation Spectroscopy of Trigonal Bipyramidal 19-electron $Ni(CO)_5^+$ Cation. *Chem. Phys. Lett.* **2012**, *542*, 33–36.

(70) Chi, C.; Cui, J.; Hua Li, Z.; Xing, X.; Wang, G.; Zhou M. Infrared Photodissociation Spectra of Mass Selected Homoleptic Dinuclear Iron Carbonyl Cluster Anions in the Gas Phase. *Chem. Sci.* **2012**, *3*, 1698–1706.

(71) Cui, J.; Xing, X.; Chi, C.; Wang, G.; Liu, Z.; Zhou M. Infrared Photodissociation Spectra of Mass-Selected Homoleptic Dinuclear Palladium Carbonyl Cluster Cations in the Gas Phase. *Chin. J. Chem.* **2012**, *30*, 2131–2137.

(72) Zhou, X.; Cui, J.; Li, Z. H,; Wang, G.; Liu, Z.; Zhou, M. Carbonyl Bonding on Oxophilic Metal Centers: Infrared Photodissociation Spectroscopy of Mononuclear and Dinuclear Titanium Carbonyl Cation Complexes. *J. Phys. Chem. A* **2013**, *117*, 1514–1521.

(73) Cui, J.; Zhou, X.; Wang, G.; Chi, C.; Liu, Z.; Zhou, M. Infrared Photodissociation Spectroscopy of Mass Selected Homoleptic Copper Carbonyl Cluster Cations in the Gas Phase. *J. Phys. Chem. A* **2013**, *117*, 7810–7817.

(74) Dicke, J. W.; Stibrich, N. J.; Schaefer, H. F., III $V(CO)_7^+$: A Capped Octahedral Structure Completes the 18-Electron Rule. *J. Chem. Phys.* **2008**, *456*, 13–18.

CHAPTER 2

EXPERIMENTAL SETUP

Transition metal carbonyls and oxide carbonyls are produced in a supersonic expansion via laser vaporization of a rotating and translating metal rod with the third harmonic (355 nm) of an Nd:YAG laser (Spectra Physics INDI). Metal carbonyl ions are produced using a pure carbon monoxide expansion at a backing pressure of 150 psig, whereas oxide complexes require a gas mixture of 5% oxygen in carbon monoxide. A General Valve Series 9 nozzle, operated at a frequency of 10Hz and pulse duration of 280 microseconds, is employed in these experiments. The apparatus used to conduct these experiments has been described previously in the literature.[1-5]

Figure 2.1 illustrates the apparatus used to conduct these experiments. Ion formation occurs in the first vacuum chamber, known as the "source". This chamber has an operating pressure of approximately 10^{-6} Torr, which is maintained by a Varian VHS-10 diffusion pump (6600 l/s of He). Laser pulse energies between 1-6 mJ/pulse of 355 nm light at 10 Hz, focused unto a metal rod, are typically used for vaporization. In these experiments, the rod is mounted in the so-called "offset" configuration, which facilitates the efficient production of cold monatomic metal-ligand complexes.[5] An illustration of this assembly is shown in Figure 2.2. The expansion gas is pulsed into the source chamber orthogonal to the laser path. When combined, these vaporization and expansion processes produce a plasma containing a variety of neutrals, cations and anions. Metal carbonyl complexes are entrained in the molecular beam which is skimmed (Beam Dynamics 3mm nozzle) into a second, differentially-pumped, mass spectrometer

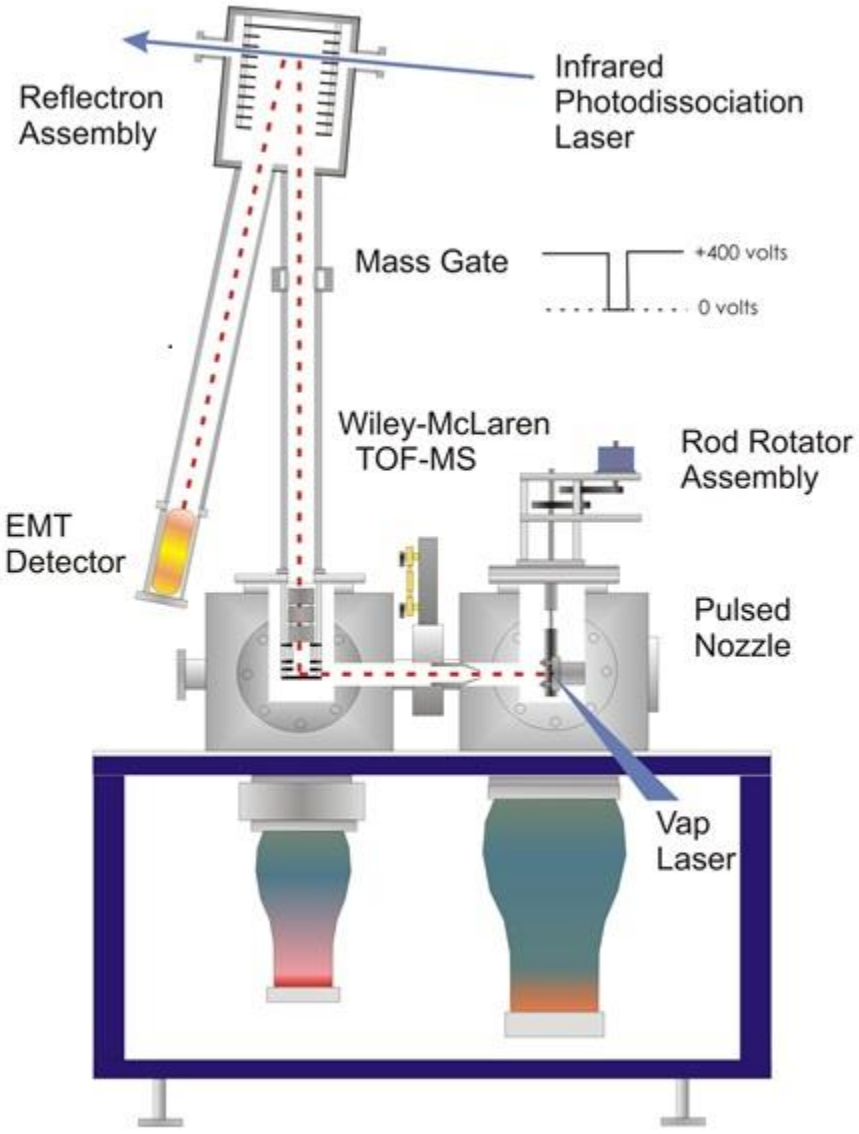

Figure 2.1 Schematic of the molecular beam apparatus.

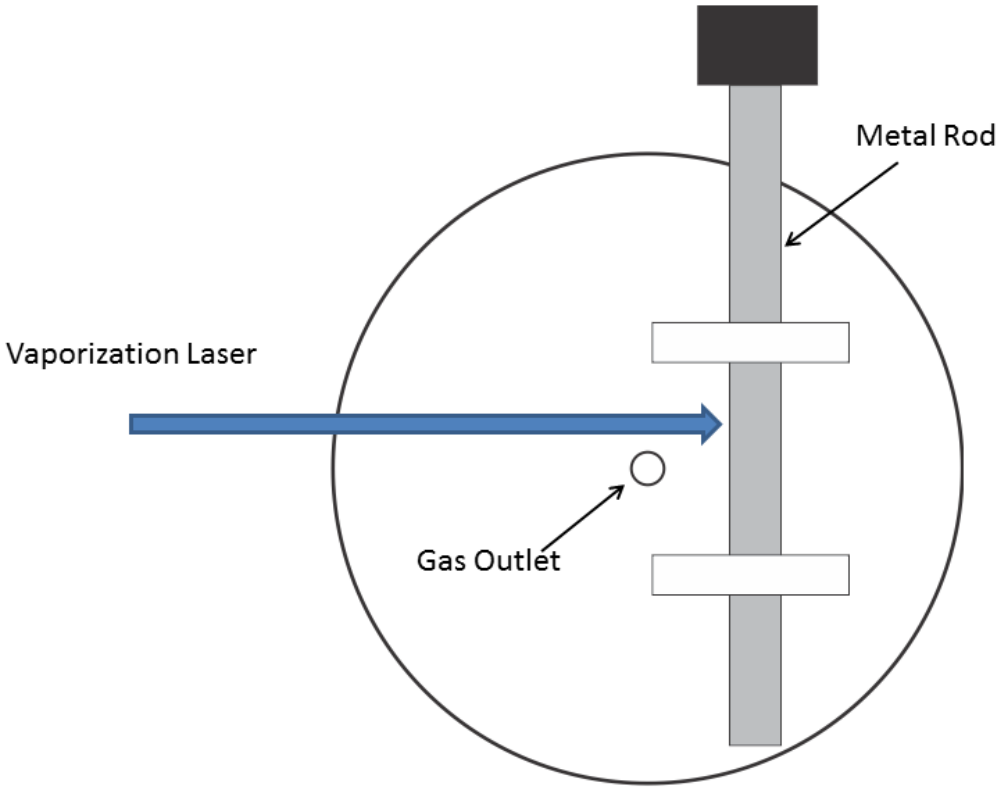

Figure 2.2 Metal rod in the offset configuration.

chamber, where cations are pulse extracted into the first flight tube of a homemade Wiley-Mclaren-type reflectron time-of-flight mass spectrometer.[6] The mass spectrometer chamber has an operating pressure of approximately 10^{-8} Torr, which is accomplished using a Varian VHS-6 diffusion pump (3000 l/s of helium). Because pulse extraction occurs perpendicularly to the flow of the molecular beam, deflection plates (~100 volts) are used to readjust the horizontal motion of the ions. The ions are extracted using a series of three pulsed plates (repeller, draw out grid, ground plate) that create a two-field acceleration region. This type of extraction helps to compensate for any spread in the energies of the ions. Voltages to the acceleration plates are supplied by a power supply (Behlke HTS-50) and the timings are controlled by Stanford Research Systems DG 535 digital delay generators. After extraction, an einzel lens is used to create a tightly focused ion packet and helps to counteract space-charge effects. Following acceleration and focusing, the ions enter a field-free region, where their mass determines the time taken for them to reach the detector.

Although all the ions are given essentially the same initial kinetic energy (same acceleration voltage), the rate at which they move through the flight tube is inversely proportional to their mass, as shown in the equation:

$$\text{Kinetic Energy} = \tfrac{1}{2} mv^2 \qquad (1)$$

Where m is the mass of the ion and v is its velocity. This equation can be alternatively expressed as:

$$\text{Kinetic Energy} = \tfrac{1}{2} m(d/t)^2 \qquad (2)$$

Where d is the distance the ions travel and t is the time taken. Thus, lighter atoms will have a greater velocity than heavier atoms, and as such, they will travel the length of the flight tube faster. By making time zero coincide with the pulsing of the acceleration plates, the exact time taken for the ions to arrive at the detector can be recorded using an oscilloscope. This information can then be transferred to a PC where ion intensities and relative abundances can be observed. Rearranging the above equation to solve for mass yields:

$$m = 2KE/(t/d)^2 \quad (3)$$

Therefore, by measuring the time taken reach the detector, the mass of an ion can be calculated using the kinetic energy and the distance to the ions travel to the detector. The error introduced by the ambiguity in the distance traveled by the ions can be removed by comparing the relationship between a reference mass (m_r) and an unknown mass (m_u). Since all ions experience the same kinetic energy, equation (2) can be expressed as:

$$m_u v_u^2 = m_r v_r^2 \quad (4)$$

As a result, the mass of an unknown ion can be calculated from the simple expression:

$$m_u = m_r(t_u/t_r)^2 \quad (5)$$

Where t_u and t_r are the times taken for the unknown ion and the reference ion to reach the detector respectively. The peak in the mass spectrum corresponding to the atomic metal ion is

usually unmistakable, owing to its enhanced abundance. As a result, this peak is often used as a reference mass to calibrate the other masses in the spectra collected in these experiments.

A reflectron is located at the end of the first flight tube. This assembly consists of a series of plates with increasingly positive voltages, connected by a series of resistors. The reflectron can be thought of as an electrostatic hill, and the ions, as a ball rolling up the hill. As the ball rolls up the hill, its kinetic energy is rapidly converted to potential energy. At a certain point they are equal, and the ball stops momentarily, before rolling back down the hill. Similarly, ions enter the reflectron and are essentially slowed to a halt, then reaccelerated out. The purpose of the reflectron is to assist with special focusing. If two ions of the same mass are extracted from different positions within the acceleration grids, their kinetic energy, and by extension, their arrival time at the detector, will be different. However, the reflectron can help to reconcile this disparity because the more energetic (faster moving) ion will penetrate further into the reflectron and therefore travel a greater distance. As a result, both ions will exit the reflectron at the same time and arrive at the detector together.

A post-accelerator, which is an inner tube to which a voltage can be pulsed, is located in the second leg of the flight tube. Prior to entering the detector, cations of interest can be accelerated by giving the tube a pulse of positive voltage. This accelerates the cations into the detector and enhances signal levels. Ions are detected using a Hamamatsu electron multiplier tube (EMT model R-595). The signal from the detector is passed through a Stanford Research Systems SR445A amplifier, before being sent to an oscilloscope. The oscilloscope is interfaced with a PC via an IEEE-488 digital card. A typical metal carbonyl mass spectrum, collected by the method described herein, is shown in the top trace of Figure 2.3. In the first leg of the flight tube, we have the ability to mass select a specific ion for further investigation using a mass gate.

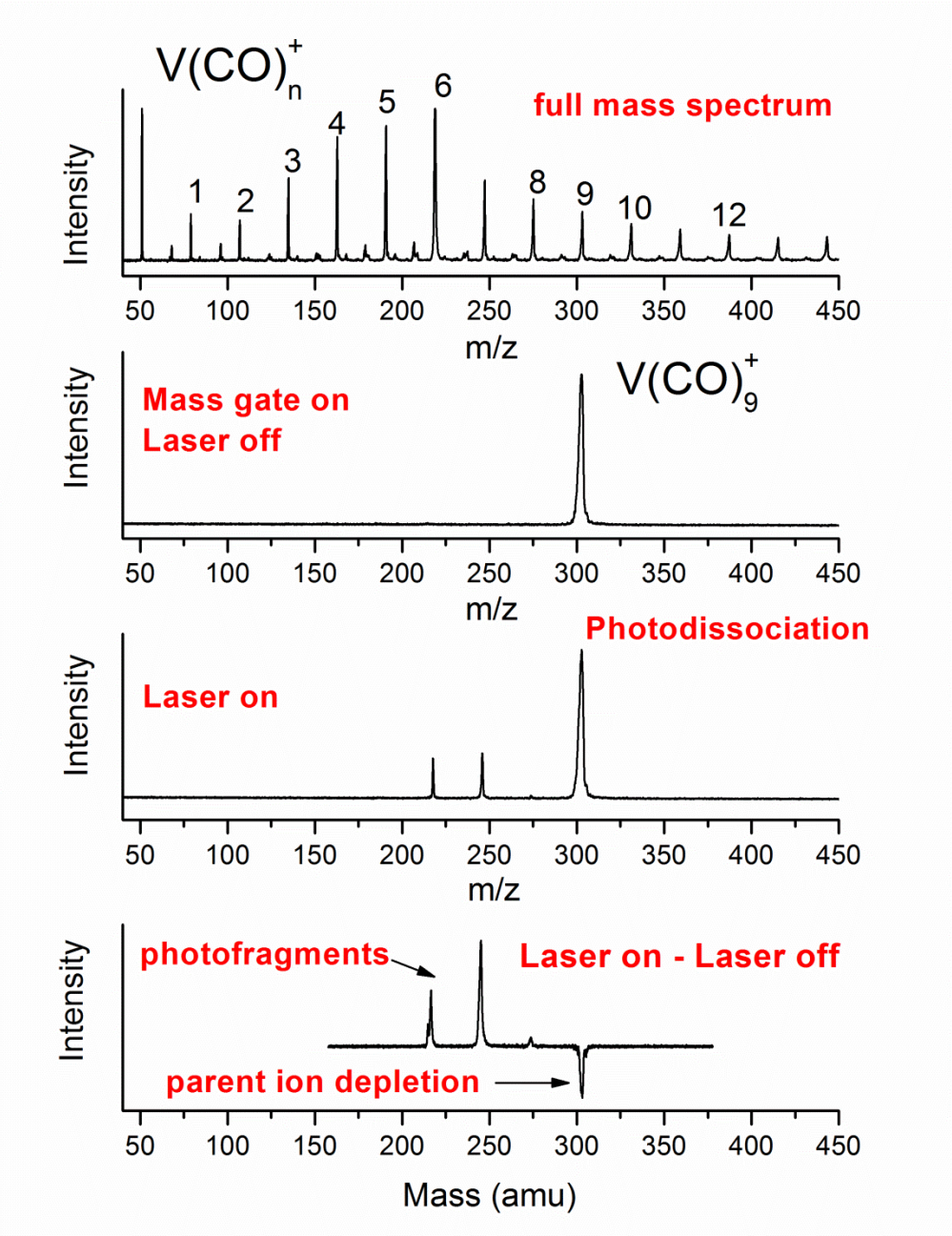

Figure 2.3. Mass spectra of all $V(CO)_n^+$ ions produced, mass-selected $V(CO)_9^+$, $V(CO)_9^+$ fragmenting to $V(CO)_7^+$ and $V(CO)_6^+$ via loss of CO, and $V(CO)_9^+$ depletion and fragment production.

The mass gate consists of two deflection plates located toward the end of the flight tube. When these plates are pulsed with a positive voltage, cations are deflected from their normal trajectory and do not reach the detector. The pulse width of the positive voltage can be varied and the plates are pulsed to ground to allow the desired ion/s to pass freely through the mass gate. The use of the mass gate allows the voltage to the detector to be turned up without overloading, as only a narrow selection of ions reach the detector. An example of a mass spectrum obtained with the mass gate "on" is shown in the second trace of Figure 2.3.

The ion densities in our experiments are too low for traditional absorption spectroscopy. Instead, we employ a type of action spectroscopy which utilizes infrared lasers to induce photodissociation. The spectroscopy of these ions can be measured because detection of a fragment ion produced via infrared laser photodissociation provides an indirect means of measuring absorption. Since the fragment ions are detected against a zero background, this technique is extremely sensitive. In order for this technique to be successful, there must be a bond in the molecule whose dissociation energy is less than that of the energy of the absorbed infrared photon. Via intramolecular vibrational energy relaxation (IVR), the energy absorbed by the IR active bond can find its way to the weakest bond in the molecule, and induce dissociation.

Following size-selection, the ions continue into the reflectron, where they remain in the turning region for approximately 1-2 microseconds. During this period, the ions can be intercepted with the tunable output of an infrared optical parametric oscillator/amplifier (OPO/OPA) laser system. If this excitation induces fragmentation, both the fragment ions and unfragmented parent ions are reaccelerated out of the reflectron. The fragment and parent ions arrive at the detector at different times because the fragment is lighter, and has a greater velocity. This is illustrated in the third trace in Figure 2.3. A computer difference of a mass spectrum

obtained with the photodissociation laser off, versus one obtained with it on, is shown in the bottom trace of Figure 2.3. The depletion of the parent ion and the production of fragment ions are clearly illustrated. Infrared spectra are measured by monitoring the appearance of fragment ions as a function of laser wavelength.

The tunable infrared light used in these experiments is generated by a LaserVision infrared OPO/OPA laser system. An illustration of this system is shown in Figure 2.4. The OPO is pumped by the fundamental (1064 nm) of a Spectra Physics Pro 230 Nd:YAG laser operated at 10 Hz and approximately 480 mJ/pulse. The pump beam enters the OPO/OPA box and is first split by a 70:30 beam splitter. The low energy beam is frequency doubled to generate light at 532 nm (~ 18800 cm^{-1}), while the 70% fraction is sent to the OPA via the delay line. A series of dichroic mirrors then directs the 532 nm light unto a potassium titanyl phosphate (KTP) crystal in the OPO. This crystal splits the incident beam into two beams (signal and idler) that are governed by the following equations:

$$\omega_{signal} \neq \omega_{idler} \tag{6}$$

$$\omega_{signal} > \omega_{idler} \tag{7}$$

$$\omega_{pump} = \omega_{signal} + \omega_{idler} \tag{8}$$

where ω is frequency in cm^{-1}. Equation 8 holds true due to the law of conservation of energy. The signal beam, which is tunable from 710 – 880 nm (14085 – 11364 cm^{-1}) is dumped and the idler beam, which is tunable from 1340 – 2120 nm (4715 – 7436 cm^{-1}), is sent to the amplification stage. In the OPA, the idler is recombined with the 70% split of the 1064 nm (~9400 cm^{-1}) pump beam through four potassium titanyl arsenate (KTA) crystals.

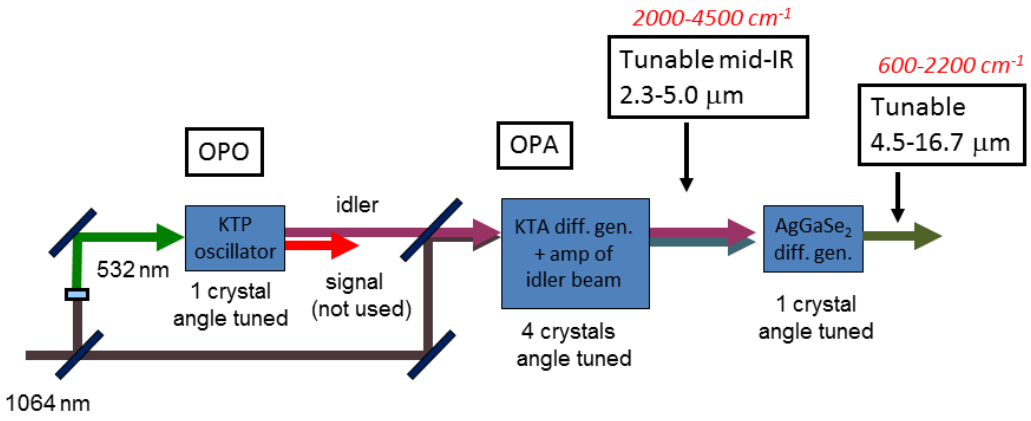

Figure 2.4. Schematic of the OPO/OPA laser system.

Difference frequency mixing generates tunable mid-IR light between 2000 and 4500 cm^{-1} with a linewidth of approximately 1 cm^{-1}. The idler and the mid-IR beams are orthogonally polarized. This allows them to be efficiently separated with a polarizer. Using a silver gallium selenide ($AgGaSe_2$) difference frequency stage, the tuning range of 600-2000 cm^{-1} is generated. Light in this region is produced by difference frequency mixing of the idler and the Mid-IR beam. The OPO/OPA laser system covers most of the infrared region, thus allowing for the vibrational spectroscopy of a wide range of metal-ligand complexes. In the studies reported herein, we focus on the carbonyl stretching region (2000 – 2300 cm^{-1}), as well as the low frequency modes (800 – 1200 cm^{-1}) of metal oxides.

References

(1) Dietz, T. G.; Duncan, M. A.; Powers, D. E.; Smalley, R. E. Laser Production of Supersonic Metal Cluster Beams. *J. Chem. Phys*. **1981**, *74*, 6511-6512.

(2) Powers, D. E.; Hansen, S. G.; Geusic, M. E.; Puiu, A. C.; Hopkins, J. B.; Dietz, T. G.; Duncan, M. A.; Langridgesmith, P. R. R.; Smalley, R. E. Supersonic Metal Cluster Beams - Laser Photo-Ionization Studies of Cu_2. *J. Phys. Chem-Us*. **1982**, *86*, 2556-2560.

(3) Laihing, K.; Cheng, P. Y.; Taylor, T. G.; Willey, K. F.; Peschke, M.; Duncan, M. A. Photodissociation in a Reflection Time-of-Flight Mass-Spectrometer - a Novel Mass-Spectrometry Mass-Spectrometry Configuration for High-Mass Systems. *Anal. Chem*. **1989**, *61*, 1458-1460.

(4) Cornett, D. S.; Peschke, M.; Laihing, K.; Cheng, P. Y.; Willey, K. F.; Duncan, M. A. Reflectron Time-of-Flight Mass-Spectrometer for Laser Photodissociation. *Rev. Sci. Instrum*. **1992**, *63*, 2177-2186.

(5) Duncan, M. A. Laser vaporization cluster sources. *Rev. Sci. Inst*. **2012**, *83*, 041101/1-19.

(6) Wiley, W. C.; McLaren, I. H. Time of Flight Mass Spectrometer with Improved Resolution. *Rev. Sci. Inst*. **1955**, *26*, 1150-1157.

CHAPTER 3

INFRARED PHOTODISSOCIATION SPECTROSCOPY OF SCANDIUM AND YTTRIUM CARBONYL CATIONS

Transition metal carbonyls provide prototypical examples of metal-ligand bonding and coordination in inorganic and organometallic chemistry.[1] A hallmark of these complexes is their adherence to the 18 electron rule, which predicts stability for complexes in which a transition metal atom has 18 electrons occupying its valence orbitals ($s^2p^6d^{10}$).[2] $Ni(CO)_4$, $Fe(CO)_5$ and $Cr(CO)_6$ are well-known examples of stable transition metal carbonyls that abide by this rule. Their isoelectronic cationic analogues, $Cu(CO)_4^+$, $Co(CO)_5^+$ and $Mn(CO)_6^+$, also demonstrate enhanced stability in the gas phase.[3-5] Following this pattern, the early transition metal cations, Sc^+ and Y^+, should form eight-coordinate (8C) carbonyl complexes. However, it is likely that significant steric crowding will occur in such systems. As a result, the coordination of eight CO ligands to Sc^+ and Y^+ is expected to test the limits of the 18 electron rule.

Our research group has previously reported the infrared spectroscopy of $U(CO)_8^+$ in the gas phase.[6] However, the coordination of ligands to actinides is not governed by the 18 electron rule. Octacoordinate metal carbonyls of scandium and yttrium have been predicted by theory and suggested in mass spectra.[7] However, the structures reported have not been confirmed via spectroscopy. Here, we report a gas-phase investigation of the carbonyl complexes of scandium and yttrium, using infrared photodissociation spectroscopy. These studies confirm an 18-electron, 8C complex for Y^+ and reveal a 7C complex for $Sc^+.Sc(CO)_n^+$ and $Y(CO)_n^+$ ions are produced and studied via previously described methods.[3-5, 8] Density Functional Theory (DFT)

computations were carried out in support of this work. The calculations were performed using the B3LYP functional[10,11] as implemented in the Gaussian 2003 computational package.[12] The LanL2DZ ECP basis set[13-15] was used for the metal atoms and the DZP basis set[16] was used for carbon and oxygen atoms. As discussed previously, the carbonyl frequencies are scaled by a factor of 0.971.[17]

The mass spectra of $Sc(CO)_n^+$ and $Y(CO)_n^+$ complexes are shown in Figure 3.1. Complexes containing over 19 carbonyl ligands are produced. However, all these ligands cannot conceivably be coordinated directly to the metal atom. Larger complexes are thought to have a strongly bound core ion, with the remaining "external" CO ligands attached via weak electrostatic and/or van der Waals interactions. Only the weakly bonded external carbonyls are expected to undergo efficient ligand elimination upon absorption of an IR photon. This type of clustering is possible due to the cold supersonic expansion employed in the production of the ions. The enhanced abundances of the n = 7 and n = 8 species for scandium and yttrium respectively, suggest stability for these complexes. However, mass spectrometry is not a reliable means of determining stability, as ion intensities can vary with source conditions and mass spectrometer focusing.[9] The insets show the fragmentation patterns of $Sc(CO)_9^+$ and $Y(CO)_9^+$ obtained by subtracting a mass spectrum obtained with the photodissociation laser off from one with it on. The negative peaks show the depletion of the parent ion, whereas the positive peaks show the fragments produced. The energy of the IR photons employed is sufficient to induce dissociation of weak bonds, but not the strong bonds of the ligands in the core ion. Ligand elimination terminates at n = 7 for scandium and n = 8 for yttrium, indicating that the $Sc(CO)_7^+$ is the fully coordinated scandium complex, whereas that of yttrium is the 18-electron $Y(CO)_8^+$ ion.

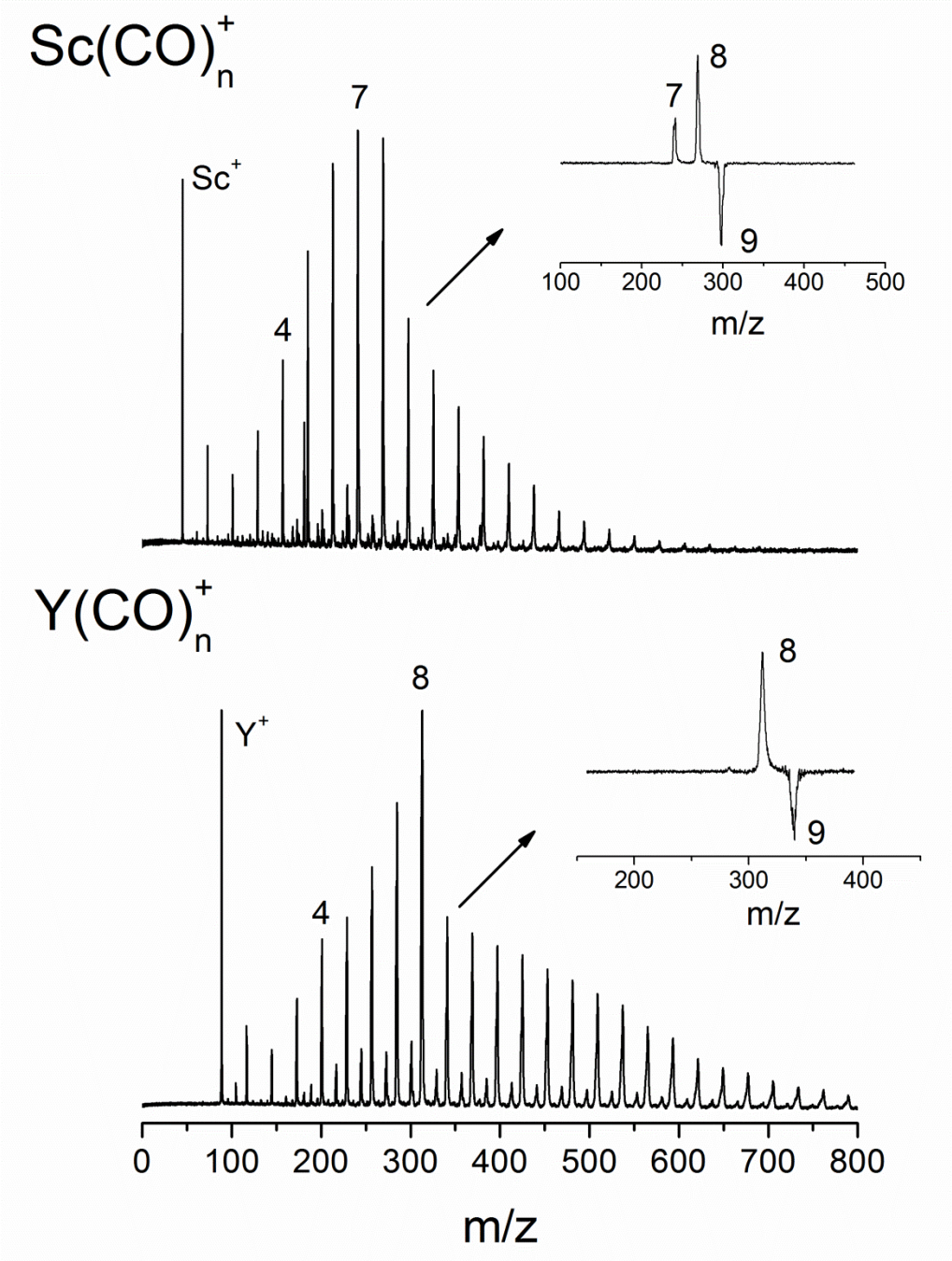

Figure 3.1. Mass spectra and photodissociation spectra for scandium and yttrium carbonyl cations.

To investigate the spectroscopy of these complexes, we measure the wavelength dependence of these fragmentation processes. The $Sc(CO)_7^+$, $Y(CO)_7^+$ and $Y(CO)_8^+$ complexes do not undergo efficient fragmentation when excited with infrared light. This is consistent with the strong binding expected for core ligands. To measure the vibrational frequencies of these complexes, we employ rare gas "tagging".[3-5,17,18] Complexes of the form $M(CO)_n^+Ar$ are produced using expansion gas mixtures containing both argon and CO. These ions fragment via the elimination of argon. Previous experiments have confirmed that tagging has a negligible effect on the spectra of metal carbonyls.[3-5,17]

To aid in the interpretation of these spectra and the assignment of structures, we employ DFT calculations. Figure 3.2 shows the infrared photodissociation spectra of $Sc(CO)_n^+$ for n = 7-9, along with vibrational spectra and structures predicted by theory for an 8C and a 7C+1 species. The 8C and 7C+1species both have the same mass and a mass spectrum is ineffective at discerning which is present. Fortunately, IR spectroscopy is a viable means of revealing the structure and bonding in these complexes. This is illustrated by the contrasting IR spectra shown in the top two traces of Figure 3.2. The bottom three traces are of the experimental spectra for the n = 7 - 9 species. The spectra of the n = 7 ion was measured via argon tagging. All experimental spectra show an intense band at 2086 cm^{-1}, along with a few weak features. This peak, which is blue-shifted from the free molecular CO stretch (2143 cm^{-1})[19] is observed at 2163 cm^{-1}, and its intensity increases with cluster size. Its position and behavior is characteristic of external CO ligands.[3-5] The observed spectral patterns and comparisons to theory allow us to rule out an 8C species for scandium and confirm a 7-coordinate capped octahedron with C_{3v} symmetry, as the fully coordinated complex.

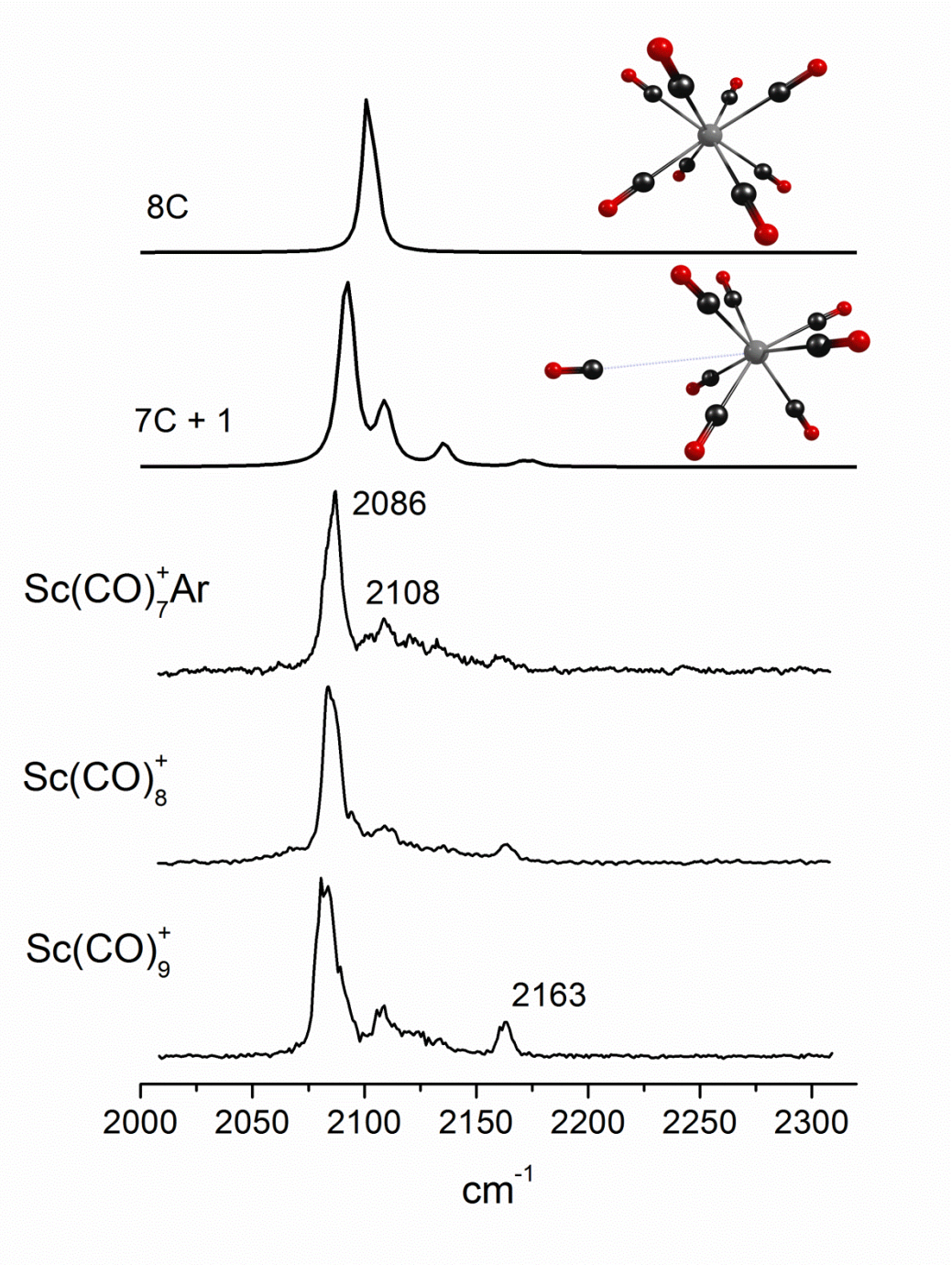

Figure 3.2. Calculated infrared spectra for 8C and 7C+1 $Sc(CO)_8^+$ complexes and experimental spectra for $Sc(CO)_7^+Ar$, $Sc(CO)_8^+$ and $Sc(CO)_9^+$.

Experimental spectra for $Y(CO)_n^+$, where n =7 -9, along with theory for the 7C and 8C complexes, are shown in Figure 3.3. The 7C+1ion was not found to be a minimum for this system. Unlike scandium, the spectra for the n = 7 and n = 8 yttrium species are not the same. The n = 7 spectrum has three infrared bands at 2071, 2104 and 2114 cm^{-1}. These frequencies and their relative intensities are in agreement with those predicted for the lowest energy 7C complex. This ion has a capped octahedral geometry and C_{3v} symmetry. Conversely, the n = 8 spectrum consists of a single band at 2087 cm^{-1}. Again, the number of bands and their frequency positions coincide with the spectrum predicted for the lowest energy n = 8 ion, which has a square antiprism geometry with D_{4d} symmetry. The experimental spectrum for $Y(CO)_9^+$ is shown in the bottom trace, and is similar to that of $Y(CO)_8^+$, with the addition of a weak blue-shifted feature at 2157 cm^{-1}. This is consistent with an 8C core ion and a weakly bound external CO ligand. Because the single infrared band measured for the n = 8 complex is in excellent agreement with the predicted spectrum, and the n = 9 spectrum has a similar intense band along with an external CO band, we conclude that the core ion is the 8C, 18-electron $Y(CO)_8^+$.

The experimental spectra measured for scandium carbonyls reveal no evidence for a stable 8C species, while the evidence for an 8C species for yttrium is compelling. This difference in coordination numbers among group members can be attributed to their ionic size; the larger yttrium ion is apparently able to accommodate the eighth ligand. However, DFT computations conducted by Tang and coworkers[7] and by our group, predict a stable 8C species for scandium that is lower in energy than the measured 7C+1 complex. The disparity between experiment and theory can be reconciled by examining the effect of spin-orbit coupling on the rate at which metal carbonyl complexes are formed.

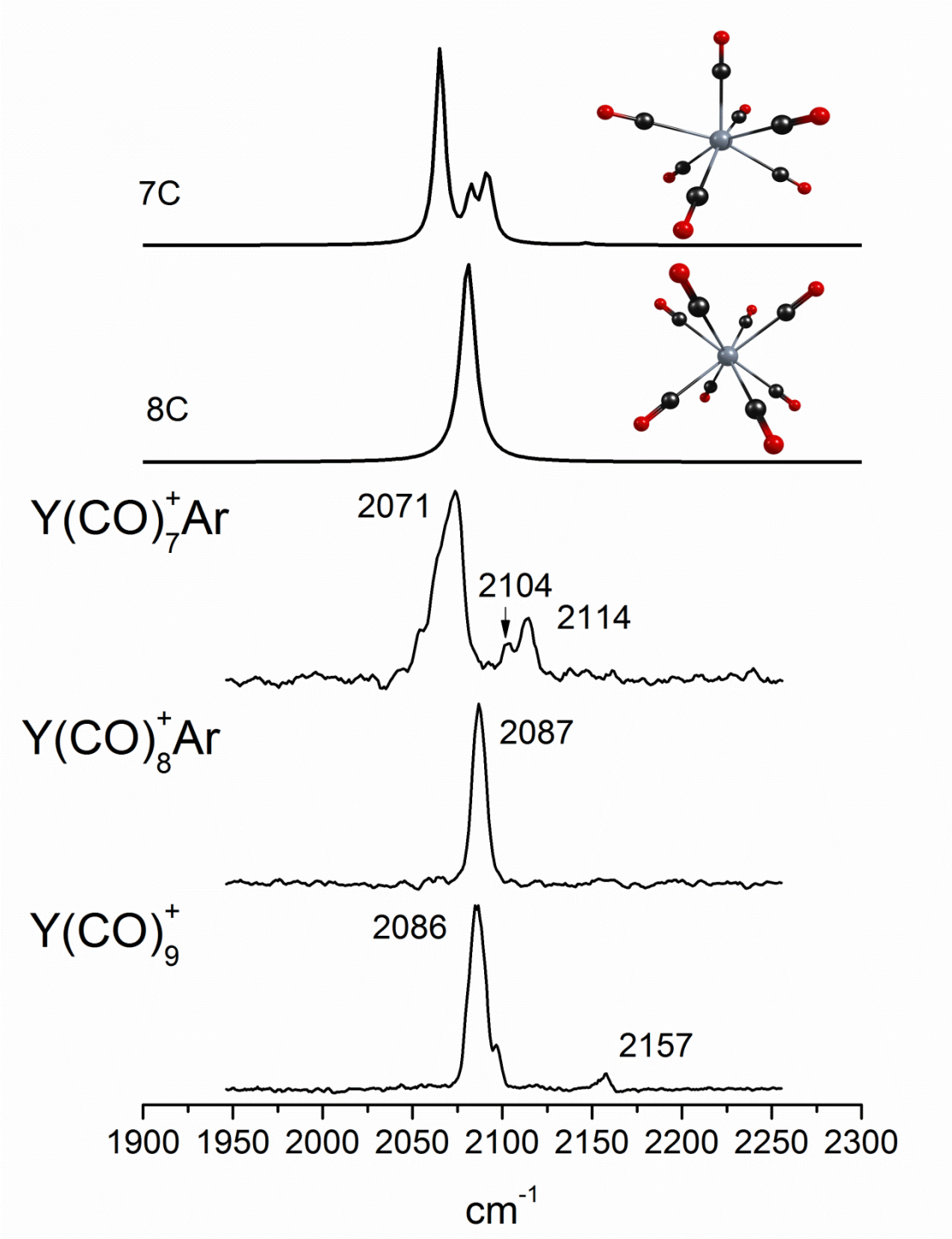

Figure 3.3. Calculated infrared spectra for 7C $Y(CO)_7^+$ and 8C $Y(CO)_8^+$ complexes, and experimental spectra for $Y(CO)_7^+Ar$, $Y(CO)_8^+Ar$ and $Y(CO)_9^+$.

The lowest energy structure for $Sc(CO)_7^+$ is a triplet, while that of $Sc(CO)_8^+$ is a singlet. If cluster growth occurs via sequential ligand coordination, it is likely that a kinetic "bottleneck" will be associated with the spin change required to produce singlet $Sc(CO)_8^+$ from triplet $Sc(CO)_7^+$ and CO. The rapid cooling in our supersonic expansions could therefore prohibit the observation of the 8C complex. Although an analogous triplet to singlet spin change was observed for yttrium, the increased spin-orbit coupling in this larger ion is likely to facilitate a more efficient spin change and a faster reaction rate. Indeed, our results follow this pattern as an 8C species is observed for yttrium, but not for scandium. The behavior exhibited by scandium and yttrium is not novel, and has been observed for group IV carbonyls. [22] Larger cations, tantalum and niobium form 7C, 18-electron complexes, but vanadium does not.

Weitz and coworkers first investigated this effect experimentally by looking at the spin-forbidden and spin-allowed recombination rates of CO to $Fe(CO)_n$ complexes.[20] This study showed that recombination reactions involving spin changes occur at a much slower rate (X400) than those in which spin is conserved. These observations were corroborated by theoretical models for curve crossing dynamics proposed by Harvey et. al.[21] Landau-Zener theory and non-adiabatic transition state theory, were used to predict the probability of a curve crossing reaction and calculate the rates from first principles. Indeed, the spin-orbit coupling of the system was shown to be proportional to the reaction rate. Harvey quantitatively reproduced the results of Weitz and coworkers. It is therefore not unreasonable to expect reactions in systems with small spin-orbit coupling to proceed via a slower rate than those with larger spin-orbit coupling. These results can be used to qualitatively explain our findings.

One final point worth discussing is the band positions measured for these complexes. The main infrared active bands for fully coordinated complexes were measured at 2086 and 2087

cm^{-1} for $Sc(CO)_7^+$ and $Y(CO)_8^+$ respectively. Since scandium and yttrium are early transition metals, their *d* orbital population is limited compared to later transition metals. However, the effective nuclear charge is also smaller in these atoms, resulting in less *d* contraction and greater orbital availability. Enhanced electron density promotes efficient π back-bonding, and leads to greater red shifts for these ions. The band positions measured here are consistent with previously established trends for transition metal carbonyl cations[22] and provide further examples of these bonding effects.

This study provides the first spectroscopic evidence for an 8C transition metal carbonyl in the gas phase and the vibrational frequencies observed are among the most red-shifted measured for such a system. Although scandium does not form a stable 8C complex, yttrium however, does form an unprecedented 18-electron, 8C complex, with D_{4d} symmetry and a square antiprism structure. The 18 electron rule is a fundamental tenet in coordination chemistry, and the formation of the $Y(CO)_8^+$ complex, even under extreme coordination conditions, reaffirms its validity. The new coordination possibilities outlined here can serve to expand the imagination of chemists' and inspire fascinating new coordination chemistry.

References

(1) Cotton, F. A. *Advanced Inorganic Chemistry*, 6th ed.; John Wiley and Sons, Inc.: New York, 1999.

(2) Huheey, J. E.; Keiter, E. A.; Keiter, R. L. *Inorganic Chemistry Principles of Structure and Reactivity*, Harper Collins: New York, 1993.

(3) Ricks, A. M.; Bakker, J. M.; Douberly, G. E.; Duncan, M. A. Infrared Spectroscopy and Structures of Cobalt Carbonyl Cations. *J. Phys. Chem. A* **2009**, *113*, 4701–4708.

(4) Reed, Z. D.; Duncan, M. A. Infrared Spectroscopy and Structures of Manganese Carbonyl Cations, $Mn(CO)_n^+$ (n = 1–9). *J. Am. Soc. Mass Spectrom.* **2010**, *21*, 739–749.

(5) Brathwaite, A. D.; Reed, Z. D.; Duncan, M. A. Infrared Photodissociation Spectroscopy of Copper Carbonyl Cations. *J. Phys. Chem. A* **2011**, *115*, 10461–10469.

(6) Ricks, A. M.; Gagliardi, L.; Duncan, M. A. Infrared Spectroscopy of Extreme Coordination: The Carbonyls of U^+ and UO_2^+. *J. Am. Chem. Soc.* **2010**, *132*, 15905–15907.

(7) Xing, X.; Wang, J.; Xie, H.; Liu, Z.; Qin, Z.; Zhao, L.; Tang, Z. Octacoordinate Metal Carbonyls of Scandium and Yttrium: Theoretical Calculations and Experimental Observation. *Rapid Commun. Mass Spectrom*. **2013**, *27*, 1403-1409.

(8) Duncan, M. A. Laser Vaporization Cluster Sources. *Rev. Sci. Inst*. **2012**, *83*, 041101/1–19.

(9) Duncan, M. A. Reflectron Time-of-Flight Mass Spectrometer for Laser Photodissociation. *Rev. Sci. Instrum.* **1992**, *63*, 2177-2186.

(10) Becke, A. D. 3 Term Correlation Functional. *J. Chem. Phys.* **1993**, *98*, 5648-5652.

(11) Lee, C.; Yang, W.; Parr, R. G. Development of the Coll-Salvetti Correlation Energy Formula into a Functional of the Electron Density. *Phys. Rev B*. **1988**, *37*, 785-789.

(12) Frisch, M. J.; Trucks, G. W.; Schlegel, H. B.; Scuseria, G. E.; Robb, M. A.; Cheeseman, J. R.; Montgomery, J. A. Jr.; Vreven, T.; Kudin, K. N.; Burant, J. C.; Millam, J. M.; Iyengar, S. S.; Tomasi, J.; Barone, V.; Mennucci, B.; Cossi, M.; Scalmani, G.; Rega, N.; Petersson, G. A.; Nakatsuji, H.; Hada, M.; Ehara, M.; Toyota, K.; Fukuda, R.; Hasegawa, J.; Ishida, M.; Nakajima, T.; Honda, Y.; Kitao, O.; Nakai, H.; Klene, M.; Li, X.; Knox, J. E.; Hratchian, H. P.; Cross, J. B.; Adamo, C.; Jaramillo, J.; Gomperts, R.; Stratmann, R. E.; Yazyev, O.; Austin, A. J.; Cammi, R.; Pomelli, C.; Ochterski, J. W.; Ayala, P. Y.; Morokuma, K.; Voth, G. A.; Salvador, P.; Dannenberg, J. J.; Zakrzewski, V. G.; Dapprich, S.; Daniels, A. D.; Strain, M. C.; Farkas, O.; Malick, D. K.; Rabuck, A. D.; Raghavachari, K.; Foresman, J. B.; Ortiz, J. V.; Cui, Q.; Baboul, A. G.; Clifford, S.; Cioslowski, J.; Stefanov, B. B.; Liu, G.; Liashenko, A.; Piskorz, P. Komaromi, I.; Martin, R. L.; Fox, D. J.; Keith, T.; Al-Laham, M. A.; Peng, C. Y.; Nanayakkara, A.; Challacombe, M.; Gill, P. M. W.; Johnson, B.; Chen, W.; Wong, M. W.; Gonzalez, C. and Pople, J. A. Gaussian 03 (Revision B.02), Gaussian, Inc., Pittsburgh PA, 2003.

(13) McLean, A. D.; Chandler, G. S. Contracted Gaussian Basis Sets For Molecular Calculations. I. Second Row Atoms, Z =11–18. *J. Chem. Phys.* **1980**, *72*, 5639-5648.

(14) Krishman, R.; Binkley, J. S.; Seeger, R.; Pople, J. A. Self-Consistent Molecular Orbital Methods. XX. A Basis Set For Correlated Wave Functions. *J. Chem. Phys.* **1980**, *72*, 650-654.

(15) Hay, P. G.; Wadt, W. R. *Ab Initio* Effective Core Potentials for Molecular Calculations. Potentials for K To Au Including the Outermost Core Orbitals. *J. Chem. Phys.* **1980**, *82*, 299-310.

(16) Dunning, T. H. Gaussian Basis Functions for Use in Molecular Calculations. I. Contraction of (9*s*5*p*) Atomic Basis Sets for the First-Row Atoms. *J. Chem. Phys.* **1970**, *53*, 2823-2833.

(17) Brathwaite, A. D.; Duncan, M. A. Infrared Photodissociation Spectroscopy of Saturated Group IV (Ti, Zr, Hf) Metal Carbonyl Cations. *J. Phys. Chem. A* ASAP DOI 10.1021/jp400793h.

(18) Duncan, M. A. Infrared Spectroscopy to Probe Structure and Dynamics in Metal Ion-Molecule Complexes. *Int. Rev. Phys. Chem.* **2003**, *22*, 407-435.

(19) Huber, K. P.; Herzberg, G. *Molecular Spectra and Molecular Structure IV. Constants of Diatomic Molecules*, Van Nostrand Reinhold Co., 1979.

(20) Ryther, R. J.; Weitz, E. Reaction Kinetics of Coordinatively Unsaturated Iron Carbonyls Formed on Gas-Phase Excimer Laser Photolysis of Iron Pentacarbonyl. *J. Phys. Chem.* **1991**, *95*, 9841-9852.

(21) Harvey, J. N.; Aschi, M. Modeling Spin-Forbidden Reactions: Recombination of Carbon Monoxide with Iron Tetracarbonyl. *Faraday Discuss*. **2003**, *124*, 129-143.

(22) Ricks, A. M.; Reed, Z. D.; Duncan, M. A. Seven-Coordinate Homoleptic Metal Carbonyls in the gas phase. *J. Am. Chem. Soc*. **2009**, *131*, 9176-9177.

CHAPTER 4

INFRARED PHOTODISSOCIATION SPECTROSCOPY OF SATURATED GROUP IV METAL CARBONYL CATIONS

Introduction

Early transition metals are relatively electron deficient and coordination to a large number of ligands is needed to achieve a stable 18-electron configuration. However, steric crowding is likely to influence the coordination in these complexes. Transition metals in the second and third rows are larger, and therefore better able to accommodate more ligands. Here, we present the first concerted investigation of group IV transition metal carbonyl cations, via infrared photodissociation spectroscopy and computational chemistry, in an effort to elucidate these coordination issues.

Group IV metal carbonyl systems have been previously investigated via both experiment and theory. Unsaturated, neutral and anionic carbonyls of Ti, Zr and Hf have been isolated and studied with infrared spectroscopy in rare gas matrices.[9]

Equilibrium geometries and vibrational frequencies of neutral saturated carbonyls of group IV metals have been predicted using Density Functional Theory (DFT).[10] Also, Zhou and coworkers have recently measured the infrared photodissociation spectra of selected titanium and titanium oxide carbonyl cations.[11]

There has been ongoing investigation of ionic and neutral early transition metal carbonyls in an effort to obtain evidence for a stable homoleptic 7-coordinate species.[12-15] Stable 18-electron complexes for the cation of the group V metal vanadium have been proposed by

theory[15] and bond dissociation energy studies by Armentrout.[12] However, until a recent publication by our group, there was no experimental spectroscopic evidence for a seven coordinate complex. In our study of the group V carbonyl cations, vanadium was observed to only form a six-coordinate species, niobium formed both six- and seven coordinate structures, while tantalum formed the seven-coordinate species exclusively. In this present study, we extend our investigation to the carbonyl congeners of group IV metals to gain insight into their coordination. Group IV cations have an odd number of electrons. Therefore, they cannot form 18-electron complexes. However, because they have even fewer valence electrons than group V cations, it is possible for them to form six-, seven-, or eight-coordinate complexes with 15, 17, or 19 electrons respectively.

Experimental Section

$Ti(CO)_n^+$, $Zr(CO)_n^+$ and $Hf(CO)_n^+$ ions are produced in a pulsed nozzle laser vaporization source via the method described in the experimental chapter. In support of the experimental studies, DFT calculations were carried out to determine the structure and bonding of these complexes. The calculations were performed using the B3LYP functional[16,17] as implemented in the Gaussian 2003 computational package.[18] The Los Alamos effective core potential (ECP) double zeta (LanL2DZ) basis set[19-21] was used for the metal atoms and the DZP basis set[22] was used for carbon and oxygen atoms. The calculated carbonyl frequencies are scaled by a factor of 0.971 and are given a 10 cm^{-1} FWHM Lorentzian line shape for comparison to the experimental spectra. This scaling factor was derived by calculating the CO stretching frequencies of the well-known stable carbonyl complexes, $Ni(CO)_4$, $Fe(CO)_5$, and $Cr(CO)_6$, and finding the average value needed to make their experimental and theoretical frequencies agree.[23-25]

Results and Discussion

A mass spectrum of the $Ti(CO)_n^+$ ions formed via laser vaporization of a titanium rod in a carbon monoxide expansion is shown in Figure 4.1. The major peaks correspond to titanium carbonyl cations, whereas the minor peaks correspond to titanium oxide-carbonyl cations. The most prominent peak in the mass spectrum corresponds to $Ti(CO)_6^+$, suggesting that this ion has enhanced stability. $Ti(CO)_n^+$ complexes with as many as 19 carbonyl ligands are produced. All of these ligands cannot possibly be coordinated directly to the central metal ion. Instead, larger complexes are thought to consist of a strongly coordinated metal-ligand core ion, with additional "external" ligands attached via electrostatic and/or van der Waals interactions. The production of large complexes with weakly bound external ligands is possible due to the cold conditions our supersonic expansion. These external or second-sphere ligands are expected to be easily eliminated upon absorption of infrared photons. The mass spectra for the zirconium and hafnium systems are similar to that of titanium, with the n = 6 species having enhanced intensity, as shown in Figures 4.2 and 4.3.

Mass spectrometry is not always a reliable means of determining stability, as ion intensities can vary significantly with the conditions of the laser vaporization source and focusing of the mass spectrometer. In an effort to gain more insight into the stability of these species, infrared photodissociation studies were conducted on larger $Ti(CO)_n^+$, $Zr(CO)_n^+$ and $Hf(CO)_n^+$ clusters, where n = 7-11. The so-called "breakdown" mass spectra for $Ti(CO)_n^+$, $Zr(CO)_n^+$ and $Hf(CO)_n^+$ are presented in Figures 4.4, 4.5 and 4.6 respectively. These mass spectra were obtained by subtracting a mass spectrum of a selected complex with the fragmentation laser “off”, from one obtained with it “on”. The negative peaks are due to depletion of the parent ion, whereas the positive peaks are photofragments. $Ti(CO)_n^+$ clusters

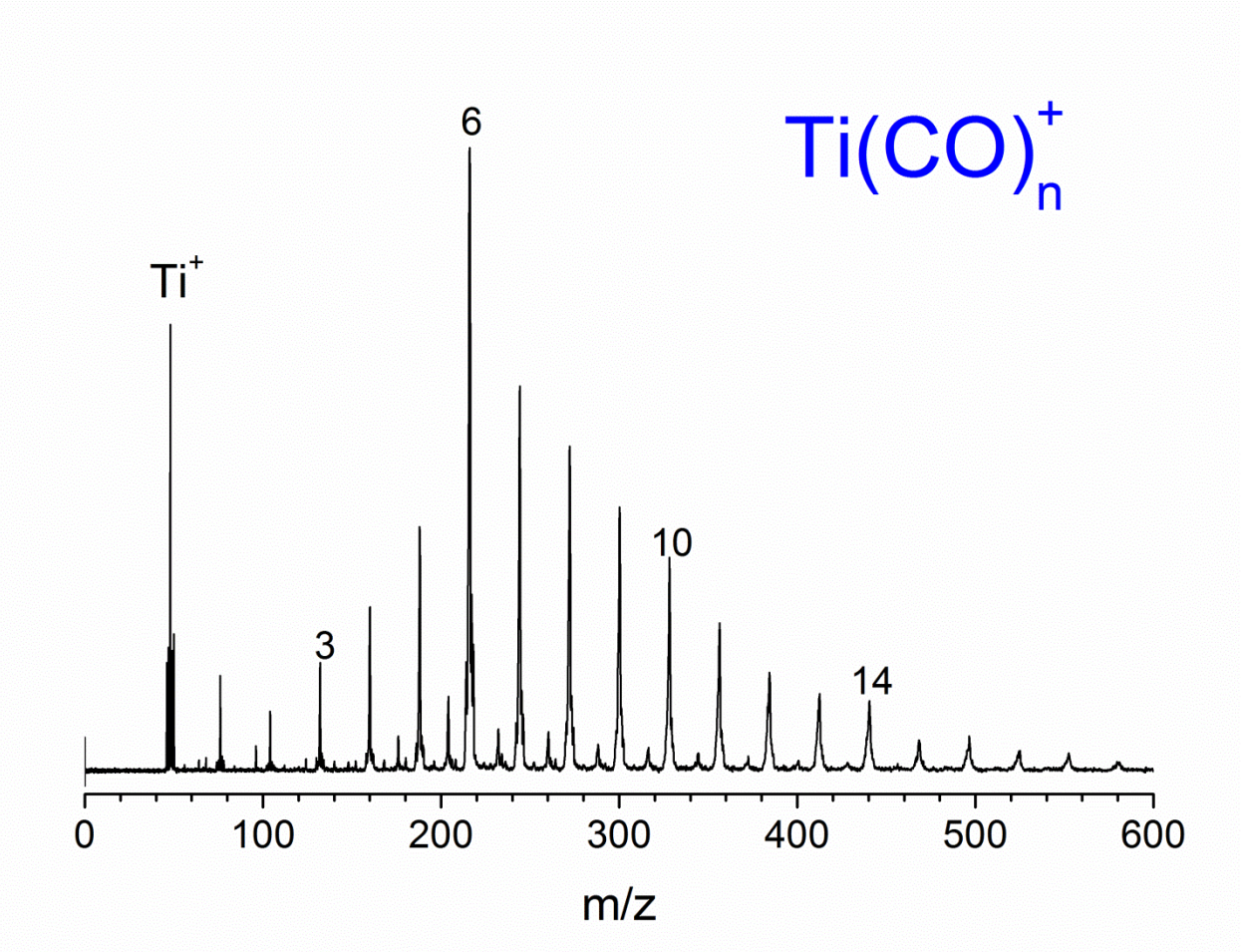

Figure 4.1. Mass spectrum of $Ti(CO)_n^+$ complexes produced via laser ablation of a titanium rod.

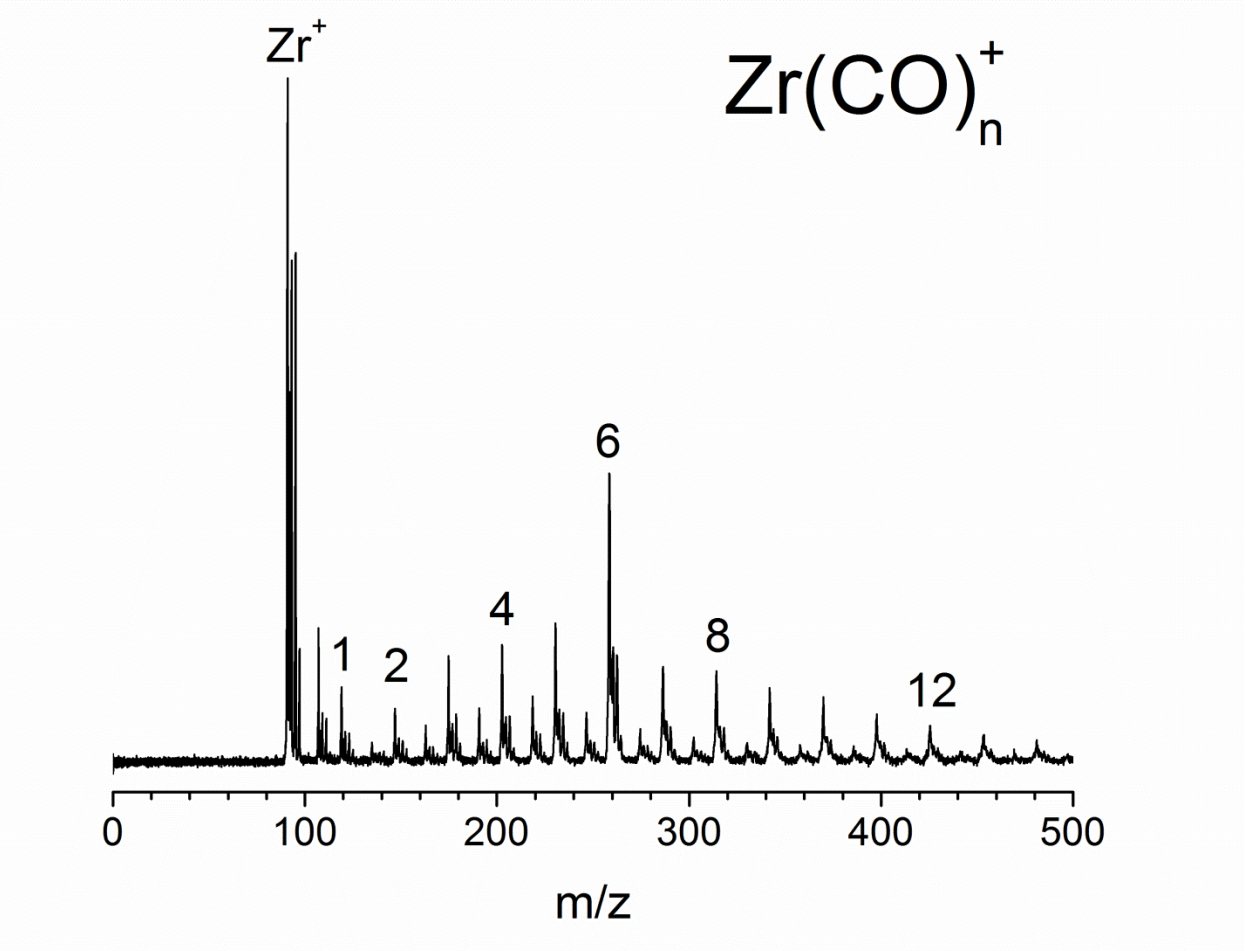

Figure 4.2. Mass spectrum of $Zr(CO)_n^+$ complexes produced via laser ablation of a zirconium rod.

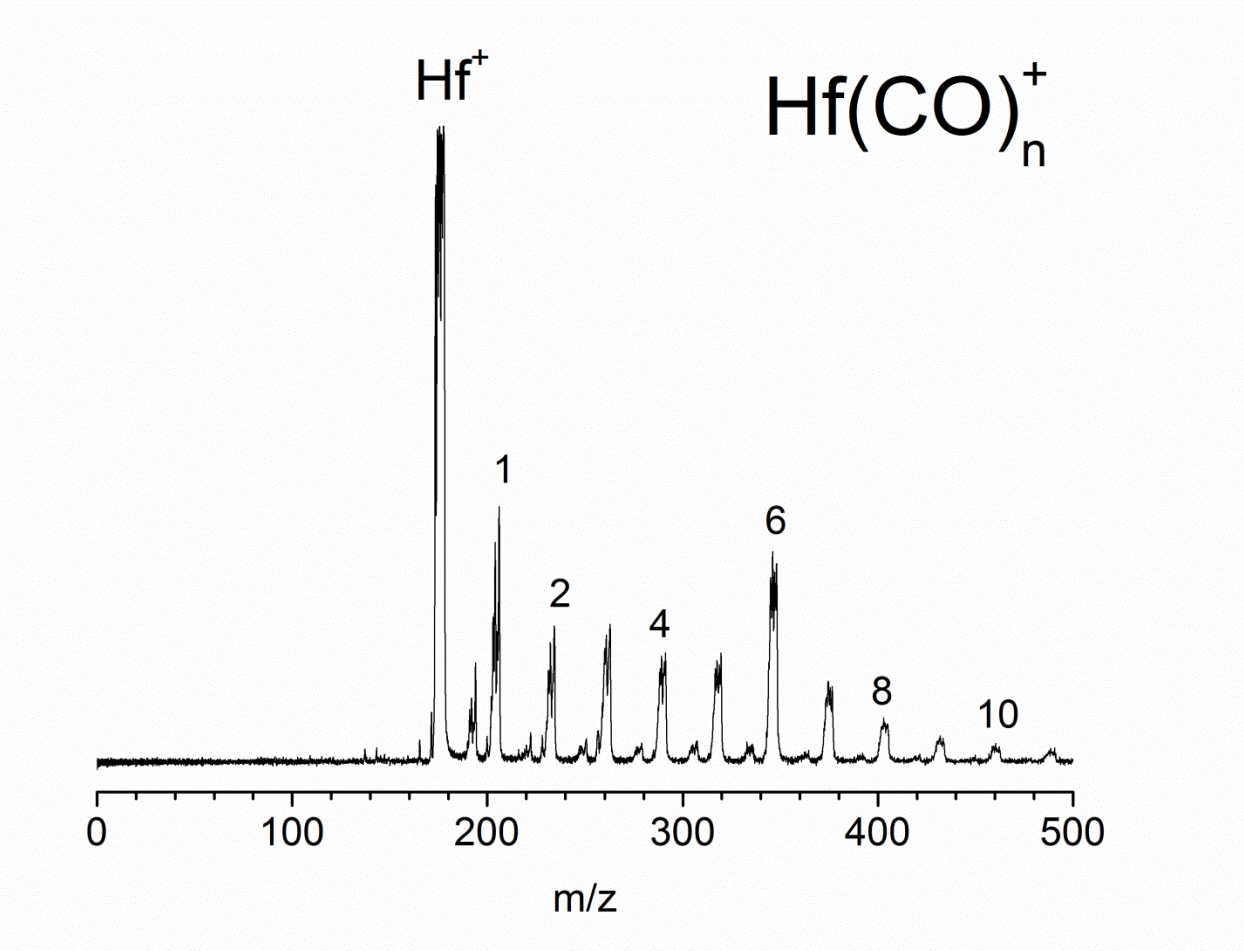

Figure 4.3. Mass spectrum of $Hf(CO)_n^+$ complexes produced via laser ablation of a hafnium rod.

smaller than n = 7 were observed to fragment inefficiently or not at all. This is not surprising, as the bond energy of the $Ti(CO)_5^+$ -CO complex has been previously measured to be approximately 6200 cm^{-1}.[13] Although this is greater than the energy of an infrared photon in the CO stretching region (~2100 cm^{-1}), some fragmentation was still observed for the $M(CO)_6^+$ (M = Ti, Zr, Hf) species. This fragmentation is attributed to multiphoton absorption and/or the presence of a small fraction of ions with some unquenched internal energy from the growth process. Larger complexes, with seven or more ligands undergo efficient fragmentation. Sequential ligand loss terminating at n = 6 is observed for these ions. This suggests that the n = 6 complex is resistant to further fragmentation, i.e., that it is relatively more stable than larger species. This is evidence for a strongly bound six-coordinate core. In all of the larger complexes the most prominent fragmentation channel is the loss of two CO ligands from the parent ion. If these ions undergo single photon dissociation, this indicates that the binding energy of the external CO molecules is less than 1000 cm^{-1}.

Figure 4.7 presents the infrared photodissociation spectra for the n = 6 complexes of titanium, zirconium and hafnium obtained via the elimination of a CO ligand. Although the fragmentation yield for these ions is not large, averaging the signal produces spectra of acceptable signal levels. The dashed line represents the free CO vibration at 2143 cm^{-1}. All spectra show a single infrared band whose frequency is red-shifted from that of free CO. However, the magnitude of this red shift notably increases with increasing atomic mass of the metal atom. The band in the titanium spectra is observed at 2110 cm^{-1}, whereas those for zirconium and hafnium are at 2094 and 2075 cm^{-1}, respectively. A single infrared band is usually indicative of a high symmetry structure, with an octahedral geometry being most common for six-coordinate systems. To aid in the assignment of the experimental spectra, DFT

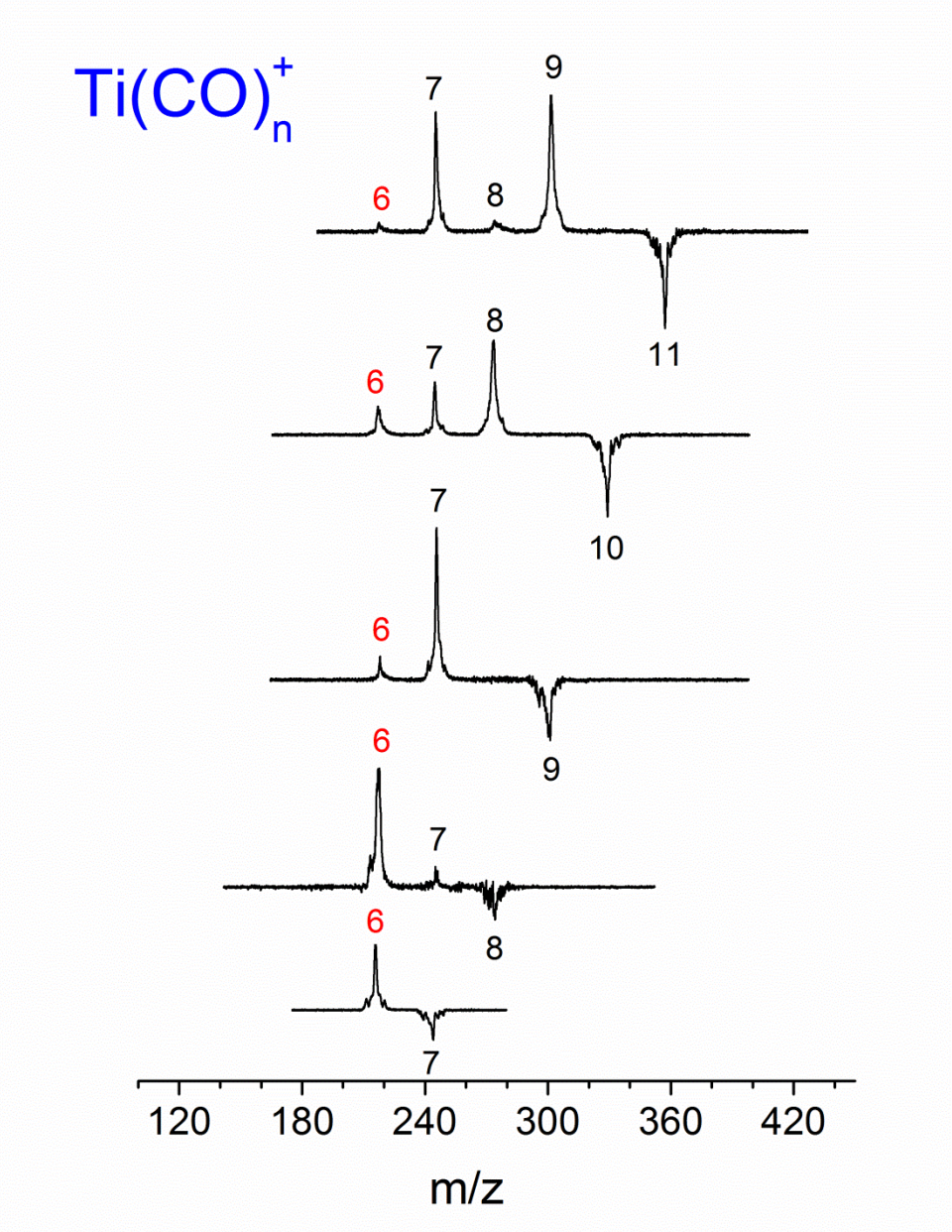

Figure 4.4. Infrared photodissociation breakdown spectra of $Ti(CO)_n^+$ (n = 7-11) complexes. These spectra were obtained by subtracting a mass spectrum of a mass-selected cluster with the laser off from one with it on.

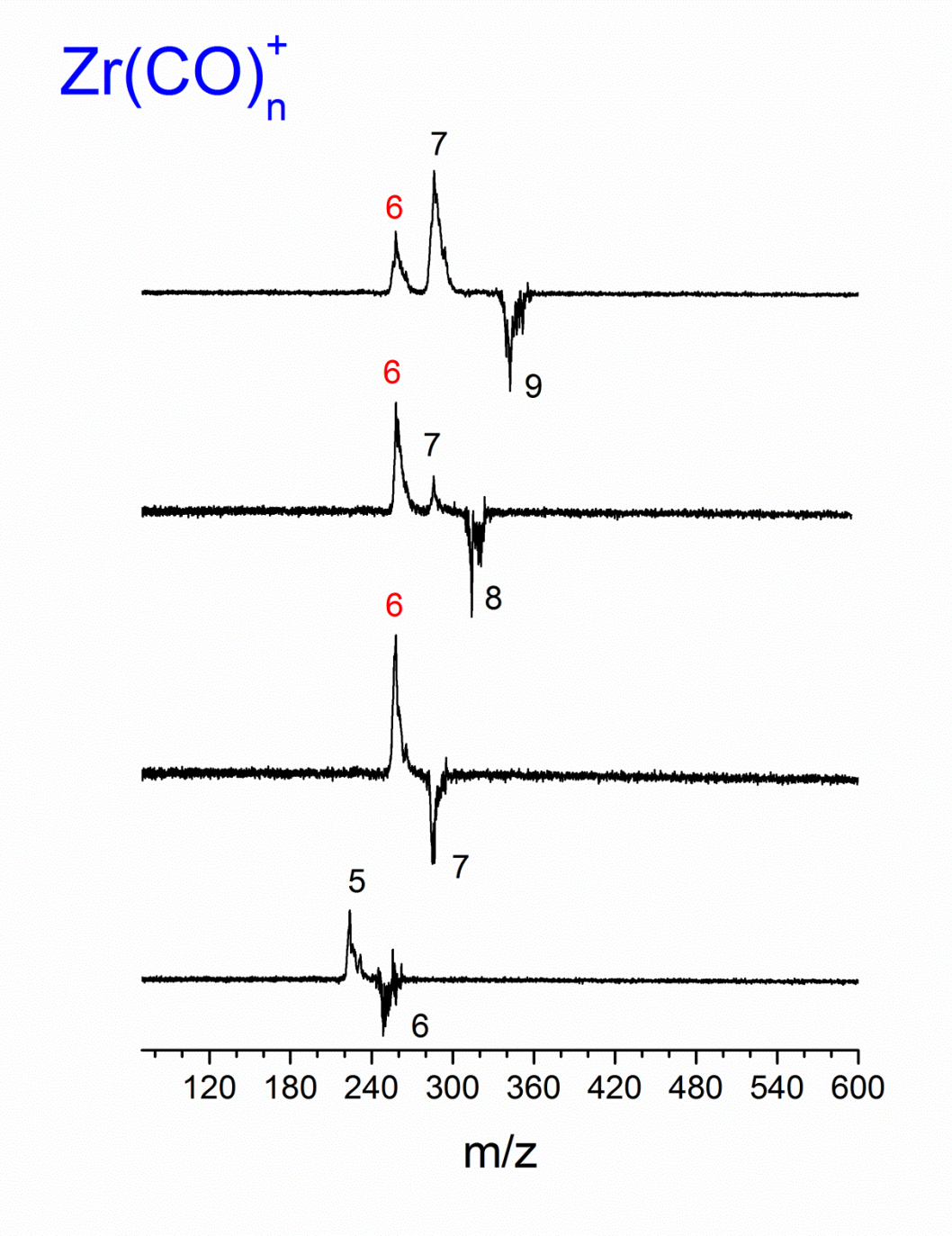

Figure 4.5. Infrared photodissociation breakdown spectra of $Zr(CO)_n^+$ (n = 6-9) complexes. These spectra were obtained by subtracting a mass spectrum of a mass-selected cluster with the laser off from one with it on.

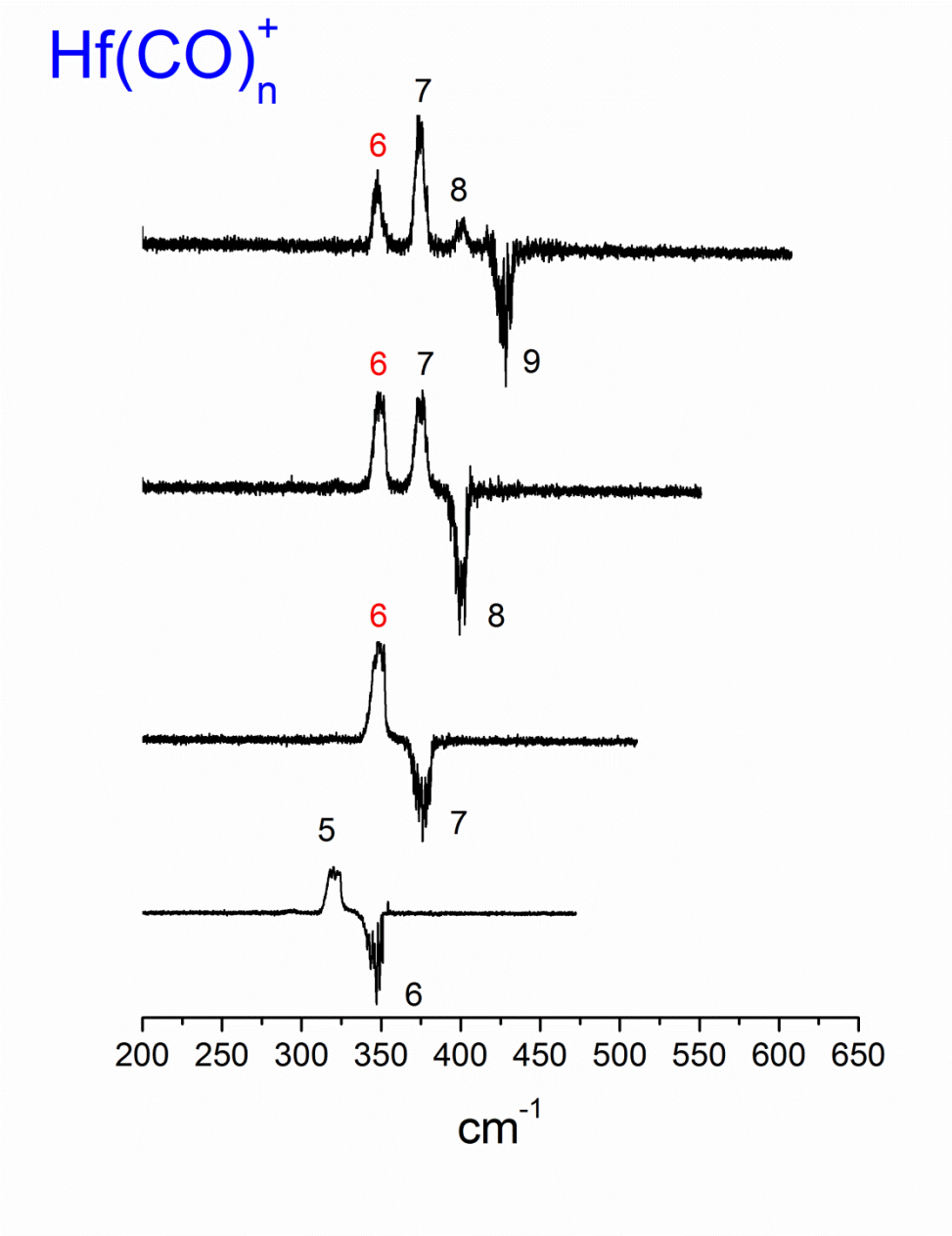

Figure 4.6. Infrared photodissociation breakdown spectra of $Hf(CO)_n^+$ (n = 6-9) complexes. These spectra were obtained by subtracting a mass spectrum of a mass-selected cluster with the laser off from one with it on.

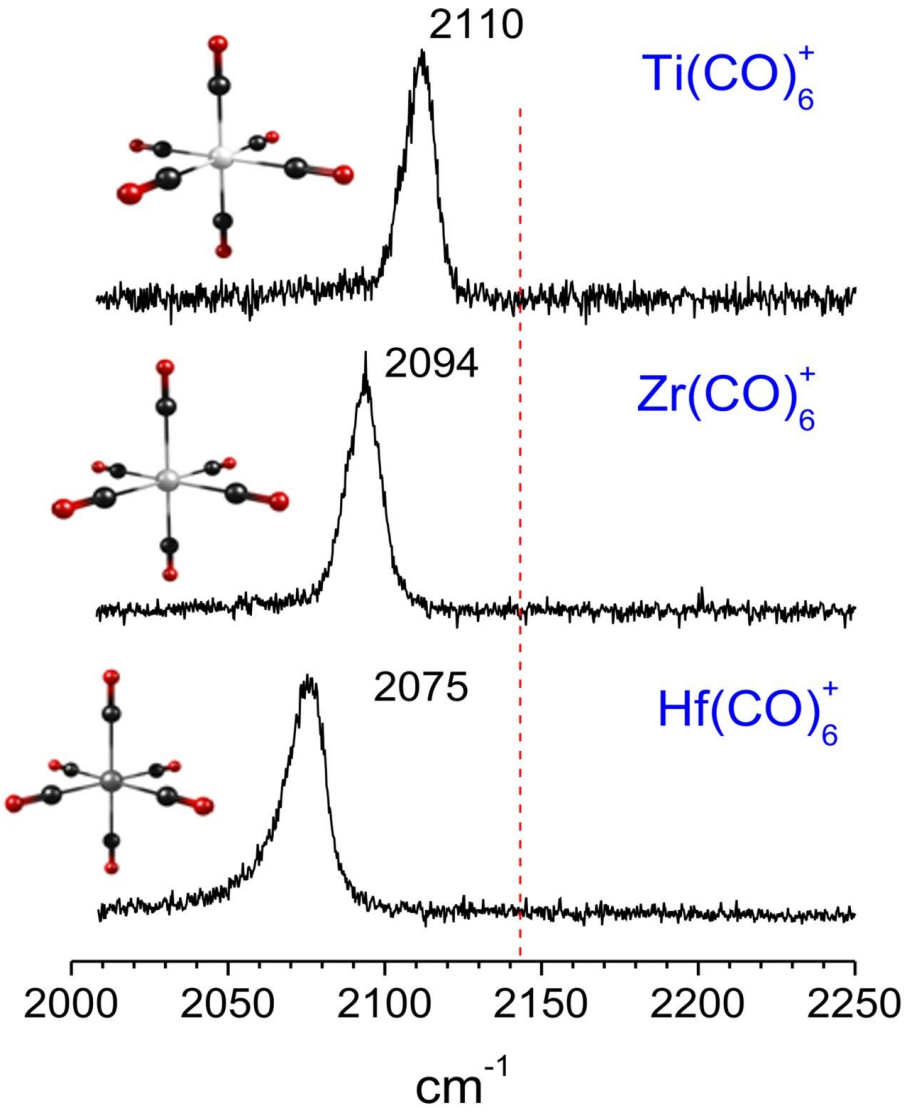

Figure 4.7. Infrared spectra of the $M(CO)_6^+$ (M = Ti, Zr, Hf) measured via CO elimination along with representative structures.

calculations using the B3LYP functional were performed on the doublet and quartet spin states for multiple $M(CO)_n^+$ (n = 6−8) isomers. The most relevant structural and numerical data from these studies are presented in Tables 4.1−4.3. The structures calculated to be stable minima are consistent with our experimental results. As expected, all n = 6 complexes were predicted to have octahedral geometries, yielding infrared spectra with a single high intensity band. The magnitude of these IR intensities can explain the observation of dissociation for these ions via multiphoton absorption. These values are shown in parentheses in Table 4.3.

As discussed previously, smaller or stable complexes have CO ligands which are strongly bound. As a result, we employ rare gas tagging to enhance the dissociation yields of these complexes.[55-60] $M(CO)_n^+Ar$ ions are produced by adding argon to the CO expansion. These ions fragment by elimination of the argon atom following photoexcitation of a CO vibration. The possible effects of tagging on the spectra are not ignored. As illustrated in Figure 4.8, both neat and tagged species are investigated to ascertain the effects of tagging on the spectra. The tagged spectrum has a better signal level and a narrower lindewidth (~12 cm^{-1} for the neat and ~7 cm^{-1} for the tagged ion). This is consistent with the argon atom being weakly bound, and thus easily eliminated. The band positions of the neat and tagged spectra are essentially the same at 2110 cm^{-1} for $Ti(CO)_6^+$ and 2109 cm^{-1} for $Ti(CO)_6Ar^+$, suggesting that any spectral shift induced by multiphoton dissociation is insignificant. The IR spectrum of the predicted quartet structure reproduces the single band pattern of the experiment, whereas the multiplet produced for the doublet species does not. Zhou and coworkers have also studied $Ti(CO)_6^+$.[11] Due to their inability to produce cold ions, the single peak in their spectrum was broader than ours (>20 cm^{-1}) and their reported band position was 2118 cm^{-1}.

Table 4.1. Structures, electronic ground states and relative energies for $M(CO)_n^+$ complexes, where M = Ti, Zr, Hf, computed using DFT. The coordination for each complex is shown in parentheses.

Complex	Spin State	Symmetry	Relative energy (kcal/mol)
$Ti(CO)_6^+$	doublet (6C)	C_{2v}	+13.0
	quartet (6C)	D_{3d}	0.0
$Ti(CO)_7^+$	doublet (7C)	C_{3v}	0.0
	quartet (6C+1)	C_1	+3.6
$Ti(CO)_8^+$	doublet (7C+1)	C_1	0.0
	quartet (6C+1)	C_{2v}	+4.2
$Zr(CO)_6^+$	doublet (6C)	C_{2v}	+4.6
	quartet (6C)	D_{3d}	0.0
$Zr(CO)_7^+$	doublet (7C)	C_{3v}	0.0
	quartet (6C+1)	C_1	+14.1
$Zr(CO)_8^+$	doublet (7C+1)	C_1	0.0
	quartet (6C+2)	C_{2v}	+15.2
$Hf(CO)_6^+$	doublet (6C)	C_{2v}	+3.5
	quartet (6C)	D_{3d}	0.0
$Hf(CO)_7^+$	doublet (7C)	C_{3v}	0.0
	quartet (6C+1)	C_1	+17.7
$Hf(CO)_8^+$	doublet (7C+1)	C_1	0.0
	quartet (6C+2)	C_{2v}	+18.5

Table 4.2. Computed binding energies in kcal/mol for the last CO in $M(CO)_n^+$ complexes, where M = Ti, Zr and Hf. The coordination for each complex is shown in parentheses.

Complex	Spin State	$E[M(CO)_{n-1}^+ - CO]$
$Ti(CO)_6^+$	doublet (6C)	25.1
	quartet (6C)	25.1
$Ti(CO)_7^+$	doublet (7C)	19.9
	quartet (6C+1)	3.2
$Ti(CO_8^+$	doublet (7C+1)	3.7
	quartet (6C+1)	3.2
$Zr(CO)_6^+$	doublet (6C)	29.5
	quartet (6C)	25.8
$Zr(CO)_7^+$	doublet (7C)	21.8
	quartet (6C+1)	3.1
$Zr(CO)_8^+$	doublet (7C+1)	4.1
	quartet (6C+2)	3.1
$Hf(CO)_6^+$	doublet (6C)	31.7
	quartet (6C)	30.4
$Hf(CO)_7^+$	doublet (7C)	24.4
	quartet (6C+1)	3.3
$Hf(CO)_8^+$	doublet (7C+1)	4.0
	quartet (6C+1)	3.2

Table 4.3. Measured vibrational frequencies and computed frequencies (Scaled by 0.971) for doublet and quartet states of $M(CO)_n^+$ complexes. All frequencies are in wavenumbers and computed IR intensities (km/mol) are listed in parentheses.

Complex	Experiment	Theory (quartet)	Theory (doublet)
$Ti(CO)_6^+$	2110	2102 (3421)	2071 (661), 2072 (844), 2085 (1404)
$Ti(CO)_7^+$	2114, 2164	2100 (2229), 2101 (1201) 2114(19), 2154 (68)	2066 (707), 2071 (816), 2078 (1009) 2092 (524), 2093 (556), 2105 (373) 2152 (81)
$Ti(CO)_8^+$	2112, 2164	2098 (1129), 2099 (2343) 2114 (43), 2153 (140)	2062 (707), 2067 (1097) 2082(1056) 2094 (575), 2098 (291) 2108 (296), 2150 (72), 2156 (74)
$Zr(CO)_6^+$	2094	2079 (4646)	2049 (716), 2055 (961), 2074 (1740) 2082 (1062), 2141 (3)
$Zr(CO)_7^+$	2097, 2164	2076 (3052), 2077 (1621) 2094 (38), 2154 (75)	2059 (750), 2062 (1201) 2076 (1578), 2083 (761), 2084 (190) 2100 (400), 2149 (51)
$Zr(CO)_8^+$	2095, 2163	2074 (1541), 2075 (3186) 2092 (48), 2153 (153)	2053 (740), 2061 (1240) 2067 (1223), 2080 (660), 2088 (544) 2092 (452), 2144 (15), 2163 (89)
$Hf(CO)_6^+$	2075	2062 (5303)	2036 (801), 2045 (1069) 2063 (1909), 2071 (1151) 2072 (6), 2140 (5)
$Hf(CO)_7^+$	2080, 2163	2059 (2465), 2060 (1872) 2081 (37), 2155 (77)	2112 (816), 2115 (1228) 2127 (1857), 2134 (792), 2154 (435) 2212 (49)
$Hf(CO)_8^+$	2079, 2163	2057 (1765), 2058 (3630) 2080 (45), 2155(155)	2047 (800), 2051 (1289) 2058 (1400), 2071 (820), 2077 (499) 2088 (475), 2146 (35), 2161 (82)

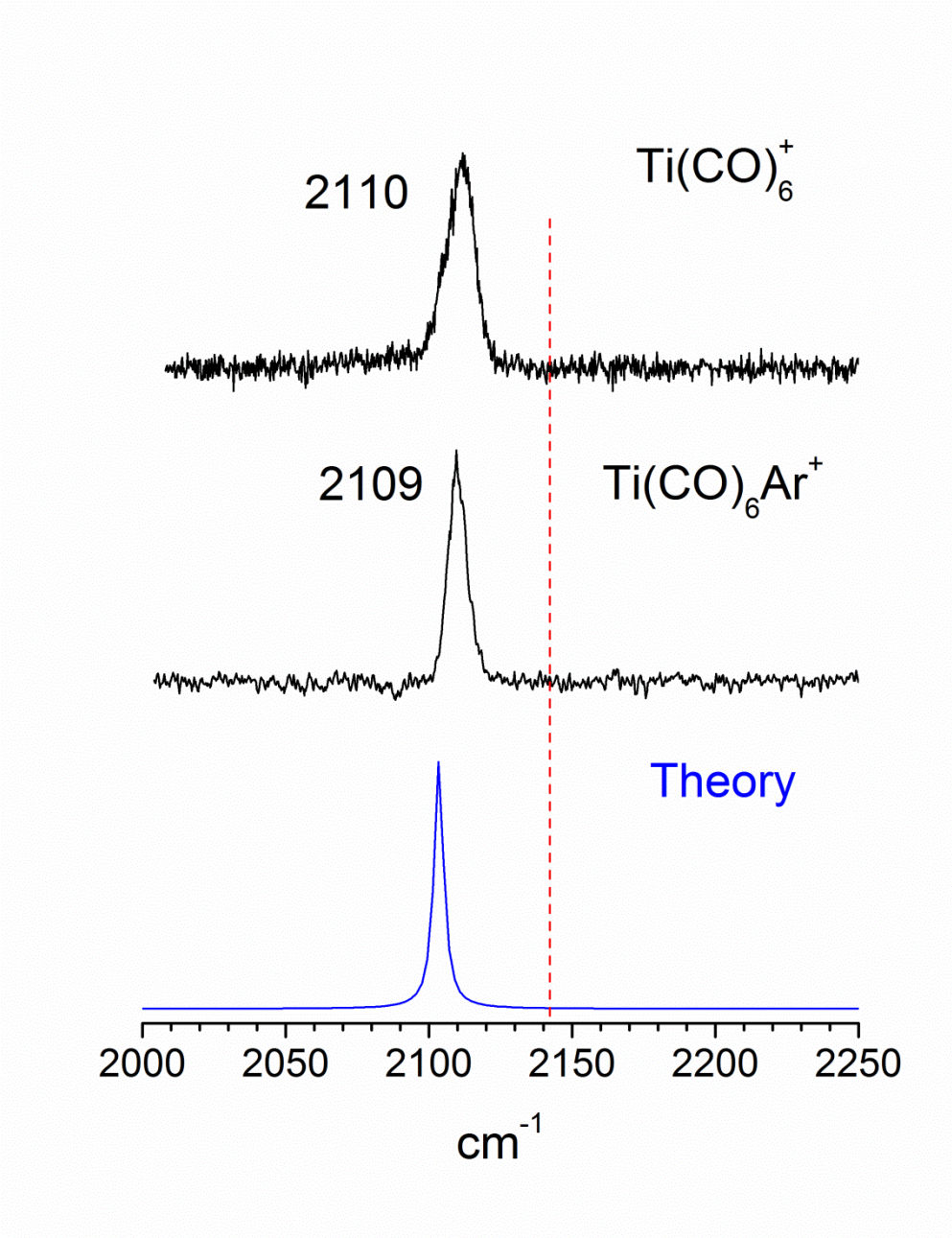

Figure 4.8. Infrared spectra of the $Ti(CO)_6^+$ ion and its argon-tagged analogue. The spectrum predicted by DFT calculations is shown in the bottom trace.

The infrared photodissociation spectra of the n = 7 complexes are presented in Figure 4.9. These complexes fragment efficiently via the elimination of a CO ligand. As a result, they have increased signal levels compared to the n = 6 spectra. Similar to the data for the n = 6 species, each n = 7 spectrum has a main band that is red-shifted from the free CO vibration, with increasing magnitude going down the group. This band is observed at 2114 cm^{-1} for the titanium complex and at 2097 and 2080 cm^{-1} for zirconium and hafnium respectively. For each $M(CO)_n^+$ system, the main band in the n = 7 spectrum is within 5 cm^{-1} of the corresponding band in the n = 6 spectrum. In addition to the main band, a blue-shifted feature whose frequency position remains virtually unchanged is also observed for all spectra. Its intensity and position is characteristic of weakly bound, second sphere CO ligands. These observations are all consistent with complexes having a hexacoordinate core and a weakly bound, external carbonyl ligand. Theoretical predictions and corresponding structures are presented in the bottom two traces for the two lowest energy n = 7 isomers of hafnium. The quartet species has a 6C+1 structure corresponding to a slightly distorted octahedral core ion with a second sphere CO ligand. The doublet species lies slightly lower in energy and has a 7C structure. Although the observed band position is less red-shifted than that predicted for the quartet, the number of infrared active bands and their relative intensities in this spectrum is a better match than the multiplet predicted for the doublet. Our n = 7 spectra are therefore assigned as being representative of a six coordinate core ion with an external CO ligand.

It is concievable that a 7C species is indeed present in our experiment, but strong ligand binding precludes its observation via the loss of a CO unit. This possibility is addressed by investigating the infrared spectra for 8C complexes, as shown in Figure 4.10. These spectra are measured by monitoring the wavelength dependence of the loss a single CO ligand. If the n = 7

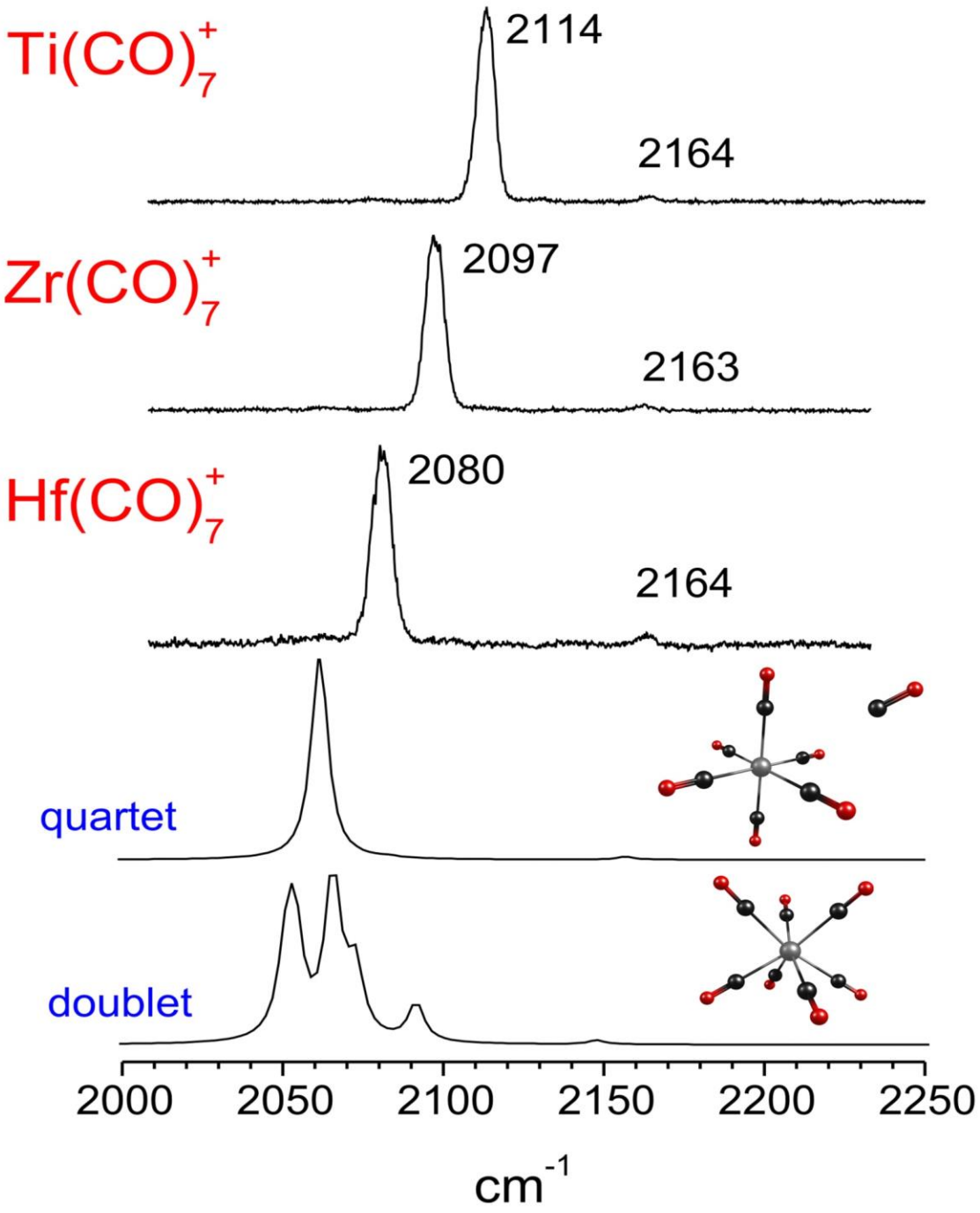

Figure 4.9. Infrared spectra of the $M(CO)_7^+$ (M = Ti, Zr, Hf) measured via CO elimination and calculated IR spectra of $Hf(CO)_7^+$ for both doublet and quartet spin states.

species is present, a multiplet similar to that predicted by theory should be observed. Indeed, similar to the n = 7 spectra, the n = 8 spectra all consist of a single intense band that is red-shifted and a weak, blue-shifted feature at 2164 cm^{-1}. As observed previously, the magnitude of the red shift of the main band increases from titanium to hafnium, whereas the band position of the weak feature remains virtually the same. Furthermore, the intensity of the blue-shifted bands is greater in the n = 8 spectra than in the n = 7 spectra. This increased intensity is consistent with the presence of two external CO ligands for the n = 8 species. The computed structures also support these observations. Compared to the n = 6 spectra, the main band in the corresponding n = 8 spectra only varies slightly (~ 4 cm^{-1}) for each metal. This provides further evidence that the n = 8 cluster also consists of an n = 6 core, with two weakly bound CO ligands. No evidence was found for a 7C complex.

Unfortunately, our experimental observations on the coordination of $Ti(CO)_n^+$ and its group IV congeners are not in agreement with our expectations for these complexes. Our theoretical results found a stable 7C complex for all metals, and binding energy studies conducted by Armentrout and coworkers determined that a stable $Ti(CO)_7^+$ species should exist.[13] In their study, the binding energy of the seventh CO ligand in $Ti(CO)_7^+$ was found to be 0.54 eV, which is much greater than expected for a second sphere ligand. However, we found no evidence for a stable seven-coordinate species for titanium, zirconium or hafnium. In our study on group V metal carbonyls, vanadium formed a 6C species, but the larger niobium and tantalum ions formed 18-electron, 7C complexes.[26] In this study, no group IV metal formed a seven-coordinate complex. Instead, a six-coordinate, 15 electron species was observed for all group IV metals.

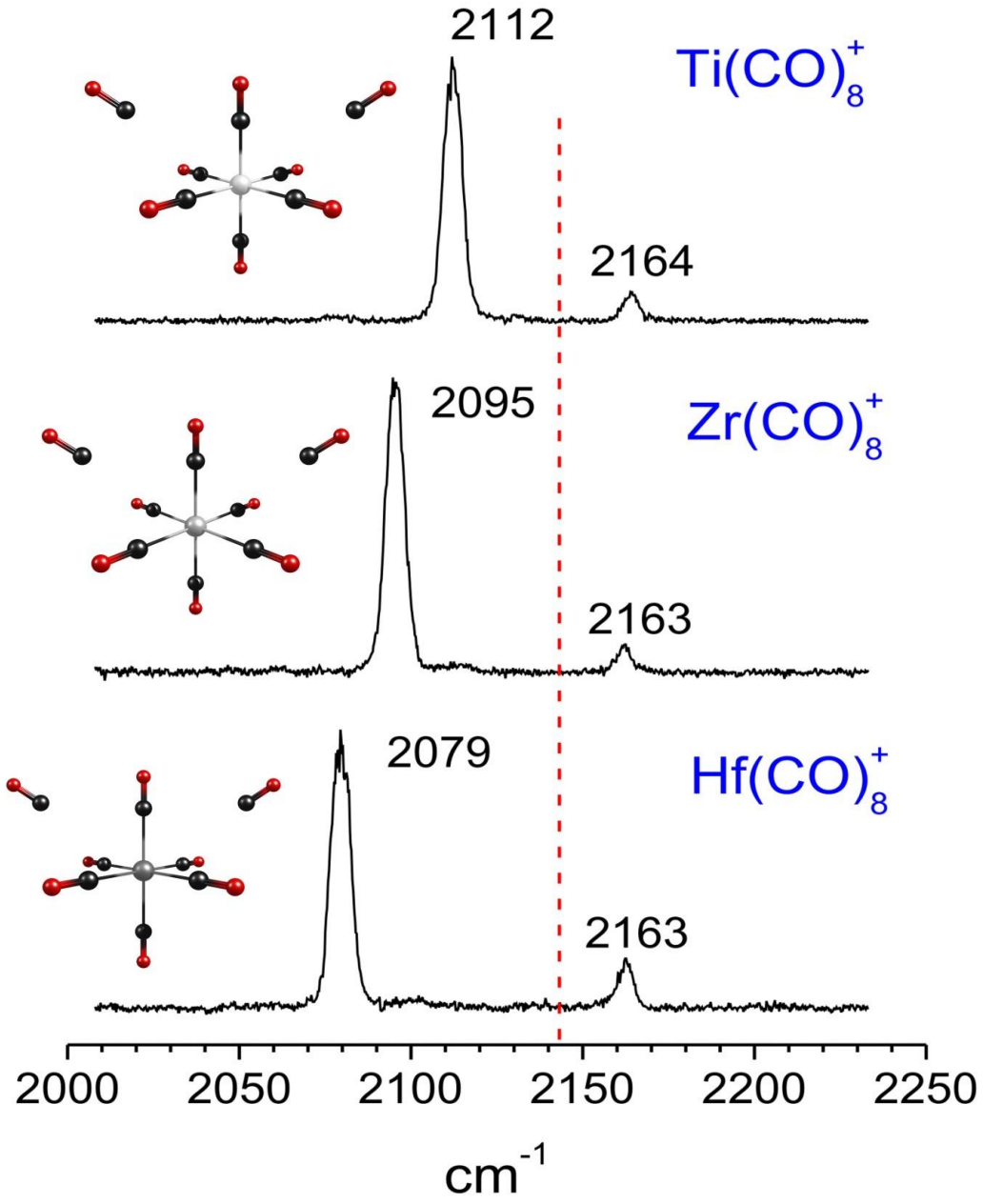

Figure 4.10. Infrared spectra of the $M(CO)_8^+$ (M = Ti, Zr, Hf) measured via CO elimination along with representative structures.

Similar inconsistencies between our experimental results and those obtained computationally and via binding energy studies conducted by Armentrout et al. have been discussed previously in our study on $V(CO)_n^+$.[26] We suggested that the disparity in results can be attributed to intrinsic differences in the mechanism of ion production in the two experiments. In the Armentrout experiment, the ions are thermalized in a flowtube which is held at room temperature. Thus, ions with ligands that are weakly bound are not expected to survive these conditions and only the strongly bound 7C species would be investigated. On the other hand, ions in our experiment are produced via laser ablation and then quickly cooled via supersonic expansion. These cold conditions are favorable for the production of ions with weakly bound external ligands. It is possible that we also produce the 7C species in our experiment, but in quantities that are unobservable relative to the significant amount of 6C+1 species.

It is possible that both species are formed initially in both experiments, but room temperature conditions preclude the observation of the 6C+1 species in Armentrout's experiment. However, it is still unclear why the 7C complexes are not formed in our experiment. To explain this, we examine the effects of spin changes on reaction rates. We discussed this issue previously in our study of group V carbonyls, where we suggested that a "kinetic bottleneck" associated with a spin change, was limiting the rate of production of the 7C species, but larger atoms with greater spin-orbit coupling were better able to undergo this reaction. The role of spin in carbonyl addition to metals was first investigated by Weitz and coworkers, who examined the spin-allowed and spin-forbidden recombination rates of CO to $Fe(CO)_n$.[27] In this study, reactions involving spin changes were found to occur at much slower rates (x400) than those that conserved spin. These results were also supported by the theoretical models for curve crossing reported by Harvey et al. which predicted so called "spin barriers" for reactions

involving a spin change.[28] As reported in Table 4.1, a spin change is observed between the n = 6 and n = 7 complexes for all three metals. For all three metals, the n = 6 cluster size has the doublet as its lowest energy structure, whereas the lowest energy structures for the n = 7 and n = 8 complexes are predicted to have quartet spin states. If cluster growth involves sequential ligand addition, then a spin change is required to go from $M(CO)_6^+$ (quartet) to $M(CO)_7^+$ (doublet). Such a spin change is likely to be the factor that limits the formation of 7C species. However, unlike the group V metals, even the second and third row metals in group IV are unable to efficiently form the 7C species.

The high symmetry of the core ions and the resulting simple spectra facilitate the observation of an interesting trend among the saturated group IV metal carbonyl cations. The magnitude of the red shift in the carbonyl stretching frequency increases systematically on going from titanium to hafnium. This trend was previously observed by Andrews and coworkers for the neutral, unsaturated titanium group carbonyls studied in a neon matrix.[9] The carbonyl stretching frequencies reported in that study were 1920, 1900 and 1869 cm^{-1} for TiCO, ZrCO and HfCO respectively. As discussed previously, π back-bonding is the most important interaction in metal-carbonyl complexes and as such, the observed trend is thought to be the result of an increase in the π back-bonding in these carbonyl systems going from titanium to hafnium.

In an attempt to rationalize this trend, we examine the ionization potentials and covalent radii of the metals. These properties are indicators of the strength with which electrons are attracted to the nucleus and the special distribution valence electrons. Both can influence the availability of valence electron density and by extension the bonding in these systems. The first IP's of titanium, zirconium and hafnium are 6.83, 6.63 and 6.83 eV respectively. Whereas, their second IP's are 13.6, 13.1, 14.9 eV respectively.[29] Although there is a decrease in the ionization

potential between titanium and zirconium, the IP of hafnium is greater than that of zirconium. These values do not corroborate the trend observed. Similar results are obtained when the covalent radii are considered. The covalent radii of group IV metals are 1.6, 1.75, 1.75 angstroms for titanium, zirconium and hafnium respectively.[30] These values also do not explain our observations. Another parameter used to express electron density availability is the Pauling electronegativity. For titanium, zirconium and hafnium, these values are 1.54, 1.33 and 1.3.2 This decrease in value is consistent with an increase in the availability of electron density for back-donation. This supports the trend observed in our experiment. This trend is also reproduced by DFT as shown in Table 4.3.

The magnitude of the red shifts observed for the C−O stretching frequencies measured in this study, relative to those measured for other systems, is another point worth discussing. As shown in Table 4.4, the carbonyl frequencies measured in this study are among the most red-shifted carbonyl frequencies measured for a transition metal carbonyl cation. Although these early transition metals have a relatively small number of electrons in their d orbitals, their effective nuclear charge is less than transition metals to their right. The increase in nuclear charge results in the well-known effect of d contraction. Early transition metals have more d electron density available for back-donation, and thus, greater red-shifts are observed for these systems. The data collected in this study are consistent with this trend and serve to provide additional examples of this effect.

Conclusion

Coordinatively saturated group IV metal-carbonyl cations of the form $M(CO)_n^+$ (M = Ti, Zr, Hf; n = 6, 7, 8) are produced in a molecular beam via laser vaporization in a pulsed nozzle

Table 4.4. Comparison of the band positions (cm^{-1}) of core CO ligands for various metal carbonyl cations.

Complex	Band Positions	Complex	Band Positions
$Ti(CO)_6^+$	2110	$V(CO)_6^+$	2097[a]
$Zr(CO)_6^+$	2094	$Mn(CO)_6^+$	2115[b]
$Hf(CO)_6^+$	2075	$Co(CO)_5^+$	2140, 2150[c]
		$Cu(CO)_4^+$	2198[d]

[a]reference [31].

[b]reference [32].

[c]reference [33].

[d]reference [34].

source. The ions are mass-selected in a reflectron time of flight mass spectrometer, and infrared laser photodissociation spectroscopy in the 2000-2300 cm^{-1} region is used to probe the carbonyl stretching vibrations. The number of infrared active bands, their relative intensities and their frequency positions provide insight into the structure and bonding of these complexes. DFT calculations were conducted in support of the experimental data. The n = 6 species was observed to be the fully coordinated complex for each metal, and all complexes have a structure with D_{3d} symmetry. These highly symmetric structures facilitated the investigation of trends in the bonding and infrared band positions of these complexes. The carbonyl stretching frequencies of the fully coordinated $M(CO)_6^+$ species are all red-shifted, (2110, 2094 and 2075 cm^{-1} for titanium, zirconium and hafnium respectively), and a systematic increase in the magnitude of the red shift, going from titanium to hafnium, is apparent. Despite the observation of 7-C complexes in a previous study on group V transition metal carbonyls, no experimental evidence for a similar 7-C carbonyl species was observed for group IV carbonyls.

References

(1) Cotton, F. A. *Advanced Inorganic Chemistry*, 6th ed.; John Wiley and Sons, Inc.: New York, 1999.

(2) Huheey, J. E.; Keiter, E. A.; Keiter, R. L. *Inorganic Chemistry Principles of Structure and Reactivity*, Harper Collins: New York, 1993.

(3) Heck, R. F. *Organotransition Metal Chemistry*, Academic Press: New York, 1974.

(4) Nakamoto, K. *Infrared and Raman Spectra of Inorganic and Coordination Compounds*; John Wiley: New York, 1997.

(5) Bertini, I.; Gray, H. B.; Stiefel, E. I.; Valentine, J. S. *Biological Inorganic Chemistry Structure and Reactivity*, University Science Books: California , 2007.

(6) Somorjai, G. A. *Introduction to Surface Chemistry and Catalysis*, John Wiley and Sons, Inc.: New York, 1994.

(7) Frenking, G.; Fröhlich, N. The nature of the bonding in transition-metal compounds. *Chem. Rev.* **2000**, *100*, 717-774.

(8) Zhou, M.; Andrews, L.; Bauschlicher, C. W., Jr. Spectroscopic and Theoretical Investigations of Vibrational Frequencies in Binary Unsaturated Transition-Metal Carbonyl Cations, Neutrals, and Anions. *Chem. Rev.* **2001**, *101*, 1931-1962.

(9) Zhou, M.; Andrews, L. Reactions of Zirconium and Hafnium Atoms with CO: Infrared Spectra and Density Functional Calculations of $M(CO)_x$, OMCCO, and $M(CO)_2^-$ (M = Zr, Hf; x = 1-4). *J. Am. Chem. Soc.* **2000**, *122*, 1531-1539.

(10) Luo, Q.; Li, Q.; Y, Z. H.; Xie, Y.; King, R. B.; Schaefer, H. F. Bonding of Seven Carbonyl Groups to a Single Metal Atom: Theoretical Study of $M(CO)_n$ (M = Ti, Zr, Hf; n = 7, 6, 5, 4). *J. Am. Chem. Soc.* **2008**, *130*, 7756-7765.

(11) Zhou, X.; Cui, J.; Li, Z. H.; Wang, G.; Liu, Z.-P.; Zhou, M. Carbonyl Bonding on Oxophilic Metal Centers: Infrared Photo-dissociation Spectroscopy of Mononuclear and Dinuclear Titanium Carbonyl Cation Complexes. *J. Phys. Chem. A* **2013**, *117*, 1514-1521.

(12) Sievers, M. R.; Armentrout, P. B. Collision-Induced Dissociation Studies of $V(CO)_7^+$, x=1-7: Sequential Bond Energies and the Heat of Formation of $V(CO)_6$. *J. Phys. Chem.* **1995**, *99*, 8135-8141.

(13) Meyer, F.; Armentrout, P. B. Sequential Bond Energies of $Ti(CO)_x^+$, x= 1-7. *Mol. Phys.* **1996**, *88*, 187-197.

(14) Luo, Q.; Li, Q.; Y, Z. H.; Xie, Y.; King, R. B.; Schaefer, H. F. Bonding of Seven Carbonyl Groups to a Single Metal Atom: Theoretical Study of $M(CO)_n$ (M = Ti, Zr, Hf; n = 7, 6, 5, 4). *J. Am. Chem. Soc.* **2008**, *130*, 7756-7765.

(15) Dicke, J. W.; Stibrich, N. J.; Schaefer, H. F., III $V(CO)_7^+$: A Capped Octahedral Structure Completes the 18-electron Rule. *J. Chem. Phys.* **2008**, *456*, 13-18.

(16) Becke, A. D. 3 Term Correlation Functional. *J. Chem. Phys.* **1993**, *98*, 5648-5652.

(17) Lee, C.; Yang, W.; Parr, R. G. Development of the Coll-Salvetti Correlation Energy Formula into a Functional of the Electron Density. *Phys. Rev B.* **1988**, *37*, 785-789.

(18) Frisch, M. J.; Trucks, G. W.; Schlegel, H. B.; Scuseria, G. E.; Robb, M. A.; Cheeseman, J. R.; Montgomery, J. A. Jr.; Vreven, T.; Kudin, K. N.; Burant, J. C.; Millam, J. M.; Iyengar, S. S.; Tomasi, J.; Barone, V.; Mennucci, B.; Cossi, M.; Scalmani, G.; Rega, N.; Petersson, G. A.; Nakatsuji, H.; Hada, M.; Ehara, M.; Toyota, K.; Fukuda, R.; Hasegawa, J.; Ishida, M.; Nakajima, T.; Honda, Y.; Kitao, O.; Nakai, H.; Klene, M.; Li, X.; Knox, J. E.; Hratchian, H. P.; Cross, J. B.; Adamo, C.; Jaramillo, J.; Gomperts, R.; Stratmann, R.

E.; Yazyev, O.; Austin, A. J.; Cammi, R.; Pomelli, C.; Ochterski, J. W.; Ayala, P. Y.; Morokuma, K.; Voth, G. A.; Salvador, P.; Dannenberg, J. J.; Zakrzewski, V. G.; Dapprich, S.; Daniels, A. D.; Strain, M. C.; Farkas, O.; Malick, D. K.; Rabuck, A. D.; Raghavachari, K.; Foresman, J. B.; Ortiz, J. V.; Cui, Q.; Baboul, A. G.; Clifford, S.; Cioslowski, J.; Stefanov, B. B.; Liu, G.; Liashenko, A.; Piskorz, P. Komaromi, I.; Martin, R. L.; Fox, D. J.; Keith, T.; Al-Laham, M. A.; Peng, C. Y.; Nanayakkara, A.; Challacombe, M.; Gill, P. M. W.; Johnson, B.; Chen, W.; Wong, M. W.; Gonzalez, C. and Pople, J. A. Gaussian 03 (Revision B.02), Gaussian, Inc., Pittsburgh PA, 2003.

(19) McLean, A. D.; Chandler, G. S. Contracted Gaussian Basis Sets for Molecular Calculations. I. Second Row Atoms, *Z*=11–18. *J. Chem. Phys.* **1980**, *72*, 5639-5648.

(20) Krishman, R.; Binkley, J. S.; Seeger, R.; Pople, J. A. Self-Consistent Molecular Orbital Methods. XX. A Basis Set for Correlated Wave Functions. *J. Chem. Phys.* **1980**, *72*, 650-654.

(21) Hay, P. G.; Wadt, W. R. *Ab Initio* Effective Core Potentials for Molecular Calculations. Potentials for K To Au Including the Outermost Core Orbitals. *J. Chem. Phys.* **1980**, *82*, 299-310.

(22) Dunning, T. H. Gaussian Basis Functions for Use in Molecular Calculations. I. Contraction of (9*s*5*p*) Atomic Basis Sets for the First-Row Atoms. *J. Chem. Phys.* **1970**, *53*, 2823-2833.

(23) Jones, L. H.; McDowell, R. S.; Goldblatt, M. Force Constants of the Hexacarbonyls of Chromium, Molybdenum, and Tungsten from the Vibrational Spectra of Isotopic Species. *Inorg. Chem.* **1969**, *8*, 2349-2363.

(24) Boquet, G.; Birgone, M. Infrared Spectra of $Ni(CO)_4$ in the Gas Phase. *Spectrochim. Acta* **1971**, *27*, 139-149.

(25) Jones, L. H.; McDowell, R. S.; Goldblatt, M.; Swanson, B. I. Potential Constants of Iron Pentacarbonyl from Vibrational Spectra of Isotopic Species. *J. Chem. Phys.* **1972**, *57*, 2050-2064.

(26) Ricks, A. M.; Reed, Z. D.; Duncan, M. A. Seven-Coordinate Homoleptic Metal Carbonyls in the Gas Phase. *J. Am. Chem. Soc*. **2009**, *131*, 9176-9177.

(27) Ryther, R. J.; Weitz, E. Reaction Kinetics of Coordinatively Unsaturated Iron Carbonyls Formed on Gas-Phase Excimer Laser Photolysis of Iron Pentacarbonyl. *J. Phys. Chem*. **1991**, *95*, 9841-9852.

(28) Harvey, J. N.; Aschi, M. Modeling Spin-Forbidden Reactions: Recombination of Carbon Monoxide with Iron Tetracarbonyl. *Faraday Discuss*. **2003**, *124*, 129-143.

(29) Kramida, A.; Ralchenko, Yu.; Reader, J.; NIST ASD Team *NIST Atomic Spectra Database*, ver. 5.0; National Institute of Standards and Technology: Gaithersburg, MD, 2011. Available: http://physics.nist.gov/asd [2012, November 8].

(30) Cordero, B.; Gomez, V.; Platero-Plats. A. E.; Reves, M.; Echeverria, J.; Cremades, E.; Barragan, F.; Alvares, S. Covalent Radii Revisited. *Dalton Trans*. **2008**, *21*, 2832-2838.

(31) Ricks, A. M.; Brathwaite, A. D.; Duncan, M. A. Coordination and Spin States in Vanadium Carbonyl Complexes ($V(CO)_n^+$, n = 1–7) Revealed with IR Spectroscopy. *J. Phys. Chem. A* **2012**, *117*, 1001-1010.

(32) Reed, Z. D.; Duncan, M. A. Infrared Spectroscopy and Structures of Manganese Carbonyl Cations, $Mn(CO)_n^+$ (n = 1–9). *J. Am. Soc. Mass Spectrom.* **2010**, *21*, 739-749.

(33) Ricks, A. M.; Bakker, J. M.; Douberly, G. E.; Duncan, M. A. Infrared Spectroscopy and Structures of Cobalt Carbonyl Cations. *J. Phys. Chem. A* **2009**, *113*, 4701-4708.

(34) Brathwaite, A. D.; Reed, Z. D.; Duncan, M. A. Infrared Photodissociation Spectroscopy of Copper Carbonyl Cations. *J. Phys. Chem. A* **2011**, *115*, 10461-10469.

CHAPTER 5

INFRARED PHOTODISSOCIATION SPECTROSCOPY OF COPPER CARBONYL CATIONS

Introduction

Although most transition metal species follow the classical bonding model, some of these complexes exhibit so-called "non-classical" bonding. This occurs for systems in which the metal d orbitals are filled, rendering them unable to accept or donate charge effectively.[1-10] C−O stretching frequencies that are blue-shifted from the free molecular CO stretch at 2143 cm^{-1} are generally observed for these species. It is widely accepted that σ donation and π back-donation are the two dominant interactions in metal-carbonyl bonding. However, recent investigations have suggested that a third interaction, electrostatic polarization, plays a pivotal role in non-classical carbonyls.[2-9] Frenking and coworkers conducted model studies on CO^+, which was found to have a higher fundamental vibrational frequency than neutral CO. They suggested that polarization in the cation redistributes the otherwise imbalanced electron density in the C-O bond. This process strengthens the bond and yields a higher C−O frequency. Electrostatic polarization adequately explains the blue-shifted frequencies observed for non-classical carbonyls. Unfortunately, there are few examples of spectroscopic studies of gas-phase metal carbonyl cations in which these interactions can be explored further.

Our research group has studied the infrared spectra of various metal cation-carbonyl complexes in the gas phase using mass-selected ion infrared photodissociation spectroscopy.[11-19] Among the systems studied, only $Au(CO)_n^+$ and $Pt(CO)_n^+$ complexes exhibited blue-shifted CO

vibrations consistent with non-classical carbonyls.[11,12] In this present study, we apply the same method to study cationic copper carbonyl complexes $Cu(CO)_n^+$ for n = 1-8.

$Cu(CO)_4^+$ is predicted to be stable as it satisfies the 18-electron rule and is isoelectronic to the well know neutral $Ni(CO)_4$. $Cu(CO)_n^+$ complexes where n = 1,3,4 have been studied in strongly acidic media.[20] The salts $[Cu(CO)_n]^-[AsF_6]^+$ (n=1-3) have been synthesized and characterized using infrared and Raman spectroscopy.[21] This solid-phase study concluded that $Cu(CO)_2^+$ and $Cu(CO)_3^+$ have $D_{\infty h}$ and D_{3h} symmetry respectively, and the ions have CO frequencies that are blue-shifted. Copper carbonyl cations have also been studied in the gas phase. The dissociation energy of $Cu(CO)_n^+$ was measured by Armentrout and co-workers for the n=1-4 complexes.[22] The bond energy of $Cu(CO)_3^+$ −CO was determined to be 0.55 eV (4436 cm^{-1}), demonstrating that up to four CO ligands are directly coordinated to the central copper ion. $Cu(CO)_n$ neutrals and ions have also been studied via matrix isolation.[23] Here, we report infrared photodissociation spectroscopy in the gas phase for both small unsaturated complexes $Cu(CO)_n^+$ (n = 1-3) and larger complexes at and beyond the first coordination shell (n= 4-8).

Experimental Section

$Cu(CO)_n^+$ ions are produced via the method described in Chapter 2. Mixed cluster ion complexes containing argon of the form $Cu(CO)_n^+Ar$ are produced using gas mixtures of 10% CO in argon. Infrared photodissociation spectra are collected for mass-selected ions. In support of the experimental results, DFT calculations were carried out to determine the structures and spin configuration of $Cu(CO)_n^+$ and $Cu(CO)_n^+Ar$. The singlet and triplet states of each ion are considered. The calculations were performed using the B3LYP functional[24,25] as implemented in the Gaussian 2003 computational package.[26] The Wachters+f basis[27] was used on Cu atoms

while the DZP basis set[28] was used for carbon and oxygen atoms, and 6-311++G** basis set was used for argon. The same functional and similar basis set was used successfully by Schaefer and coworkers to calculate the structure and infrared frequencies of binuclear copper carbonyls.[29]

Results and Discussion

A mass spectrum of the $Cu(CO)_n^+$ complexes produced by our source is shown in Figure 5.1. All peaks are doubled because of the 63 and 65 amu isotopes of copper. The most intense peak in the mass spectrum corresponds to the $Cu(CO)_4^+$ ion, indicating that this complex is preferentially formed, and suggesting that it may have enhanced stability. This cation is expected to be stable, as it satisfies the 18-electron rule and is isoelectronic to the stable neutral $Ni(CO)_4$. $Cu(CO)_n^+$ complexes with more than twenty ligands are observed. All of these ligands cannot be coordinated to the central metal ion. Instead, complexes larger than n = 4 are thought to contain a strongly bound core, with additional "external" ligands coordinated to other CO's via weaker electrostatic forces. Larger complexes are produced efficiently in our source due to the cold supersonic expansion conditions. Thus, they are not likely to be stable at room temperature.

Further insight into the stability and ligand binding energies of these complexes can be obtained by their fragmentation patterns. Small $Cu(CO)_n^+$ complexes (n = 1, 2) do not fragment when excited with infrared light. This is consistent with the binding energies (1.54 and 1.78 eV, respectively for the elimination of CO from n = 1, 2) which have been measured by Armentrout and co-workers.[22] The energy of IR photons in the CO stretching region is approximately 0.27 eV (2200 cm^{-1}). Therefore, it is not surprising that no fragmentation is observed for these complexes. Larger complexes do dissociate, and the infrared fragmentation mass spectra for

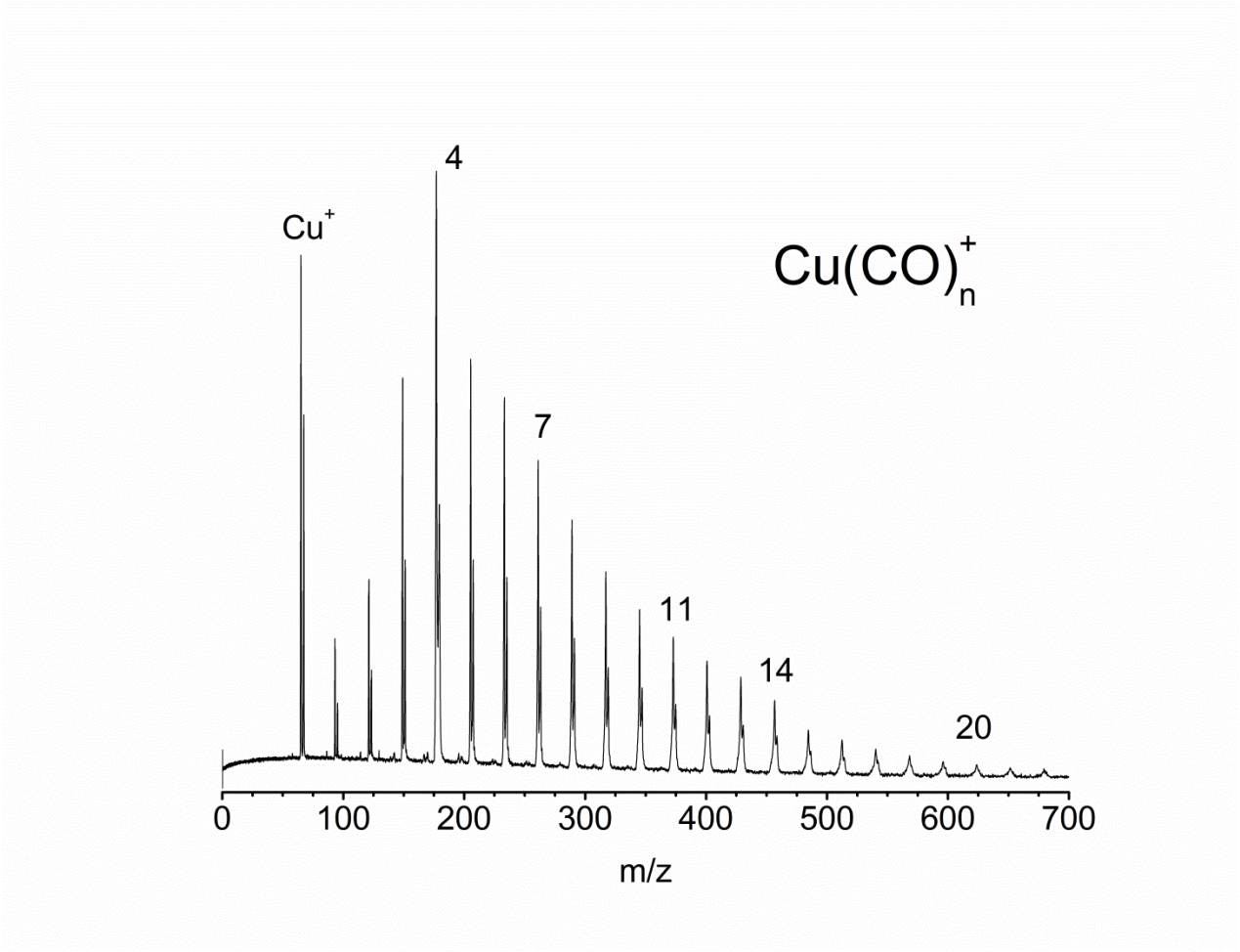

Figure 5.1. The mass spectrum of $Cu(CO)_n^+$ complexes produced by laser ablation of a copper rod in an expansion of carbon monoxide.

$Cu(CO)_n^+$ (n = 3 – 7) complexes are shown in Figure 5.2. For complexes n = 3 and 4, only a small amount of photodissociation is observed. This is consistent with the relatively high binding energies measured for these complexes by Armentrout and co-workers (0.78 and 0.55 eV respectively). Single-photon dissociation is not possible for these complexes, and the small amount of fragmentation observed is likely due to multiphoton absorption or from a fraction of the ions containing residual internal energy from the production process. Multiphoton absorption is not expected to be very efficient at the low laser pulse energies used here (about 1mJ/pulse). Residual internal energy could add to the photon energy, making photodissociation below the one-photon level possible.

Complexes larger than n = 4 undergo efficient CO elimination, terminating at n = 4. The signal levels in these spectra are also greater. All these observations are consistent with a strongly coordinated n = 4 core ion, with weakly bound external ligands. As shown in Figure 5.2, complexes larger than n = 4 show substantial tailing in time. This type of metastable dissociation indicates that the dissociation of these clusters takes place on a timescale comparable to their residence time in the reflectron (~ 1-2 microseconds). Other metal carbonyls have not exhibited such behavior, and it is still not apparent why these species dissociate at such a slow rate.

The energy of an IR photon near the CO stretching region is not sufficient to cause efficient dissociation of the smaller clusters. As a result, we employ the "rare gas tagging" technique to study these systems.[30-36] We produce mixed complexes of the form $Cu(CO)_n^+Ar$, which can fragment by eliminating argon due to photoexcitation of the ligand vibrations. This technique provides an alternative way to measure the IR spectra of ions with strongly bound ligands. The effect of tagging on these complexes is a valid concern. In some systems argon can

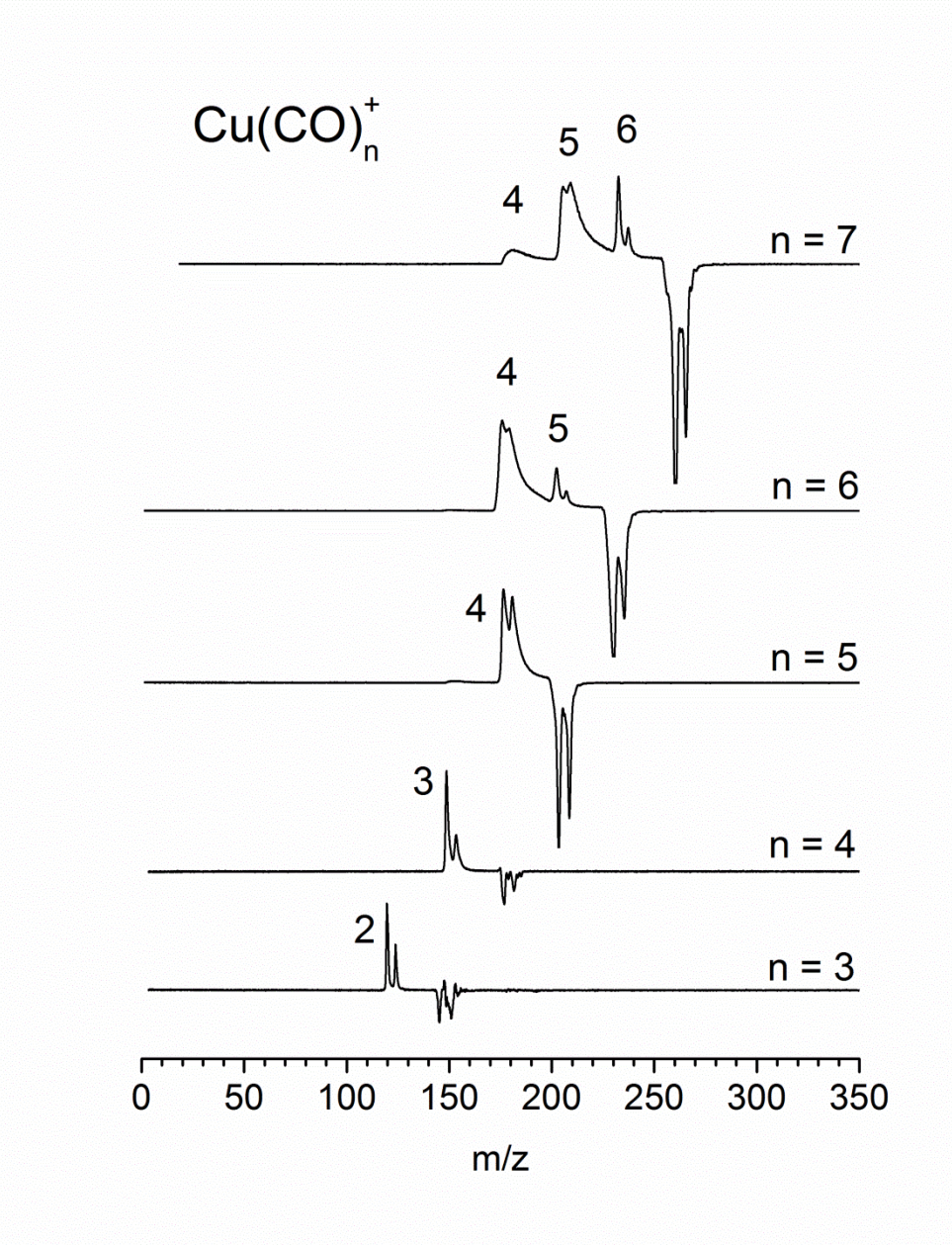

Figure 5.2. The photofragmentation mass spectra of $Cu(CO)_n^+$ species, showing the fragmentation channels resulting from infrared excitation near the carbonyl stretch. The negative peak represents the depletion of the mass-selected parent ion, while the positive peaks represent the resulting fragments.

bind strongly, essentially acting as a ligand. This can cause the spectrum of the tagged complex to be strongly perturbed in comparison to the neat species. The Cu^+−Ar binding energy has not been measured, but is calculated to be 0.405 eV (3267 cm^{-1}).[37] Although the metal-argon binding energy is more than the energy of an IR photon in the CO stretching region, the addition of ligands results in a significant decrease in this value. Previous experience with similar systems indicates that tagging usually has a negligible effect on the structure and spectrum of these complexes. However, we exercise due caution in interpreting these spectra and conduct computations on both tagged and neat complexes.

Figure 5.3 shows the spectra of the n = 1-4 complexes measured by tagging with argon. Tagging with one argon atom is sufficient to achieve efficient photodissociation for all complexes. The spectrum obtained for $Cu(CO)^+Ar$ is relatively broad. This is not surprising since argon binding to a mono ligand complex is likely to be relatively strong. The dashed vertical line indicates the position of the molecular CO vibration (2143 cm^{-1}). All spectra for the $Cu(CO)_n^+Ar$ complexes show a single intense band that is higher in frequency than free CO. This kind of blue-shifted frequency is a signature of non-classical carbonyls and the single-band spectra observed suggest structures with high symmetry. We employ DFT calculations to elucidate the structures and ligand binding energies of these systems.

Complexes containing three or more carbonyl ligands dissociate without tagging by the elimination of one or more carbonyl ligands. Though relatively inefficient, photodissociation via loss of CO ligands was observed for the neat n = 3 and 4 complexes. This facilitates the investigation of the effect of tagging by comparing neat and tagged spectra for these species. These results are presented in Figure 5.4. The tagged spectra have lower signal levels because the initial ion density of these complexes is far less than that of the neat complexes. In both

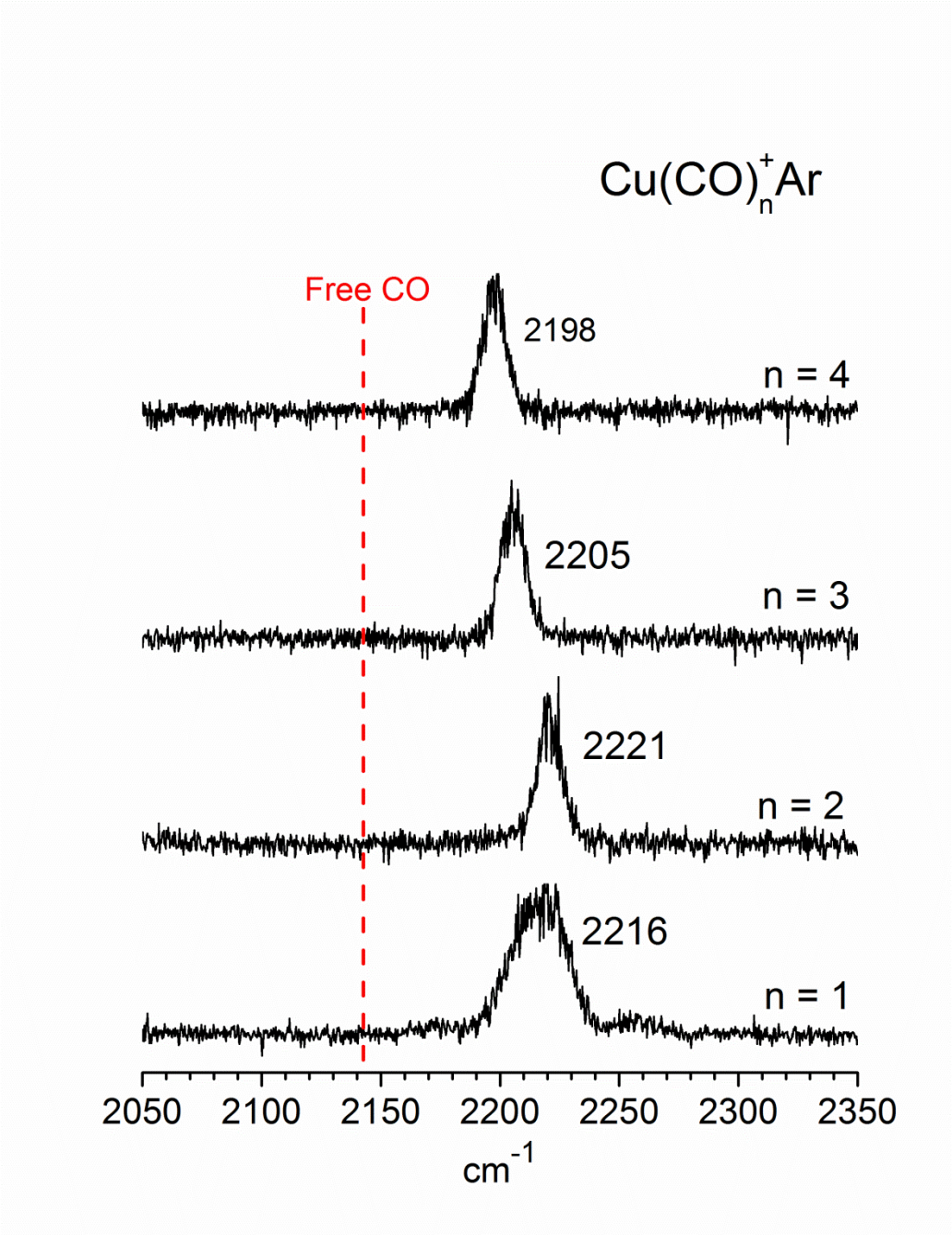

Figure 5.3. The infrared photodissociation spectra of the small $Cu(CO)_n^+Ar$ complexes detected by the elimination of argon. The dashed red line indicates the frequency of gas-phase CO.

examples, the peak positions in the tagged spectra are approximately 5 cm^{-1} higher in energy than the neat complexes. Also, for both sizes, the neat spectra are broader than those obtained with tagging. This is not surprising because fragmentation of the neat ion is likely to result from multi-photon absorption. Conversely, the tagged ions are expected to fragment via a single-photon process, due to the weak argon binding energy. As a result, the tagged spectra are expected to provide the most accurate representation of the results.

Spectra measured for larger complexes n = 4-8, are shown in figure 5.5. These spectra are obtained by monitoring the loss of CO ligands. All spectra show a single band that is blue-shifted by approximately 50 cm^{-1} from the free CO stretch. A second weaker band is observed for complexes larger than n = 4. This band increases in intensity with cluster size and its position remains unchanged at 2162 cm^{-1}. We assign this band as the C−O stretch of the external carbonyl ligands, which are bound to other carbonyls, and not directly to the metal cation. This vibration has been seen previously in other metal carbonyl complexes.[13-19] The single intense peak in the C-O stretching range, along with the weaker external CO band which increases in intensity, supports the conclusion of a tetra-coordinate $Cu(CO)_4^+$, with weakly bound external CO ligands.

In an effort to gain further insight into these spectra, we have performed DFT calculations on $Cu(CO)_n^+$ complexes for n = 1 – 8. We have investigated various isomers and spin states for each complex, and have also included the corresponding argon tagged complexes in an effort to elucidate the effects of tagging on band position, spin state and structure. Figure 5.6 shows selected structures and the most relevant numerical data are presented in Tables 5.1 and 5.2. All the structures calculated to be stable minima are consistent with those calculated

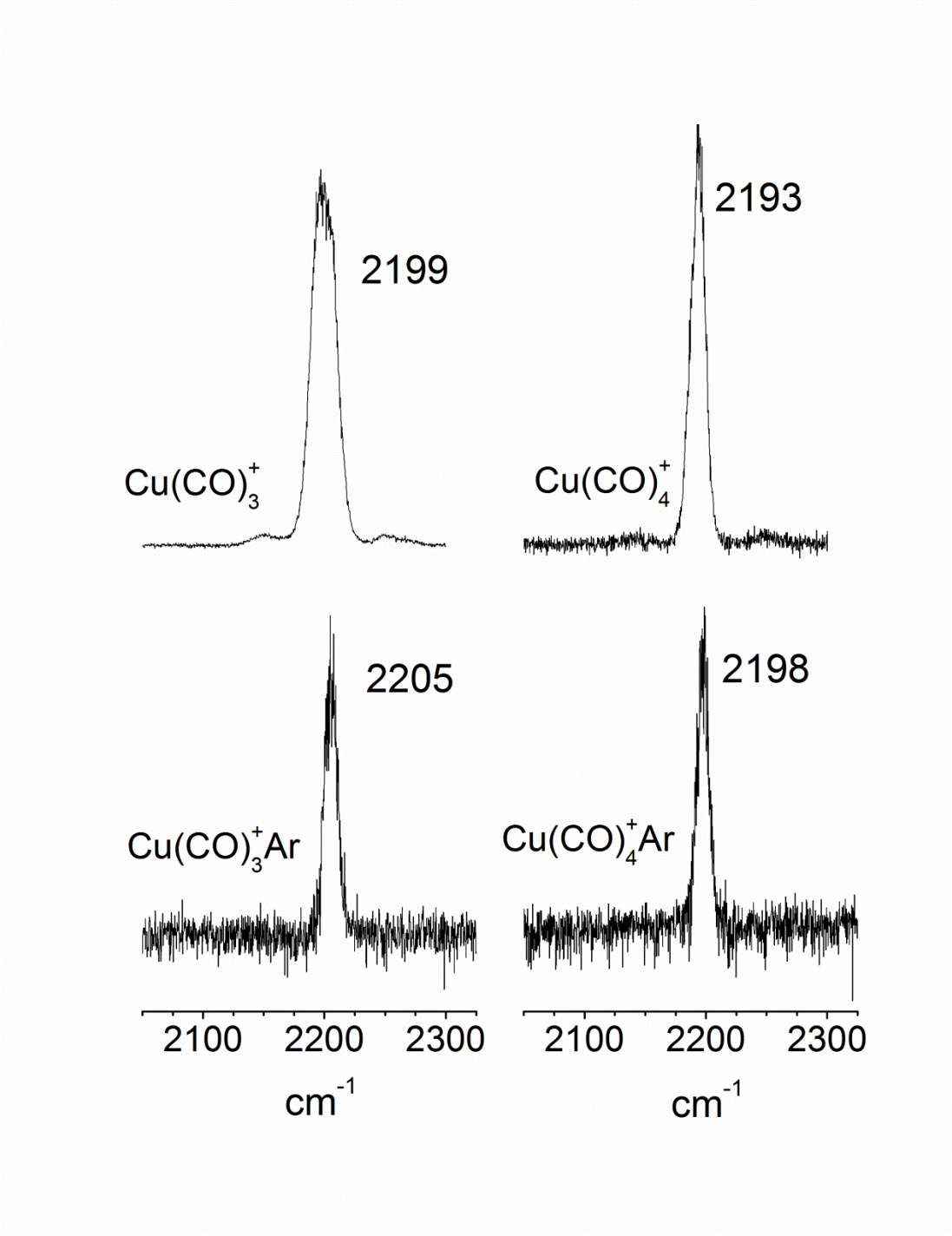

Figure 5.4. The infrared spectra of $Cu(CO)_3^+$ and $Cu(CO)_4^+$ and their corresponding argon tagged analogues.

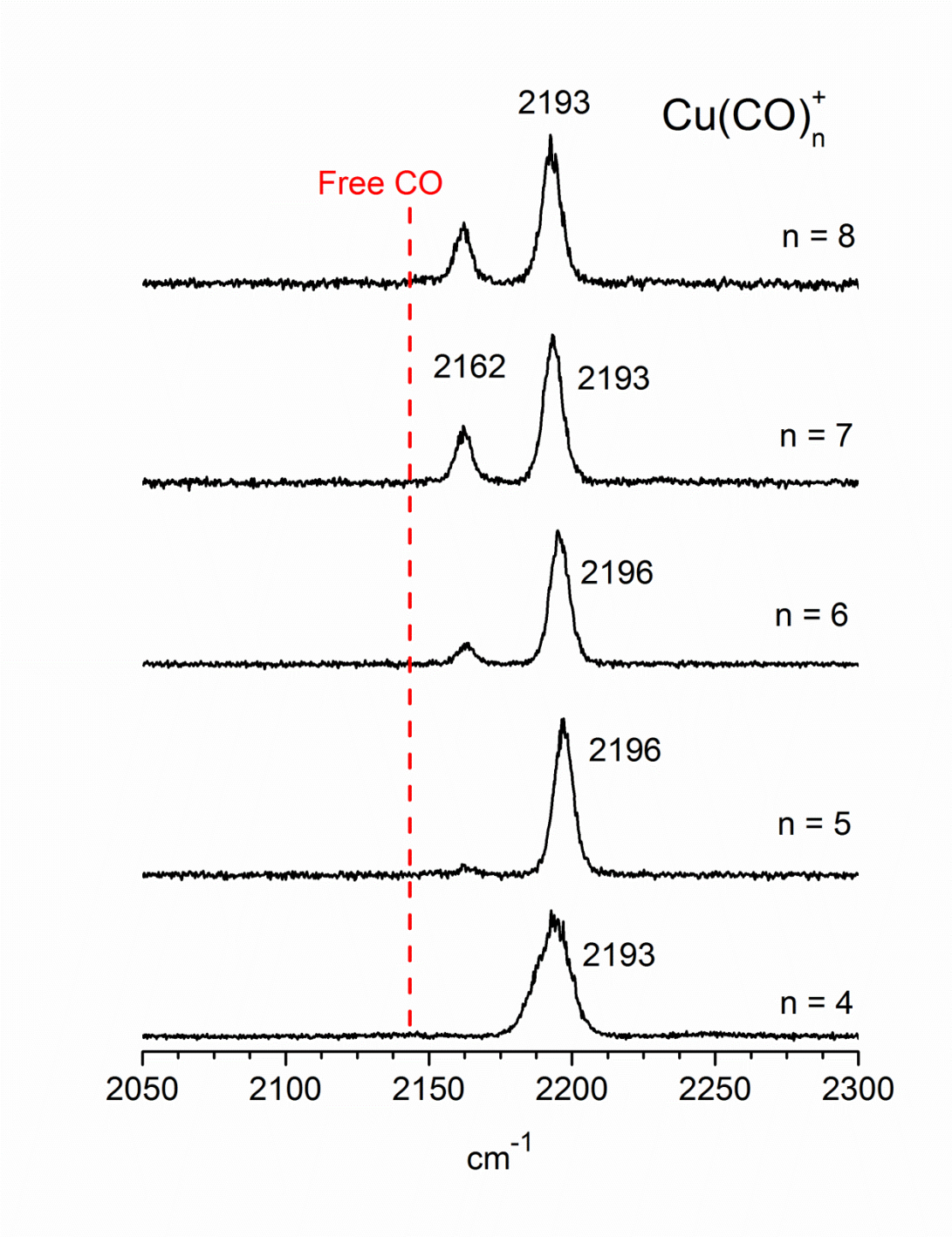

Figure 5.5. The infrared spectra of the $Cu(CO)_n^+$ complexes detected in the loss of CO mass channel.

previously by Andrews and Zhou.[23] The n = 1 species is bent, n = 2 is linear, n = 3 has a D_{3h} structure and the n = 4 complex is tetrahedral. The addition of argon causes a noticeable change in the geometry of the n = 1 and 2 complexes, but not in the other sizes. Tagging causes the n = 1 complex to go from being bent to linear, whereas the n = 2 complex goes from being linear to a slightly bent C_{2v} structure. Perturbation of the geometries of smaller complexes is not surprising due to the relatively high Cu^+-Ar binding energy (3267 cm^{-1}).[37] This binding energy is expected to decrease with increased CO coordination. However, in these small ions, argon binds strongly and essentially occupies a vacant ligand site. These theoretical results can also help to explain the photodissociation efficiency of these complexes. The calculated intensities of the CO stretches are quite high (> 250 km/mol), validating the multiphoton absorption as a possible dissociation pathway for some ions. Also, external or second-sphere CO molecules are calculated to be bound by approximately 1300 cm^{-1}. Although DFT is not expected to handle these van der Waals interactions accurately, the relatively low energies suggest that the bonding is weak enough to facilitate efficient single-photon photodissociation. The argon binding energy in the n = 1 complex is computed to be quite high (16.3 kcal/mol). This is consistent with it occupying a ligand binding site in this complex. However, in all the other complexes, the argon binding is extremely weak ($\leq$ 1 kcal/mol). These results corroborate the efficient argon elimination observed for these ions.

A comparison of the frequencies measured in the present work and previous experiments, to those computed by theory, is presented in Table 5.3. As shown in the table, the level of theory employed yields high symmetry structures which are consistent with the single band spectra measured. All the experimental frequencies are also reasonably reproduced. For the tagged species, theory seems to increasingly overestimate the perturbation caused by argon, resulting in

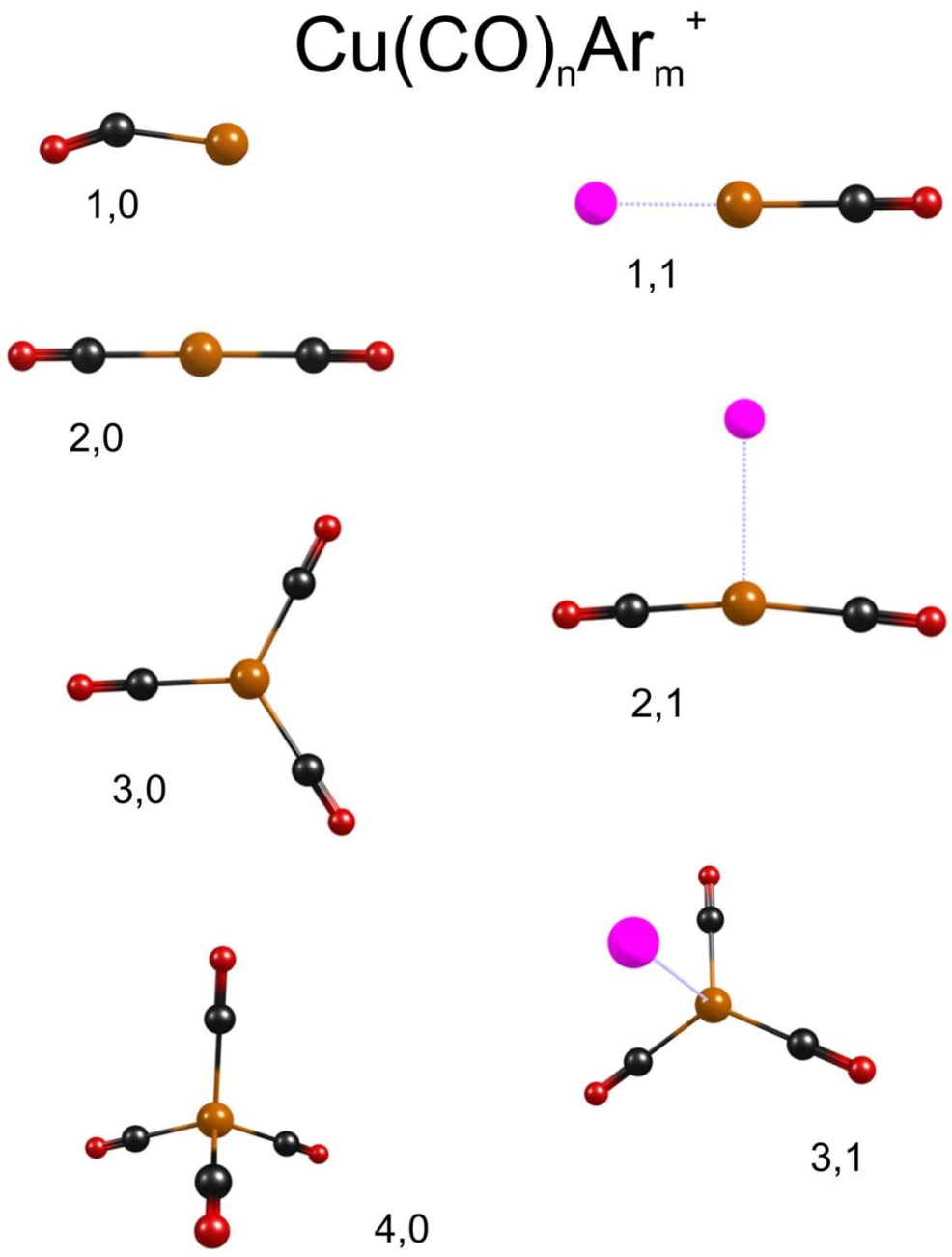

Figure 5.6. The structures for copper cation carbonyls resulting from DFT computational studies.

Table 5.1. Structures, electronic ground states and relative energies for $Cu(CO)_n^+$ complexes computed using DFT.

Complex	Spin State	Symmetry	Relative energy (kcal/mol)
$Cu(CO)^+$	singlet	C_s	0.0
triplet C_s		+80.0	
$Cu(CO)_2^+$	singlet	$D_{\infty h}$	0.0
	triplet	C_{2v}	+106.8
$Cu(CO)_3^+$	singlet	D_{3h}	0.0
	triplet	D_{3h}	+114.5
$Cu(CO)_4^+$	singlet	T_d	0.0
	triplet	D_{4h}	+79.2

Table 5.2. Computed binding energies in kcal/mol for the CO ligands in $Cu(CO)_n^+$ and argon in $Cu(CO)_nAr^+$ complexes.

Complex	$E[Cu(CO)_{n-1}^+-CO]$	$E[Cu(CO)_n^+-Ar]$
$Cu(CO)^+$	38.24	
$Cu(CO)Ar^+$		16.3
$Cu(CO)_2^+$	45.35	
$Cu(CO)_2Ar^+$		1.01
$Cu(CO)_3^+$	21.47	
$Cu(CO)_3Ar^+$		0.97
$Cu(CO)_4^+$	17.01	
$Cu(CO)_4Ar^+$		0.23
$Cu(CO)_5^+$	3.74	
$Cu(CO)_6^+$	3.65	

band positions that are lower than those measured experimentally. This effect is attributed to the inability of DFT to handle weak bonding interactions. This trend does not apply to the argon tagged n = 1 complex, in which the argon is thought to be strongly bound. The experimental frequencies reported by Souma for complexes in acidic media,[20] and by Strauss for salts with counterions present,[21] are noticeably lower than those measured in this experiment and by Andrews via matrix isolation.[23] Also, the acidic media and condensed phase frequencies appear to increase with complex size, whereas those measured in this work and by Andrews decrease from n = 1 – 4. These observations suggest that the condensed phase environment causes some perturbation of the vibrations. The band positions measured for $Cu(CO)_4^+$ and $Cu(CO)_3^+$ are remarkably similar to those measured for the same ions by Andrews and coworkers in a neon matrix (2202 cm^{-1} and 2211 cm^{-1} respectively).[22b] Andrews and coworkers calculated band positions for $Cu(CO)_n^+$ complexes where n = 1 – 4. These values (2208, 2228, 2203, 2167 cm^{-1} for n = 1 – 4 respectively) differ from those calculated in this experiment. This is understandable as they employed a different functional, basis set and scaling factor. Only the spectra corresponding to singlet species are found to be in agreement with our experiment. Computations on the d^9s^1 triplet species were conducted for each cluster. However, the relative intensities and band positions of these spectra do not coincide with the experimental spectra, as shown in Table 5.3. The IR frequencies for some of the triplet state complexes are so strongly red-shifted that they appear at the edge of the range under investigation (1977 and 2079, 2021 and 2043, 2070 cm^{-1} for n = 2, 3 and 4 respectively). Due to the strong frequency shifts predicted for the smaller triplet state complexes and the large energy difference favoring the singlet complexes, we conclude that all the species have singlet spin states. This is expected for the d^{10} ground state configuration.

It is interesting to compare cationic metal-carbonyls to their isoelectronic analogues. Table 5.4 presents the results of experimental and computational work, comparing CO frequencies of neutral and cationic isoelectronic analogues. The $Fe(CO)_5$ and $Co(CO)_5^+$ complexes both have trigonal bipyramidal structures, whereas the $Cr(CO)_6$ and $Mn(CO)_6^+$ complexes both have octahedral structures. As shown in the Table 5.4, the frequencies of the two IR bands for $Fe(CO)_5$ are 2013 and 2034 cm^{-1}, while those of $Co(CO)_5^+$ are 2140 and 2150 cm^{-1}. In the case of $Cr(CO)_6$, the lone IR band occurs at 2003 cm^{-1}, while that of $Mn(CO)_6^+$ occurs at 2115 cm^{-1}. The $Cu(CO)_4^+$ complex has been found to have the same tetrahedral structure and singlet ground state as its isoelectronic neutral $Ni(CO)_4$. However, the vibrational frequencies of these two complexes are quite different. $Cu(CO)_4^+$ has a frequency of 2198 cm^{-1}, which is blue-shifted by over 100 cm^{-1} from that of neutral $Ni(CO)_4$ (2056 cm^{-1}).[24] It is apparent that the red shift of the carbonyl stretching frequency is much greater for the neutral complexes. As discussed earlier, the carbonyl shift results from the combined effects of σ donation, electrostatic polarization, and π back-bonding. σ donation and electrostatic polarization should be stronger for cations, as these cause charge transfer from the CO towards the metal, while π back-bonding should be stronger for neutrals, as it involves transfer of charge in the other direction. The charge on the metal ion center contracts the valence electrons, limiting their back-donation. The significant red shifts for the neutrals indicate that π back-bonding is the most important interaction in these systems. This is consistent with conclusions from other previous systems.[5,17]

The dependence of π back-bonding on charge has been documented previously for the isoelectronic series $Ni(CO)_4$, $Co(CO)_4^-$ and $Fe(CO)_4^{2-}$, in which the CO stretching frequencies are 2056, 1946 and 1799 cm^{-1} respectively.[38-40] In this series, the anions have more charge

Table 5.3. Vibrational frequencies (in cm^{-1}) computed (scaled by 0.971) and measured for singlet and triplet states of $Cu(CO)_n^+$ and $Cu(CO)_n^+Ar$ complexes, along with comparisons to previous experiments. All complexes have a singlet ground state unless otherwise noted. IR intensities (km/mol) are shown in parentheses.

Complex	This exp	Theory	Andrews	Straus	Souma
$Cu(CO)^+$		2241 (132)	2234.4	2178	2160
triplet		2156 (279)			
$Cu(CO)^+Ar$	2216	2225.2 (187)			
triplet		2218 (24)			
$Cu(CO)_2^+$		2218 (405)	2230.4	2164	
triplet		2014 (2458), 2092(1)			
$Cu(CO)_2^+Ar$	2221	2213.8 (416), 2237(4)			
triplet		1977 (2856), 2079(8)			
$Cu(CO)_3^+$	2199	2197 (639)	2211.3	2183	2177
triplet		2093 (3682)			
$Cu(CO)_3^+Ar$	2205	2195 (646), 2217 (2)			
triplet (C_{2v})		2021(1094), 2043(2570)			
$Cu(CO)_4^+$	2193	2186 (838)	2202.1		2185
$Cu(CO)_4^+Ar$	2198	2185 (834)			
triplet		2070 (3969)			

density, hence they have greater π back-bonding, and larger red shifts. This present study enables us to add a cationic species to this isoelectronic series. The CO stretching frequency of the carbonyls in $Cu(CO)_4^+$ was measured to 2198 cm^{-1}. This result fits the trend seamlessly and is consistent with the previous understanding of the importance of π back-bonding on the red shifts of CO frequencies in metal-carbonyls.

The data presented in Table 5.4 also allows for the comparison of computed IR intensities of the CO vibrations for neutrals and cations. As shown in the table, neutral species have significantly more intense vibrations than the cationic analogues. This trend is surprising as the IR oscillator strength of vibrational motion depends on the dipole derivative and is generally enhanced when it involves a charge. For example, the recently measured O-H stretches in cation-water complexes are much stronger than in the free water molecule, and the doubly charged complexes were found to have much stronger transitions than those of the singly charged complexes.[41]

One final interesting point is the behavior of the external CO ligands in these systems. The n = 4 complex is the core ion for this system, and larger clusters are CO-solvated versions of tetrahedral $Cu(CO)_4^+$. A lone band around 2198 cm^{-1} is observed for these larger clusters. In addition to this main band, a less intense feature is observed at 2162 cm^{-1}. This feature, which is blue-shifted by 19 cm^{-1}, is observed for all larger clusters and its intensity increases with increasing cluster size. This behavior is consistent with previous observations for this type of second sphere CO vibration in analogous $Co(CO)_n^+$ and $Mn(CO)_n^+$ complexes.[13,15]
In a computational study by Goldman and Krogh-Jespersen[5], it was shown that CO can be slightly polarized by a nearby charge, resulting in a blue shift of its stretching frequency. Since the external ligands are not interacting with the charged metal center, but instead with the

Table 5.4. Comparison of experimental frequencies and calculated oscillator strengths for the isoelectronic analogues $Mn(CO)_6^+$ and $Cr(CO)_6$, $Co(CO)_5^+$and $Fe(CO)_5$, $Cu(CO)_n^+$ and $Ni(CO)_4$.

Complex	Experimental frequency (cm^{-1})	Oscillator strength (km/mol)
$Mn(CO)_6^+$	2115[a]	1061
$Cr(CO)_6$	2002.9[b]	1861
$Co(CO)_5^+$	2140, 2150[c]	644, 761
$Fe(CO)_5$	2013, 2034[d]	1268, 1456
$Cu(CO)_4^+$	2198	279
$Ni(CO)_4$	2056[e]	986

[a]reference [15].

[b]reference [42].

[c]reference [13].

[d]reference [43,44].

[e]reference [38].

$Cu(CO)_4^+$ core, the induced polarization is less and the increase in vibrational frequency is smaller.

Conclusion

Copper carbonyl cations of the form $Cu(CO)_n^+$ (n=1-8), and their argon-tagged analogues, $Cu(CO)_nAr^+$, were produced and studied with mass-selected infrared photodissociation in the carbonyl stretching region. The geometries and electronic states of these complexes are determined by examining the distinctive patterns provided by the number of infrared-active bands, their frequency positions, and relative intensities, and then comparing them to theoretical predictions. All $Cu(CO)_n^+$ complexes were found to have a d^{10} singlet ground state configuration. $Cu(CO)_4^+$ has a completed coordination sphere, consistent with its expected 18-electron stability. It also has a tetrahedral structure similar to that of its neutral isoelectronic analog $Ni(CO)_4$. The carbonyl stretch in $Ni(CO)_4$ is significantly red-shifted compared to that in $Cu(CO)_4^+$ due to charge induced reduction in π back-bonding. The carbonyl stretch in $Cu(CO)_4^+$ (2197 cm^{-1}) is blue-shifted with respect to the free CO vibration (2143 cm^{-1}), as observed previously in both condensed phase measurements and matrix isolation studies, providing evidence that this species is a non-classical metal carbonyl.

References

(1) Zhou, M.; Andrews, L.; Bauschlicher, C. W. Spectroscopic and Theoretical Investigations of Vibrational Frequencies in Binary Unsaturated Transition-Metal Carbonyl Cations, Neutrals, and Anions. *Chem. Rev.* **2001**, *101*, 1931-1962.

(2) Bauschlicher, C. W. Jr. Transition Metal-Ligand Bonding, II. *J. Chem. Phys*. **1986**. *84,* 260-267.

(3) Barnes, L. A.; Rosi, M.; Bauschlicher, C. W. Jr. Theoretical Studies of the First- and Second-Row Mono- and Di-Carbonyl Positive Ions. *J. Chem. Phys*. **1990**, *93*, 609-624.

(4) Sodupe, M.; Bauschlicher, C. W. Jr.; Lee, T. J. The Calculation of the Vibrational Frequencies of $CuCO^+$, NiCO and $CuCH_3$. *Chem. Phys. Lett*. **1992**, *189*, 266-272.

(5) Goldman, A. S.; Krogh-Jespersen, K. Why Do Cationic Carbon Monoxide Complexes Have High CO Stretching Force Constants and Short CO Bonds? Electrostatic Effects, not σ Bonding. *J. Am. Chem. Soc*. **1996**, *118*, 12159-12166.

(6) Lupinetti, A. J.; Fau, S.; Frenking, G.; Strauss, S. H. Theoretical Analysis of the Bonding between CO and Positively Charged Atoms. *J. Phys. Chem.* **1997**, *101*, 9551-9559.

(7) Lupinetti, A. J.; Frenking, G.; Strauss, S. H. Nonclassical Metal Carbonyls. *Angew. Chem. Int. Ed.* **1998**, *37*, 2113-2116.

(8) Lupinetti, A. J.; Jonas , V.; Thiel, W.; Strauss, S. H.; Frenking, G. Trends in Molecular Geometries and Bond Strengths of the Homoleptic d^{10} Metal Carbonyl Cations: A Theoretical Study. *Chem. Eur. J.* **1999**, *5*, 2573-2583.

(9) Lupinetti, A. J.; Strauss, S. H.; Frenking, G. Non-Classical Metal Carbonyls. *Prog. Inorg. Chem.* **2001**, *49*, 1-112.

(10) Aubke, F.; Wang, C. Carbon Monoxide as a σ-Donor Ligand in Coordination Chemistry. *Coord. Chem. Rev.* **1994**, *137*, 483-524.

(11) Velasquez III, J.; Duncan, M. A. IR Photodissociation Spectroscopy of Gas Phase $Pt^+(CO)_n$ (n=4-6). *Chem. Phys. Lett.* **2008**, *461*, 28-32.

(12) Velasquez III, J.; Njegic, B.; Gordon, M. S.; Duncan, M. A. IR Photodissociation Spectroscopy and Theory of $Au^+(CO)_n$ complexes: Nonclassical Carbonyls in the Gas Phase. *J. Phys. Chem. A* **2008**, *112*, 1907-1913.

(13) Ricks, A. M.; Bakker, J. M.; Douberly, G. E.; Duncan, M. A. Infrared Spectroscopy and Structures of Cobalt Carbonyl Cations. *J. Phys. Chem. A* **2009**, *113*, 4701-4708.

(14) Ricks, A. M.; Reed, Z. D.; Duncan, M. A. Seven-coordinate Homoleptic Metal Carbonyls in the Gas Phase. *J. Am. Chem. Soc*. **2009**, *131*, 9176-9177.

(15) Reed, Z. D.; Duncan, M. A. Infrared Spectroscopy and Structures of Manganese Carbonyl Cations, $Mn(CO)_n^+$ (n=1-9). *J. Am. Soc. Mass Spectrom.* **2010**, *21*, 739-749.

(16) Ricks, A. M.; Gagliardi, L.; Duncan, M. A. Infrared Spectroscopy of Extreme Coordination: The carbonyls of U^+ and UO_2^+. *J. Am. Chem. Soc*. **2010**, *132*, 15905-15907.

(17) Brathwaite, A. D.; Reed, Z. D.; Duncan, M. A. Infrared Photodissociation Spectroscopy of Copper Carbonyl Cations. *J. Phys. Chem. A* **2011**, *115*, 10461-10469.

(18) Ricks, A. M.; Brathwaite, A. D.; Duncan, M. A. Coordination and Spin States in Vanadium Carbonyl Complexes ($V(CO)_n^+$, n = 1–7) Revealed with IR Spectroscopy. *J. Phys Chem. A* **2013**, *117*, 1001-1010.

(19) Brathwaite, A. D.; M. A. Infrared Photodissociation Spectroscopy of Saturated Group IV (Ti, Zr, Hf) metal carbonyl cations. *J. Phys. Chem. A* **2013**, **DOI:** 10.1021/jp400793h.

(20) Souma, Y.; Iyoda, J.; Sano, H. Formation and Properties of Group 1B Metal Carbonyl Cations. *Inorg. Chem.* **1976**, *15*, 968-970.

(21) Rack, J. J.; Webb, J. D.; Strauss, S. H. Polycarbonyl Cations of Cu(I), Ag(I), and Au(I): $[M(CO)_n]$,$^+$. *Inorg. Chem.* **1996**, *35*, 277-278.

(22) Meyer, F.; Chen, Y. M.; Armentrout, P.B. Sequential Bond Energies of $Cu(CO)_x^+$ and $Ag(CO)_x^+$ (x=1-4). *J. Am. Chem. Soc.* **1995**, *117*, 4071-4081.

(23) Zhou, M.; Andrews, L. Infrared Spectra and Density Functional Calculations of $Cu(CO)_n^+$ (n=1-4), $Cu(CO)_n$ (n=1-3), and $Cu(CO)_n^-$ (n=1-3), in Solid Neon. *J. Chem. Phys.* **1999**, *111*, 4548-4557.

(24) Becke, A. D. 3 Term Correlation Functional. *J. Chem. Phys.* **1993**, *98*, 5648-5652.

(25) Lee, C.; Yang, W.; Parr, R. G. Development of the Coll-Salvetti Correlation Energy Formula into a Functional of the Electron Density. *Phys. Rev B.* **1988**, *37*, 785-789.

(26) Frisch, M. J.; Trucks, G. W.; Schlegel, H. B.; Scuseria, G. E.; Robb, M. A.; Cheeseman, J. R.; Montgomery, J. A. Jr.; Vreven, T.; Kudin, K. N.; Burant, J. C.; Millam, J. M.; Iyengar, S. S.; Tomasi, J.; Barone, V.; Mennucci, B.; Cossi, M.; Scalmani, G.; Rega, N.; Petersson, G. A.; Nakatsuji, H.; Hada, M.; Ehara, M.; Toyota, K.; Fukuda, R.; Hasegawa, J.; Ishida, M.; Nakajima, T.; Honda, Y.; Kitao, O.; Nakai, H.; Klene, M.; Li, X.; Knox, J. E.; Hratchian, H. P.; Cross, J. B.; Adamo, C.;Jaramillo, J.; Gomperts, R.; Stratmann, R. E.; Yazyev, O.; Austin, A. J.; Cammi, R.; Pomelli, C.; Ochterski, J. W.; Ayala, P. Y.; Morokuma, K.; Voth, G. A.; Salvador, P.; Dannenberg, J. J.; Zakrzewski, V. G.; Dapprich, S.; Daniels, A. D.; Strain, M. C.; Farkas, O.; Malick, D. K.; Rabuck, A. D.; Raghavachari, K.; Foresman, J. B.; Ortiz, J. V.; Cui, Q.; Baboul, A. G.; Clifford, S.; Cioslowski, J.; Stefanov, B. B.; Liu, G.; Liashenko, A.; Piskorz, P. Komaromi, I.; Martin,

R. L.; Fox, D. J.; Keith, T.; Al-Laham, M. A.; Peng, C. Y.; Nanayakkara, A.; Challacombe, M.; Gill, P. M. W.; Johnson, B.; Chen, W.; Wong, M. W.; Gonzalez, C. and Pople, J. A. Gaussian 03 (Revision B.02), Gaussian, Inc., Pittsburgh PA, 2003.

(27) Wachters, A. J. H. Gaussian Basis Set for Molecular Wavefunctions Containing Third-Row Atoms. *J. Chem. Phys.* **1970**, *52*, 1033-1036.

(28) Dunning, T. H. Gaussian Basis Functions for Use in Molecular Calculations. I. Contraction of (9*s*5*p*) Atomic Basis Sets for the First-Row Atoms. *J. Chem. Phys.* **1970**, *53*, 2823-2833.

(29) Li, Q.; Liu, Y.; Xie, Y.; King, R. B.; Schaefer, H. F. Binuclear Homoleptic Copper Carbonyls $Cu_2(CO)_x$ (x = 1-6): Remarkable Structures Contrasting Metal-Metal Multiple Bonding with Low-Dimensional Copper Bonding Manifolds. *Inorg. Chem.* **2001**, *40*. 5842-5850.

(30) Duncan, M. A. Infrared Spectroscopy to Probe Structure and Dynamics in Metal Ion-Molecule Complexes. *Int. Rev. Phys. Chem.* **2003**, *22*, 407-437.

(31) Okumura, M.; Yeh, L. I.; Myers, J. D.; Lee, Y. T. Infrared Spectra of the Cluster Ions $H_7O_3^+$-H_2 and $H_9O_4^+$-H_2. *J. Chem. Phys.* **1986**, *85*, 2328-2329.

(32) Okumura, M.; Yeh, L. I.; Myers, J. D.; Lee, Y. T. Infrared spectra of the solvated hydronium ion: Vibrational Predissociation Spectroscopy of Mass-Selected $H_3O^+(H_2O)_n(H_2)_m$. *J. Phys. Chem.* **1990**, *94*, 3416-3427.

(33) Yeh, L. I.; Okumura, M.; Myers, J. D.; Price, J. M.; Lee, Y. T. Vibrational Spectroscopy of the Hydrated Hydronium Cluster Ions $H_3O^+(H_2O)_n$ (n=1,2,3). *J. Chem. Phys.* **1989**, *91*, 7319-7330.

(34) Ebata, T.; Fujii, A.; Mikami, N. Vibrational Spectroscopy of Small-Sized Hydrogen-Bonded Clusters, Their Ions. *Intl. Rev. Phys. Chem.* **1998**, *17*, 331-361.

(35) Bieske, E. J.; Dopfer, O. High-resolution Spectroscopy of Cluster Ions. *Chem. Rev.* **2000**, *100*, 3963-3998.

(36) Robertson, W. H.; Johnson, M. A. Molecular Aspects of Halide Hydration: The Cluster Approach. *Ann. Rev. Phys. Chem.* **2003**, *54*, 173-213.

(37) Partridge, H.; Bauschlicher, C. W.; Langhoff, S. R. Theoretical Study of Metal Ions Bound to Helium, Neon and Argon. *J. Phys. Chem.* **1992**, 96, 5350-5355.

(38) Boquet, G.; Birgone, M. Infrared Spectra of $Ni(CO)_4$ in the Gas Phase. *Spectrochim. Acta* **1971**, *27*, 139-149.

(39) Stammerich, H.; Kawai, K.; Tavares, Y.; Krumholz, P.; Behmoiras, J.; Bril, S. Infrared Spectra of $Fe(CO)_4^{2-}$ in Aqueous Solution. *J. Chem. Phys.* **1960**, *32*, 1482-1487.

(40) Edgell, W. F.; Lyford, J. I. Infrared spectra of $Co(CO)_4^-$ in DMF Solution. *J. Chem. Phys.* **1970**, *52*, 4329-4333.

(41) Carnegie, P. D.; Bandyopadhyay, B.; Duncan, M. A. Infrared Spectroscopy of $Cr^+(H_2O)$ and $Cr^{2+}(H_2O)$: The Role of Charge in Cation Hydration. *J. Phys. Chem. A* **2008**, *112*, 6237-6243.

(42) Shufler, S. L.; Sternberg, H. W.; Friedel, R. A. Infrared Spectrum and Structure of Chromium Hexacarbonyl, $Cr(CO)_6$. *J. Am. Chem. Soc*. **1956**, *78*, 2687-2688.

(43) O'Dwyer, M. F. Infrared Spectra and Normal Coordinate Analysis of Iron Pentacarbonyl. *J. Mol. Spectrosc.* **1958**, *2*, 144-151.

(44) Jones, L. H.; McDowell, R. S.; Goldblatt, M.; Swanson, B. I. Potential Constants of Iron Pentacarbonyl from Vibrational Spectra of Isotopic Species. *J. Chem. Phys.* **1972**, *57*, 2050-2064.

CHAPTER 6

INFRARED PHOTODISSOCIATION SPECTROSCOPY OF VANADIUM OXIDE-CARBONYL CATIONS

Introduction

Transition metal oxides have unique structural, electrical and magnetic properties, with widespread applications in catalysis, fuel cells, chemical sensors and magnetic materials.[1-11] In addition, transition metal oxides are ubiquitous throughout surface science, and their interactions with organic and inorganic molecules are the subject of extensive investigation.[12-14] Gas phase experiments provide a perturbation-free environment in which transition metal oxides and their molecular interactions can be studied. Furthermore, these gas phase ions can be size-selected, allowing for the systematic investigation of well-defined complexes. Effective characterization of small transition metal oxides and their interactions with molecules can provide simple models for understanding more complex systems. In this study, we utilize infrared photodissociation spectroscopy to probe both the oxide stretches and carbonyl stretches of vanadium oxide, dioxide and trioxide carbonyl cations.

Carbon monoxide is the most widely studied molecular adsorbate in surface science,[12,13] where it is a sensitive probe of bonding sites for both pure metal and metal oxide surfaces. The C-O stretching vibrations have characteristic frequencies, depending on the type of binding (on-top, bridging, 3-fold).[12,13,15] The interaction of the CO ligand with pure metal atoms is also well characterized in inorganic and organometallic chemistry.[16-19] The bonding in transition metal carbonyl systems can be understood using the Dewar-Chatt-Duncanson complexation model,[16-24]

and a detailed explanation of its application to gas phase metal carbonyls has been previously provided.[20-31] Briefly, in classical metal carbonyl systems, π back-bonding, which involves partially filled metal *d* orbitals donating charge into the antibonding LUMO on CO, is usually the dominant interaction. This results in the observation of C-O stretches that are lower in frequency (i.e., red-shifted) than that of the free CO molecule (fundamental = 2143 cm^{-1}) for these systems.[32] Oxidation of the metal atom is likely to reduce its charge donating ability, as electron density will now be utilized in forming metal-oxygen bonds. As a result of this reduced charge donation, reduced red-shifts, or even blue shifts, are likely to be observed for these metal oxide-carbonyl complexes. It is interesting to investigate the magnitude and direction of the observed shifts in the carbonyl stretching frequency for these $VO(CO)_n^+$, $VO_2(CO)_n^+$ and $VO_3(CO)_n^+$ complexes.

Metal carbonyl ions have been studied extensively in the gas phase. The structure and bonding of these species have also been investigated with theory.[20-30] Both saturated and unsaturated complexes have been produced in cryogenic rare gas matrices and investigated using infrared spectroscopy.[33-39] There is also an increasing body of work on metal carbonyl ions investigated via infrared photodissociation spectroscopy.[40-58] One particularly interesting study was recently conducted by our research group on the coordination number and spectroscopy of carbonyl ligands bound to vanadium.[48,52] Small vanadium oxides and vanadium oxide carbonyls have also been previously investigated. Asmis and coworkers have measured infrared photodissociation spectra for VO^+, VO_2^+ and VO_3^+ using a free electron laser.[59,60] Infrared spectra for the CO_2 insertion products, OVCO and $OVCO^+$, have been measured by Andrews et. al. via matrix isolation.[61] CO molecules coordinated to vanadium oxides are likely to exhibit different vibrational frequencies compared to those coordinated to pure vanadium. The data

collected in this present study provides insight into the effect of oxidation on the CO stretching frequency. In addition, the effects of carbonyl ligand coordination on the vanadium oxide frequencies can be elucidated from this work. Here, we report the first study detailing the direct production of gas phase $VO(CO)_n^+$, $VO_2(CO)_n^+$ and $VO_3(CO)_n^+$ ions and their investigation via infrared spectroscopy in the V-O and C-O stretching regions.

Experimental Section

$VO_m(CO)_n^+$ ions are produced in a molecular beam via the method described in chapter 2. Instead of a pure carbon monoxide expansion, a gas mixture of 5% O_2 in carbon monoxide is used. In support of the experimental studies, DFT calculations were carried out to determine the structure and bonding of these complexes. The calculations were performed using the B3LYP functional[62,63] as implemented in the Gaussian 2003 computational package.[64] The Def2-TZVP basis set[65] was used for vanadium atoms and the DZP basis set[66] was used for carbon and oxygen atoms. In the present work, the computed carbonyl frequencies are scaled by a factor of 0.968, as discussed previously,[52] and given an 8 cm^{-1} FWHM Lorentzian line shape for comparison to the experimental spectra. The computed metal oxide frequencies are adjusted using a scaling factor of 0.9167, derived by Asmis and coworkers for vanadium oxide cations.[59]

Results and Discussion

Laser vaporization of a vanadium rod in an expansion of pure CO predominantly produces complexes of the form $V(CO)_n^+$, as previously described. [48, 52] The $VO(CO)_n^+$ species are present as minor peaks in the $V(CO)_n^+$ mass spectrum, due to residual vanadium oxides on the surface of the rod. In this study, the abundance of the desired metal oxide-carbonyls is

enhanced by seeding oxygen into the carbon monoxide expansion gas. This process generates $VO_m(CO)_n^+$ ions with sufficient ion yield to conduct infrared photodissociation spectroscopy studies, and a mass spectrum is shown in Figure 6.1.

Figure 6.2 shows the infrared induced fragmentation of $VO(CO)_n^+$ ions (n = 5−8). Ideally, the integrated area of the parent ion peak should be equivalent to the sum of the areas of the fragment ion peaks. However, this is not the case due to mass discrimination in our instrument, i.e. we cannot focus on the parent and fragment ions simultaneously. As shown in the bottom trace, $VO(CO)_n^+$ ions smaller than n = 5 do not fragment efficiently. This is evident from the limited parent depletion and fragment production exhibited by the n = 5 ion. The binding energy of CO in $VO(CO)_5^+$ has been calculated to be approximately 13.5 kcal/mol (4721 cm^{-1}). Since this is significantly more than the energy of an infrared photon in the CO stretching region (~2100 cm^{-1}), the fragmentation for this complex is attributed to multiphoton absorption. Efficient fragmentation via loss of carbonyl ligands is observed for cations larger than n = 5. As illustrated in Figure 6.2, these complexes undergo efficient CO ligand elimination terminating at n = 5. This indicates that only the first five carbonyl ligands are strongly bound and the $VO(CO)_5^+$ species is the fully coordinated vanadium monoxide-carbonyl ion. Similar photodissociation mass spectra were measured for $VO_2(CO)_n^+$ and $VO_3(CO)_n^+$ and are presented in Figure 6.3 and 6.4 respectively. All $VO_m(CO)_n^+$ species were observed to have a total coordination number of 6 (m + n = 6), analogous to the fully coordinated $V(CO)_6^+$ ion observed for pure vanadium carbonyls.

To examine the vibrational spectroscopy of these systems, we measure the wavelength dependence of these fragmentation processes. Figure 6.5 compares the carbonyl stretching frequencies of CO ligands coordinated to pure vanadium, with those coordinated to its monoxide

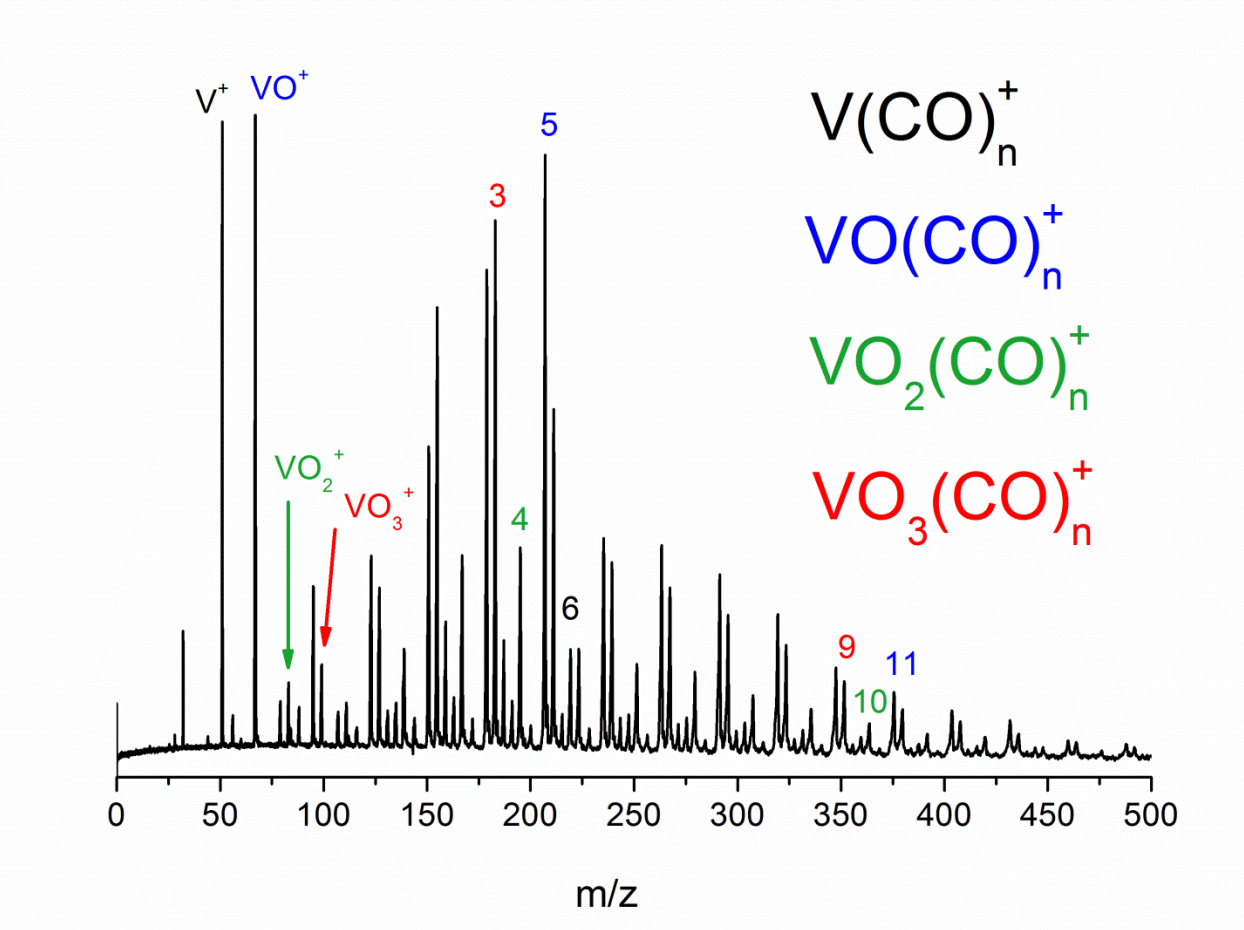

Figure 6.1. Mass spectrum of the vanadium oxide carbonyl complexes produced in our experiment.

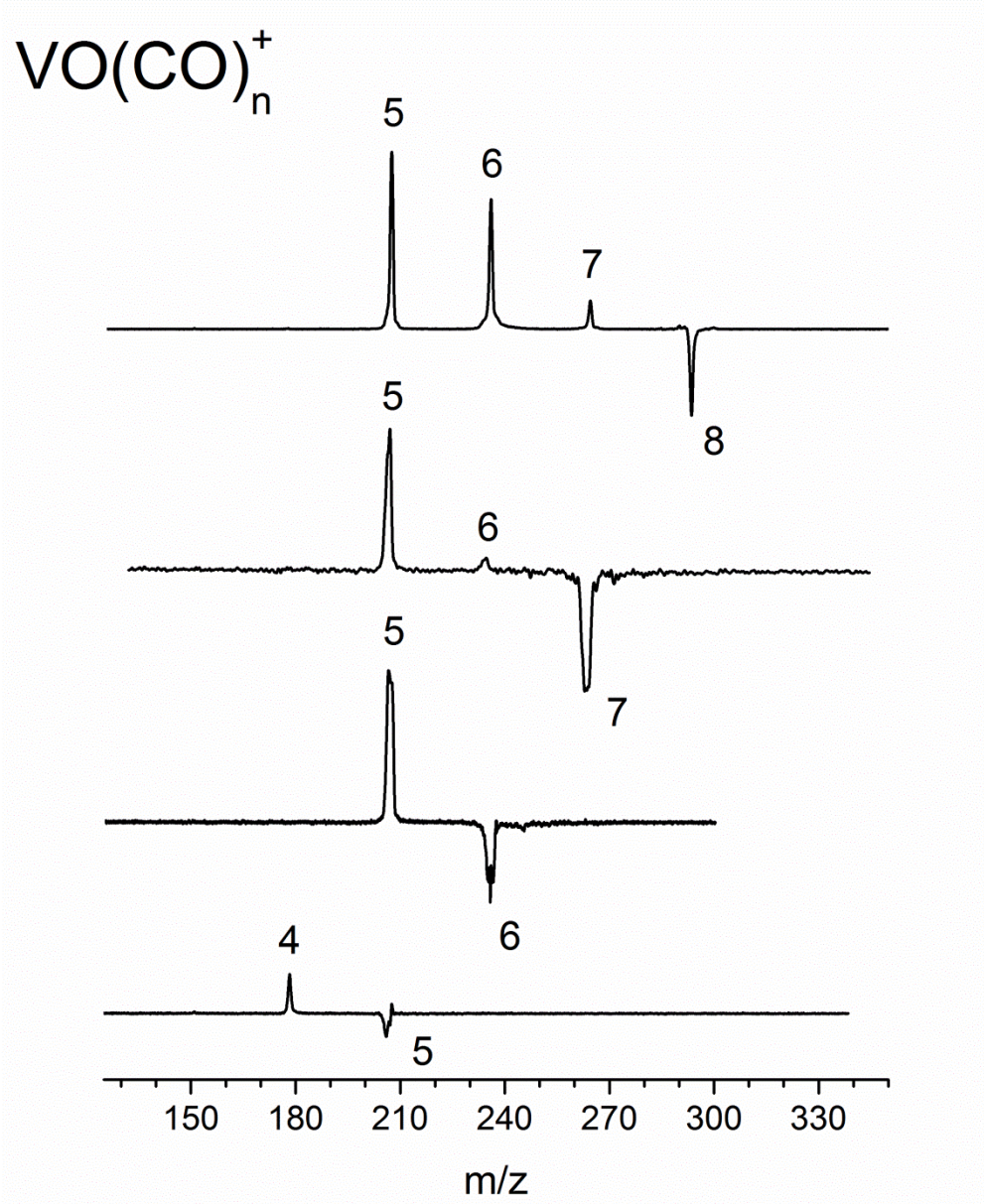

Figure 6.2. Infrared photodissociation breakdown spectra of $VO(CO)_n^+$ (n = 5-8) complexes. These spectra were obtained by subtracting a mass spectrum of a mass selected cluster with the laser off from one with it on.

and trioxide. These photodissociation spectra for $V(CO)_6^+$, $VO(CO)_5^+$ and $VO_3(CO)_3^+$ ions are measured by monitoring the loss of a CO ligand. As previously discussed, the sixth ligand in these systems is relatively strongly bound and fragmentation is likely to proceed via a multiphoton process. This inefficient fragmentation mechanism is responsible for the low signal levels observed in these spectra. The $V(CO)_6^+$ spectrum shown in the top trace has an intense, broad feature at 2103 cm^{-1}, red-shifted from the free CO stretch at 2143 cm^{-1}. This band is produced by CO ligands directly coordinated to the central vanadium ion, forming a D_{3d} structure. The width of this peak is due to the nearly degenerate oscillations of the CO ligands.[48] The spectrum of the $VO(CO)_5^+$ ion is shown in the middle trace. This spectrum consists of an intense band that is unshifted from the molecular CO stretch, along with a minor peak at 2204 cm^{-1}. The bottom trace of this figure shows the spectrum of the $VO_3(CO)_3^+$ complex. A single intense band at 2228 cm^{-1} is observed for this ion.

Figure 6.6 illustrates spectra for the complexes studied in Figure 6.5, but with an additional external CO. The CO ligand eliminated from these ions is weakly bound, and these spectra show a noticeable improvement in the signal levels when compared to the spectra of the core ions. The $V(CO)_7^+$ spectrum shown in the top trace has a broad, intense red-shifted feature at 2103 cm^{-1}, as well as a less intense band at 2166 cm^{-1}. This blue-shifted band is consistent with the presence of a second sphere CO ligand. As discussed previously, electrostatic polarization of the external CO ligand by the core ion leads to an increase in its stretching frequency.[48,52] The width of the main peak in the $V(CO)_7^+$ spectrum is likely due to multiple isomeric structures with external CO ligands in different positions around the core D_{3d} ion. These isomers are close in energy and have slightly different spectra. The $VO(CO)_6^+$ spectrum in the middle trace, like that of $VO(CO)_5^+$ has an intense band at 2143 cm^{-1}. In addition, two

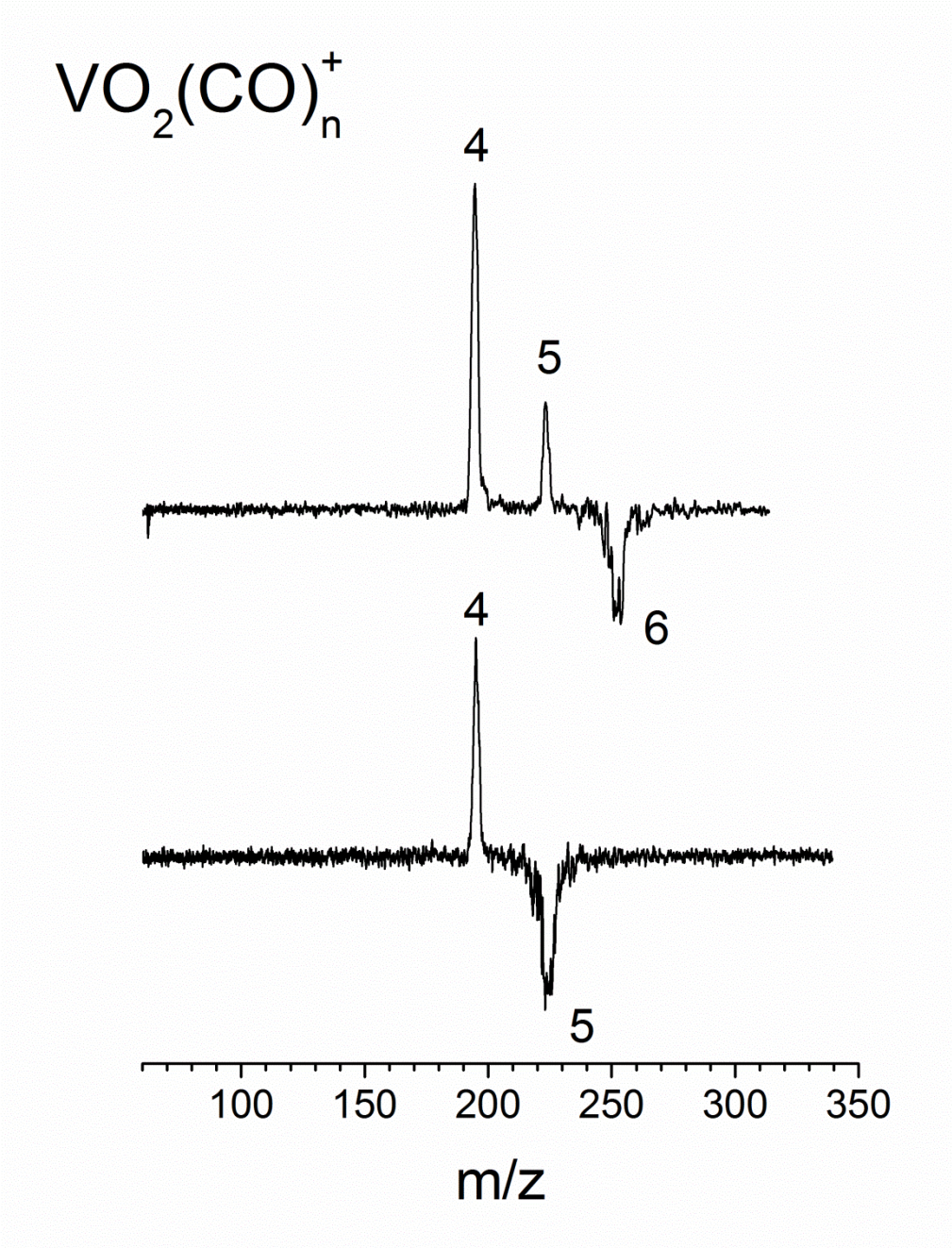

Figure 6.3. Photodissociation mass spectrum of $VO_2(CO)_n^+$.

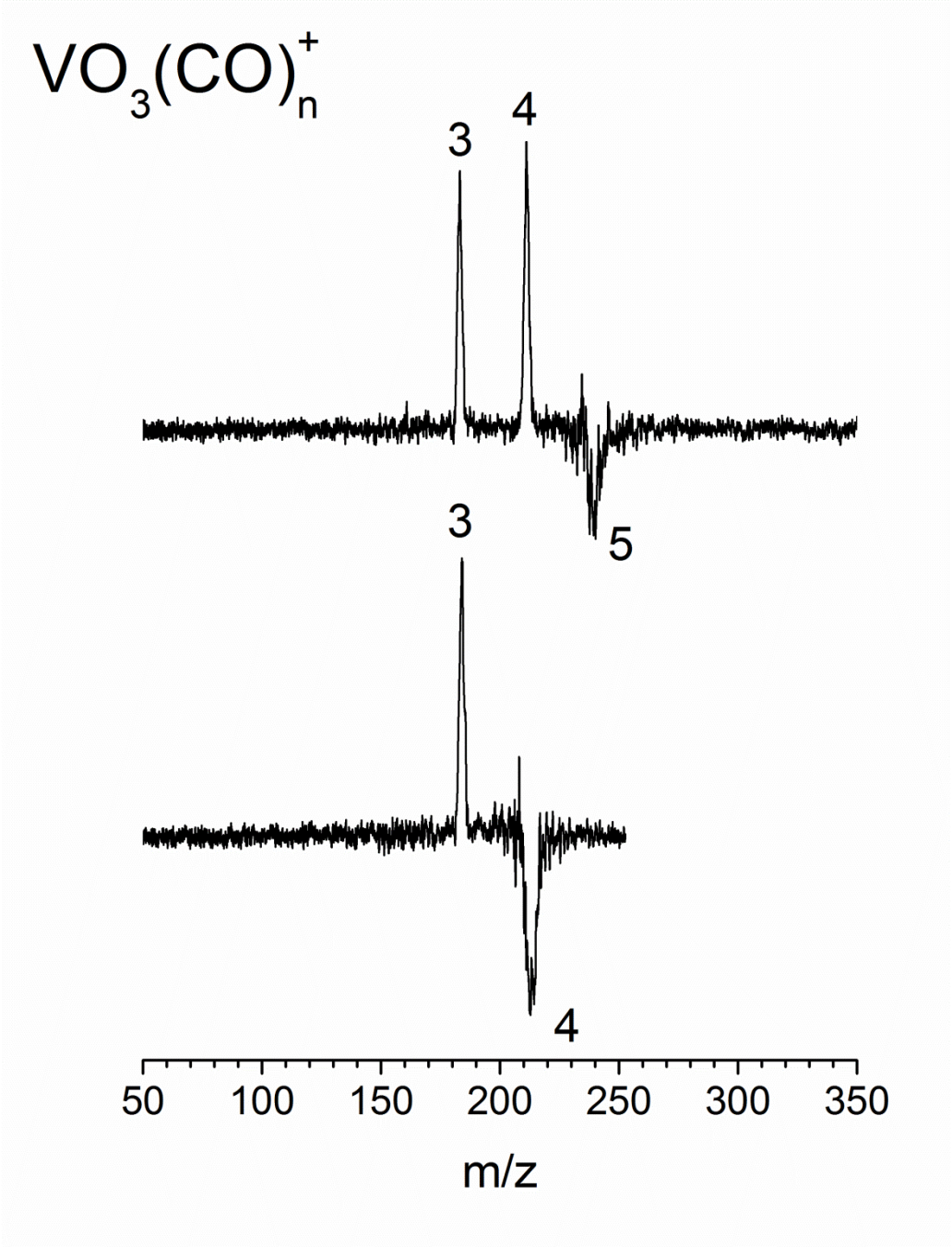

Figure 6.4. Photodissociation mass spectrum of $VO_3(CO)_n^+$.

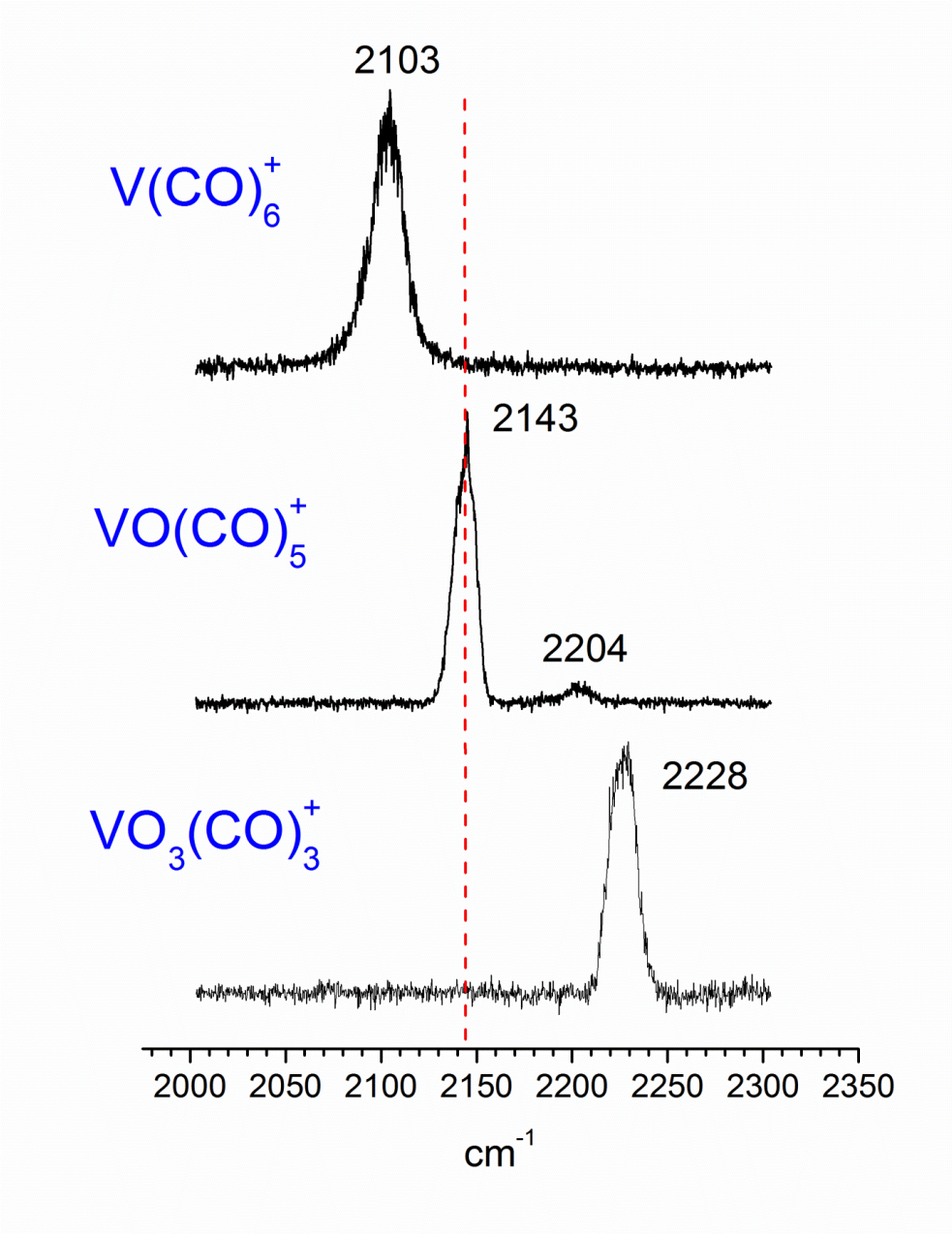

Figure 6.5. Infrared photodissociation spectra of the $V(CO)_6^+$, $VO(CO)_5^+$ and $VO_3(CO)_3^+$ ions in the carbonyl stretching region.

minor blue-shifted features are observed. The peak at 2169 cm^{-1} is assigned to the second-sphere CO ligand. The bottom trace of this figure shows the spectrum of $VO_3(CO)_4^+$. Two blue-shifted peaks are observed for this ion: an intense band at 2232 cm^{-1} and a weaker one at 2175 cm^{-1}. These are representative of core and second-sphere carbonyl ligands respectively.

Infrared spectra (black traces) in the 600 – 1200 cm^{-1} range are presented in Figure 6.7 for the $VO(CO)_6^+$, $VO_2(CO)_5^+$ and $VO_3(CO)_4^+$ complexes. All these were measured via the elimination of a weakly-bound, second-sphere CO ligand. Again, the low binding energies of these ligands facilitated the collection of spectra with good signal levels. Asmis and coworkers have investigated these oxide ions via helium tagging using a free electron laser.[59] Simulations of their results are shown in the red traces. A single band at 1000 cm^{-1} is observed in the low-frequency region for the $VO(CO)_6^+$ species. This band has a FWHM of approximately 8 cm^{-1} and is attributed to the V-O stretch. The spectrum of the bare metal oxide cation also has a single peak, however, its position is 1053 cm^{-1}. Two bands are observed in the low frequency region of the spectrum for the $VO_2(CO)_5^+$ ion. These bands at 944 cm^{-1} and 971 cm^{-1} are likely due to the asymmetric and symmetric O-V-O stretches. The results of DFT calculations aid in the assignment of these modes. The intensities and splitting between the bands observed in the bare oxide spectrum are well replicated by our data. However, yet again, the frequencies are red-shifted compared to the bare oxide (by 46 cm^{-1}). The $VO_3(CO)_4^+$ complex yields a spectrum with two main peaks at 991 and 1084 cm^{-1}, and a minor one at 1045 cm^{-1}, whereas the data obtained using the free electron laser for infrared experiments (FELIX) only shows two bands at 1037 cm^{-1} and 1069 cm^{-1}. It is possible that the low intensity spectral feature observed in our data was also present in the Asmis experiment. However, due to the inherently broad linewidths (~ 30 cm^{-1}) of the main bands in their spectra, it might have gone undetected.

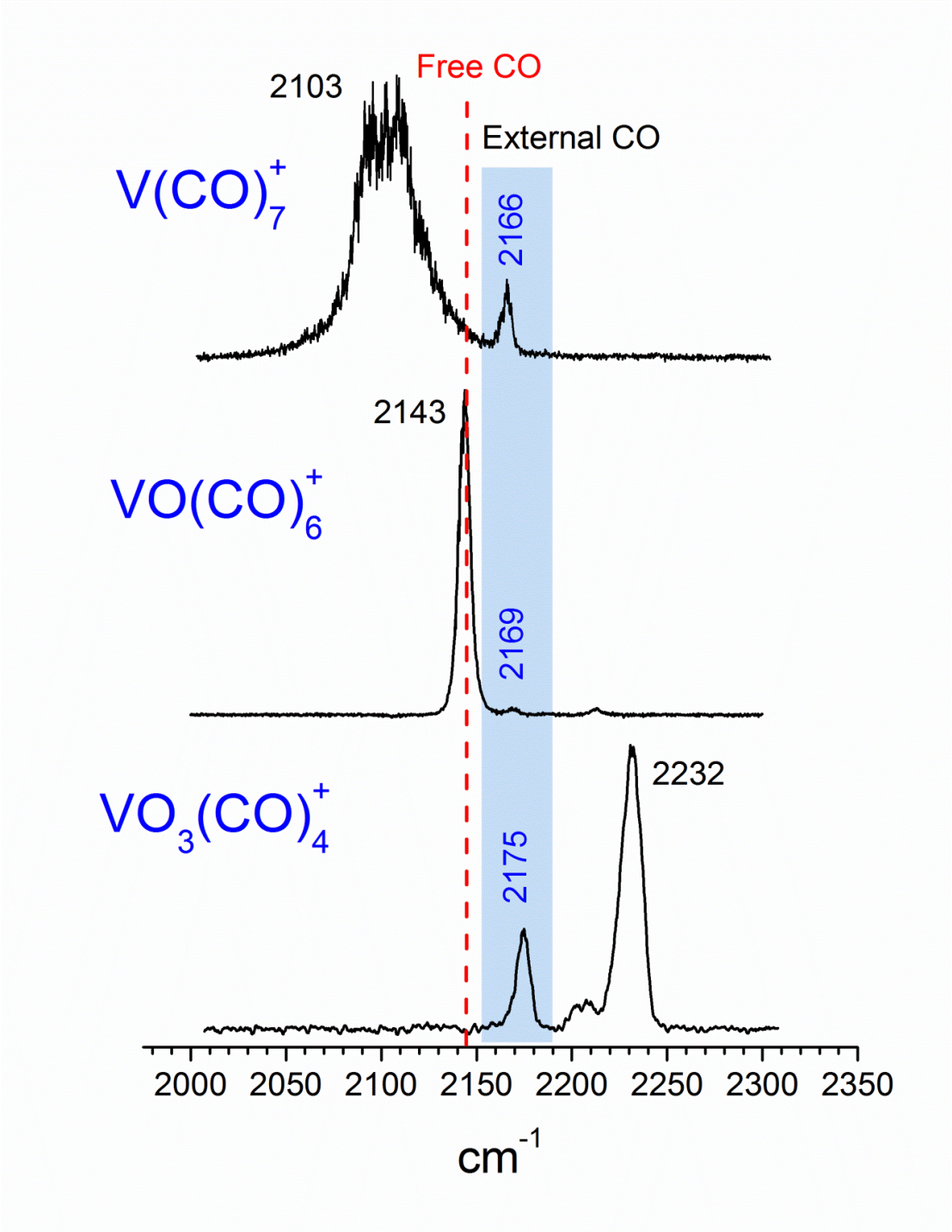

Figure 6.6. Infrared photodissociation spectra of the $V(CO)_7^+$, $VO(CO)_6^+$ and $VO_3(CO)_4^+$ ions in the carbonyl stretching region.

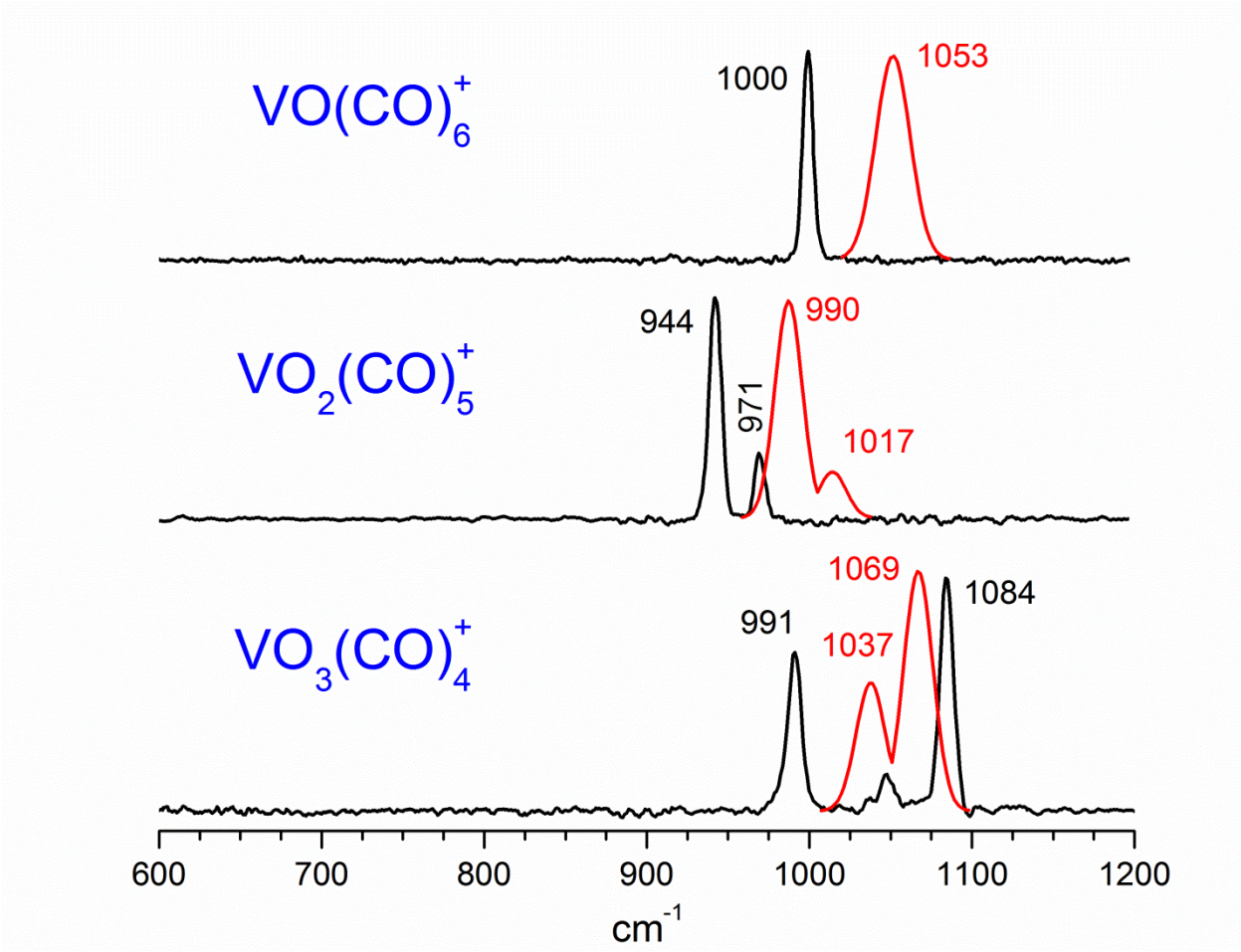

Figure 6.7. Low-frequency infrared photodissociation spectra of $VO(CO)_6^+$, $VO_2(CO)_5^+$ and $VO_3(CO)_4^+$ compared to simulated spectra (red) for VO^+, VO_2^+ and VO_3^+ ions using frequencies reported by Asmis and coworkers.

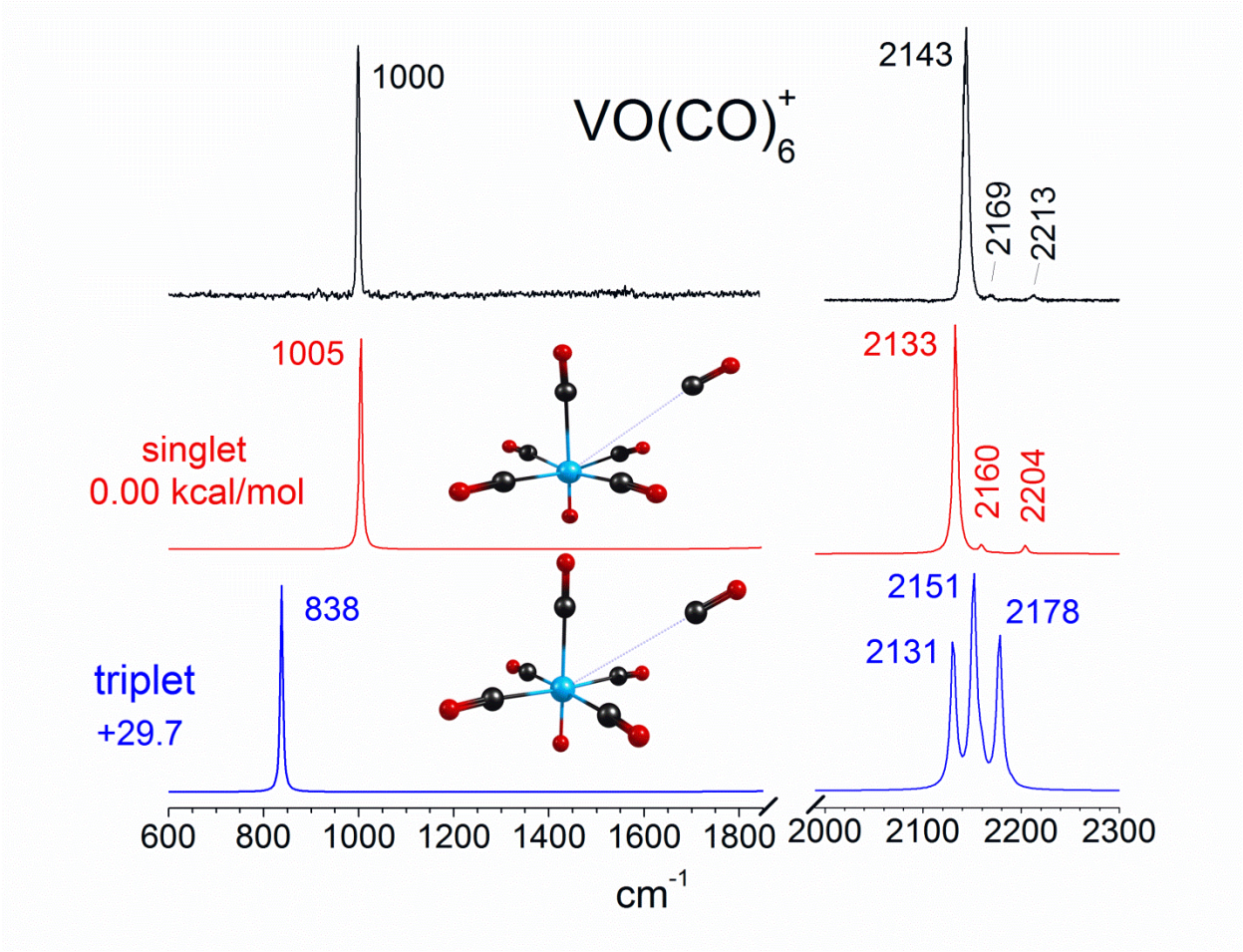

Figure 6.8. Infrared spectrum of $VO(CO)_6^+$ compared to the spectra predicted by DFT theory.

Figure 6.8 shows the experimental spectrum of the $VO(CO)_6^+$ complex along with that predicted by theory for this complex in two different spin states. In the carbonyl stretching region (2000−2300 cm^{-1}), the experimental spectrum contains a single intense band along with two barely noticeable features. The singlet structure is predicted to be lower in energy than the triplet by 29.7 kcal/mol. Despite the ions having seemingly indistinguishable structures, the predicted spectra for ions with a singlet and triplet spin states are conspicuously dissimilar. In the CO stretching region the singlet spectrum reproduces the experiment almost perfectly, whereas the triad of intense peaks in the triplet spectrum does not match the experiment. Both experiment and theory yield low frequency spectra with a single intense band. Again, the predicted singlet spectrum matches well with the experiment; conversely, the triplet has a band that is lower in frequency. Because the singlet is predicted to lie lowest in energy and because of the correspondence in the relative intensities and frequency positions with the predicted spectrum, we assign the observed spectrum of the $VO(CO)_6^+$ species to the singlet ground state.

The spectrum of the $VO_2(CO)_5^+$ ion measured via CO elimination is shown in Figure 6.9. This has three peaks in the carbonyl stretching region and two barely resolved peaks in the low frequency region. DFT calculations predict a singlet ground state for this complex, with a triplet state lying 33.9 kcal/mol higher in energy. Indeed, the predicted singlet spectrum demonstrates outstanding agreement with the experiment. The number of infrared bands and their relative intensities in the predicted triplet spectrum are not consistent with the experiment. We therefore assign the experimental spectrum to be the singlet ground state. DFT calculations on the singlet structure indicate that the more intense feature in the low frequency region corresponds to the asymmetric O-V-O stretch, whereas the band with lesser intensity corresponds to the symmetric stretch.

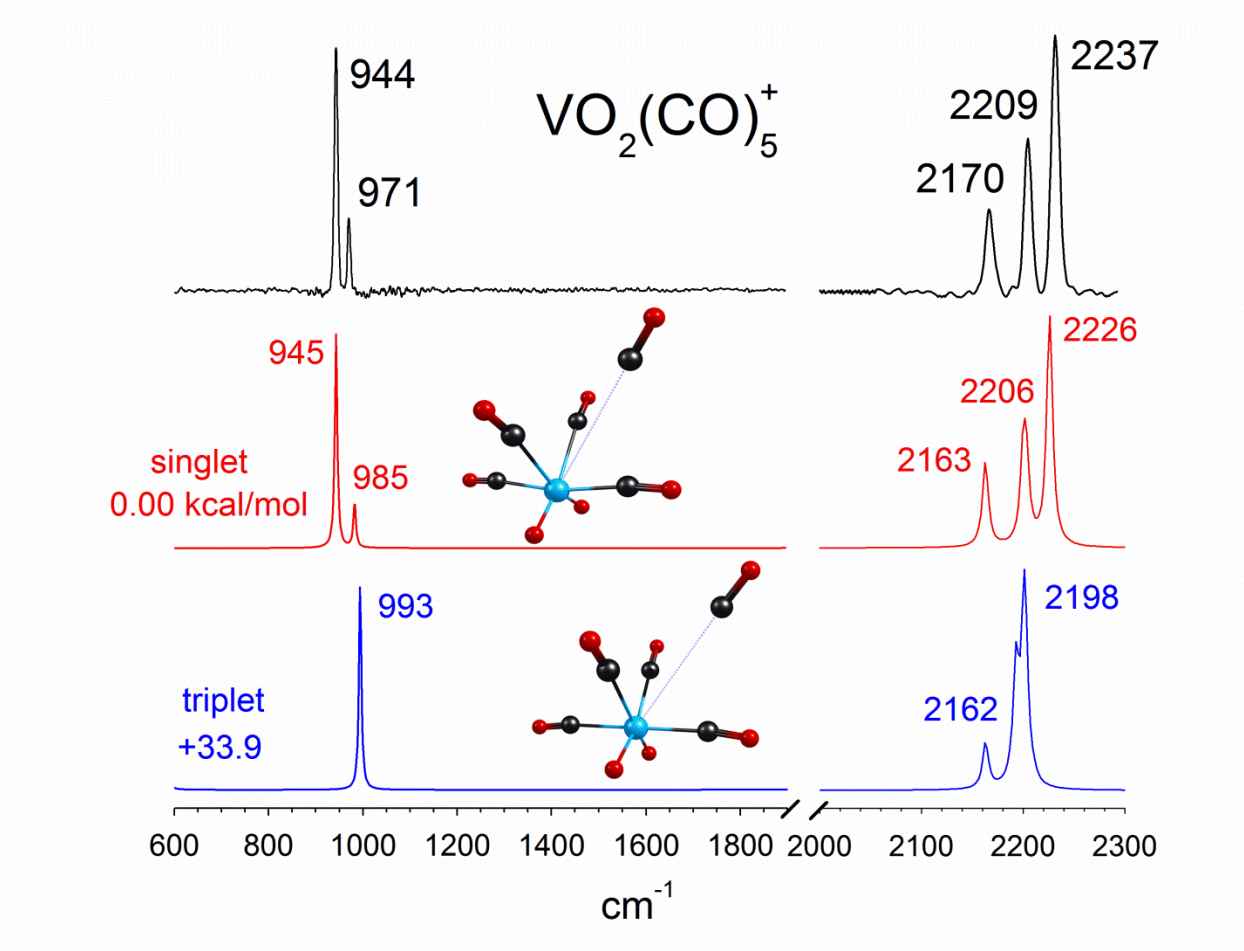

Figure 6.9. Infrared spectrum of $VO_2(CO)_5^+$ compared to the spectra predicted by DFT theory.

Figure 6.10 shows the experimental spectrum for the $VO_3(CO)_4^+$ ion, as well as those predicted for the lowest energy singlet and triplet states. The experiment has two intense bands in the CO stretching region, with the more intense of these having a noticeable shoulder on the low frequency side. Coincidentally, this same pattern is repeated in the metal oxide stretch region. DFT calculations on these complexes produce a lowest energy singlet structure that differs in energy from the triplet by 5.3 kcal/mol. The singlet structure is not a symmetric trioxide, but instead has both a V=O (vanadyl) and V–O_2 (superoxide) mode. Unfortunately, none of the theoretical spectra agree with the experiment in the oxide stretching region. Asmis and coworkers left the spectrum of VO_3^+ unassigned due to a disagreement in the intensity ordering of their experimental and theoretical results. We observed a similar discrepancy in our experiment/theory comparison. It is apparent that DFT does not reliably predict the vanadyl and superoxide modes of the VO_3^+ species. However, we have the carbonyl stretching region as another basis for comparison to theory. The relative intensity and splitting of the two main bands observed experimentally in the CO stretching region are consistent with the pattern predicted for the triplet structure. As a result, we assign our experimental spectrum as being representative of a complex having a triplet spin state. The minor features observed in both the oxide and carbonyl stretching regions, in conjunction with the similarity in calculated relative energies for the singlet and triplet structures, lead us to conclude that we also have a small amount of the singlet species present in the ions sampled.

The magnitude and direction of the CO frequency shifts measured for the vanadium oxide ions in this experiment are noticeably different from those of pure vanadium carbonyls. While pure metal complexes have slightly red-shifted bands, oxides have either no shift or blue shifts. This observation indicates that oxidation of the metal atom does indeed have an effect on

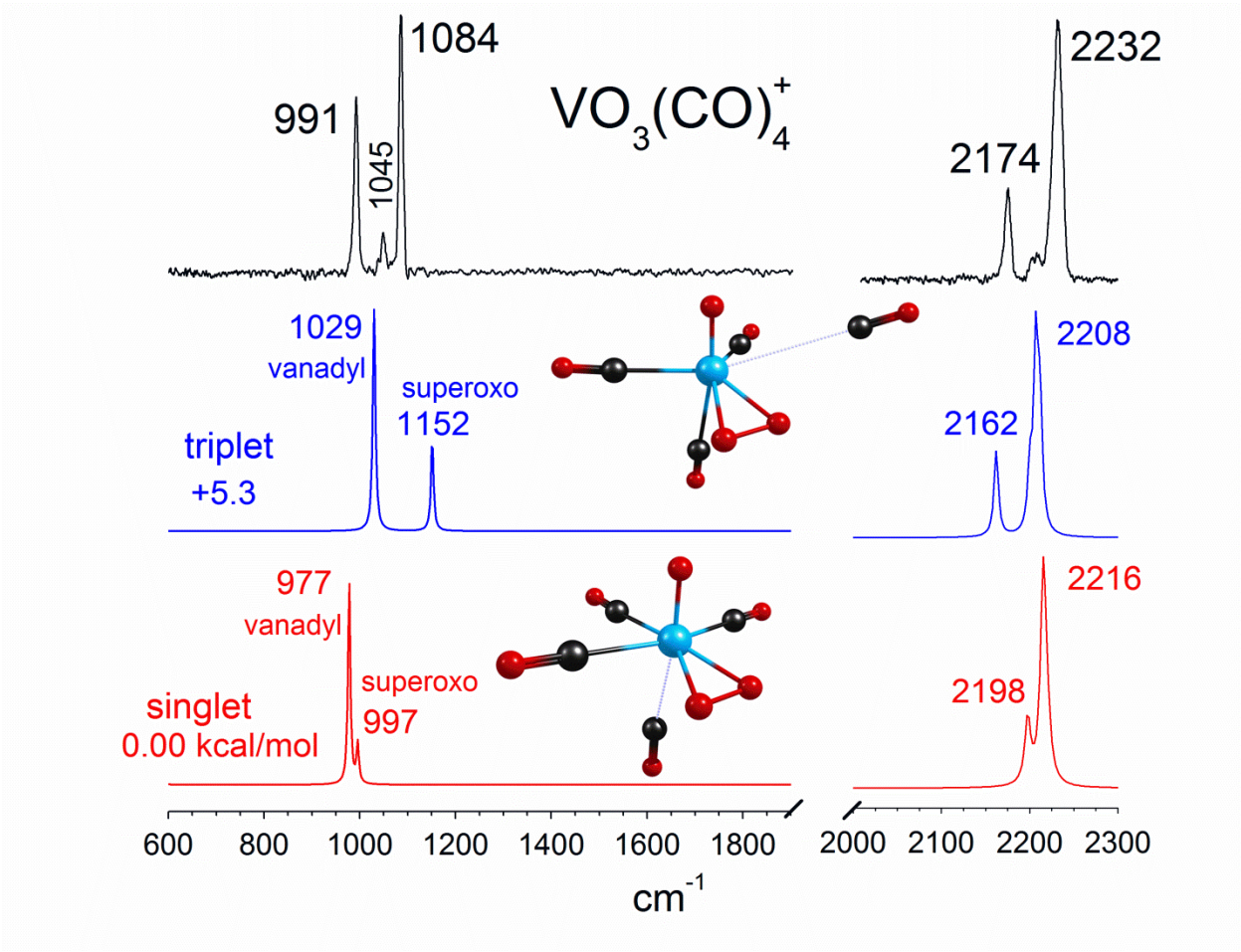

Figure 6.10. Infrared spectrum of $VO_3(CO)_4^+$ compared to the spectra predicted by DFT theory.

carbonyl bonding. In pure metal carbonyls, π back-bonding is the most dominant interaction, and red-shifted CO frequencies are customary for these systems. However, in oxide carbonyl complexes, the *d* electrons on the metal atom are utilized in forming strong metal oxide bonds, and their availability for back-donation is reduced.[26] This is shown by the monoxide-carbonyl cation, in which the main CO stretching band is observed to coincide with the free molecular CO stretch at 2143 cm^{-1}. Further oxidation leads to a significant blue shift in the observed CO stretching frequencies. Since π back-bonding is reduced in these systems, σ donation and electrostatic polarization, both of which induce blue shifts, dominate the bonding. This effect has also been observed for $UO_2(CO)_n^+$, relative to $U(CO)_n^+$.[67] A similar effect has been observed in the carbonyl complexes of late transition metals (gold, copper).[46,51] Filled *d* orbitals in these systems limit the availability of electron density for π back-bonding, resulting in blue-shifted carbonyl frequencies. Blue-shifted frequencies for carbonyl ligands bound to metal oxides are well known in surface science.[12-14] It is therefore not surprising that subsequent oxidation leads to significant blue shifts in the frequencies of the dioxide and trioxide species.

To ascertain the effect of carbonyl ligand bonding on metal oxide frequencies, we compare our results to those of Asmis and coworkers who measured infrared spectra for bare vanadium oxide cations. This comparison is shown in Figure 6.7. The number of bands and the relative peak intensities are comparable for both sets of data for the monoxide and dioxide species. However, our spectra are noticeably red-shifted (53 and 46 cm^{-1} for the monoxide and dioxide respectively). In an effort to explain this, we examine orbital occupation in the metal oxides. It is well known that the bonding in simple metal oxides is complicated due to the $3d-3d$ exchange energy being greater than the orbital separations.[68] Because of this, it can be more energetically favorable to add electron density to a π* orbital than to a nonbonding orbital. If

CO ligands donate electron density into such an orbital, the V−O bond order will be lowered, its length should increase, and its stretching frequency should be reduced. Indeed, this is observed for the monoxide and dioxide species. A similar reduction in the frequency of the M−O vibration upon carbonyl binding has been previously observed for uranium oxide carbonyl ions.[67] We have not ignored the possible effect of the metal spin state on these oxide frequencies. As stated above, the VO^+ species was found to have a triplet ground state by Asmis and coworkers, whereas our $VO(CO)_6^+$ complex has a singlet ground state. As illustrated in Figure 6.11, the frequency of the triplet state in VO^+ is lower than the singlet. Therefore, it is likely that the red shift resulting from carbonyl bonding is even more significant. The dioxide and trioxide species reported by Asmis and those presented here have the same ground spin state.

Conclusion

$VO_m(CO)_n^+$ (m=0-3 and n=3-6) complexes are produced in a molecular beam via laser vaporization in a pulsed nozzle source. The ions were mass-selected and studied using infrared photodissociation spectroscopy in both the carbonyl and oxide stretching regions. DFT calculations were conducted to facilitate the interpretation of the experimental spectra. Insight into the structure and bonding of these complexes is obtained from the number of infrared active bands, their relative intensities, and their frequency positions. The effect of oxidation on the carbonyl stretching frequencies of $VO(CO)_n^+$, $VO_2(CO)_n^+$ and $VO_3(CO)_n^+$ complexes is investigated. All oxide-carbonyl species are observed to have C-O vibrations that are blue-shifted from those of pure vanadium carbonyl cations due to a reduction in the availability of *d* electron density for π back-bonding. The metal-oxygen modes of these complexes are also investigated and the effects of CO coordination on the V-O and O-V-O stretches are revealed.

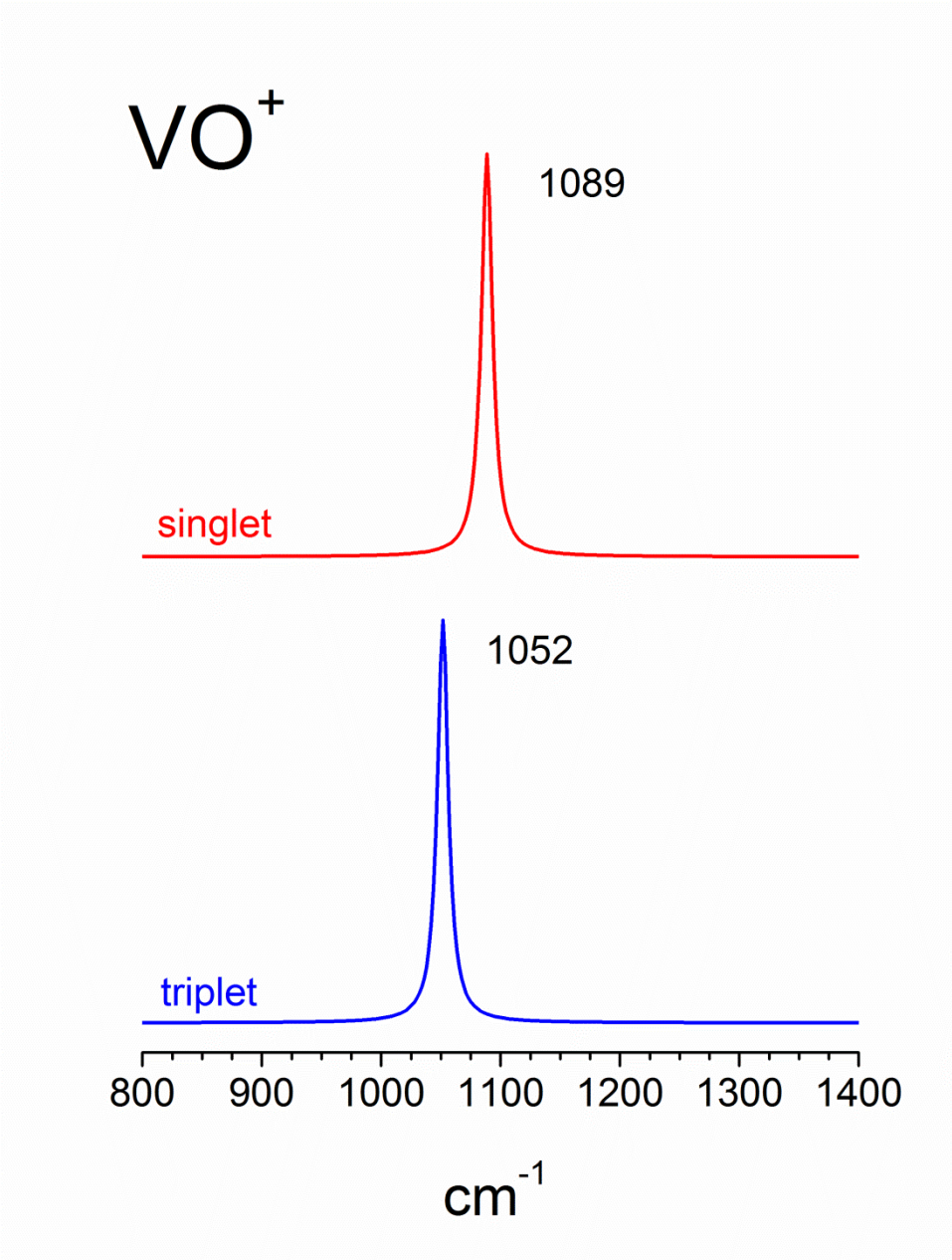

Figure 6.11. Theoretical spectra for VO^+ calculated using B3LYP/TZVP. Frequencies are scaled by 0.9167.

CO coordination causes these modes to red-shift due to the introduction of electron density into antibonding modes. The metal oxide-carbonyl complexes investigated all have a hexa-coordinate core, analogous to that of pure vanadium carbonyl. The fully coordinated vanadium monoxide-carbonyl species is of the form $VO(CO)_5^+$, while those of the dioxide and trioxide are $VO_2(CO)_4^+$ and $VO_3(CO)_3^+$ respectively.

References

(1) Cox, P. A. *Transition Metal Oxides*; Clarendon: Oxford, U.K., 1992.

(2) Rao, C. N.; Raveau, B. *Transition Metal Oxides*; Wiley: New York, 1998.

(3) Campbell, C. T. Ultrathin Metal films and Particles on Oxide Surfaces: Structural, Electronic and Chemisorptive Properties. *Surf. Sci. Rep.* **1997**, *27*, 1-111.

(4) Aiken, J. D.; Finke, R. G. A Review of Modern Transition-Metal Nanoclusters: Their Synthesis, Characterization, and Applications in Catalysis. *J. Mol. Catal. A: Chem.* **1999**, *145*, 1-44.

(5) Kodama, R. H. Magnetic Nanoparticles. *J. Magn. Magn. Matter.* **1999**, *200*, 359-372.

(6) Hill, C. L. Introduction: Polyoxametalates – Multicomponent Molecular Vehicles to Probe Fundamental Issues and Practical Problems. *Chem Rev* **1988**, *98*, 1-2.

(7) Hill, C. L. Progress and Challenges in Polyoxometalate-Based Catalysis and Catalytic Materials Chemistry. *J. Mol. Catal. A: Chem.* **2007**, *262*, 2-6.

(8) Luo, X. L.; Morrin, A.; Killard, A. J.; Smyth, M. R. Application of Nanoparticles in Electrochemical Sensors and Biosensors. *Eletroanalysis* **2006**, *18*, 319-326.

(9) Franke, M. E.; Koplin, T. J.; Simon, U. Metal and Metal Oxide Nanoparticles in Chemiresistors: Does the Nanoscale Matter? *Small* **2006**, *2*, 36-50.

(10) Dorcioman, G.; Ebrasu, D.; Enculescu, I.; Serban, N.; Axente, E.; Sima, F.; Ristoscu, C.; Mihailescu, I. N. Metal Oxide Nanoparticles Synthesized by Pulsed Laser Ablation for Proton Exchange Membrane Fuel Cells. *J Power Sources* **2010**, *195*, 7776-7780.

(11) Joshi, U.; Palasyuk, A.; Arney, D.; Maggard, P. A. Semiconducting Oxides to Facilitate the Conversion of Solar Energy to Chemical Fuels. *J. Phys. Chem. Lett.* **2010**, *1*, 2719-2726.

(12) Somorjai, G. A. *Introduction to Surface Chemistry and Catalysis*, John Wiley and Sons, Inc.: New York, 1994.

(13) Yates, J. T., Jr.; Madey, T. E. *Vibrational Spectroscopy of Molecules at Surfaces*; Plenum: New York, 1987

(14) Eischens, R. P. Infrared Spectroscopy and Catalysis Research. *Science* **1964**, *146*, 486-493.

(15) Ohtani, H.; Van Hove, M. A.; Sormaji, G. A. Leed Intensity Analysis of the Surface Structures of Pd(111) and of CO Adsorbed on Pd(111) in a ($\sqrt{3} \times \sqrt{3}$) R30° Arrangement. *Surf. Sci*. **1987**, *187*, 372-386

(16) Cotton, F. A. *Advanced Inorganic Chemistry*, 6th ed.; John Wiley and Sons, Inc.: New York, 1999.

(17) Huheey, J. E.; Keiter, E. A.; Keiter, R. L. *Inorganic Chemistry Principles of Structure and Reactivity*, Harper Collins: New York, 1993.

(18) Heck, R. F. *Organotransition Metal Chemistry*, Academic Press: New York, 1974.

(19) Nakamoto, K. *Infrared and Raman Spectra of Inorganic and Coordination Compounds*; John Wiley: New York, 1997.

(20) Frenking, G.; Fröhlich, N. The nature of the bonding in transition-metal compounds. *Chem. Rev.* **2000**, *100*, 717-774.

(21) Zhou, M.; Andrews, L.; Bauschlicher, C. W., Jr. Spectroscopic and Theoretical Investigations of Vibrational Frequencies in Binary Unsaturated Transition-Metal Carbonyl Cations, Neutrals, and Anions. *Chem. Rev.* **2001**, *101*, 1931-1962.

(22) a) Bauschlicher, C. W., Jr. Transition Metal-Ligand Bonding, II. *J. Chem. Phys*. **1986**, *84*, 260-267.

(23) Bauschlicher, C. W., Jr.; Bagus, P. S.; Nelin, C. J.; Roos, B. J.; The Nature of Bonding in XCO for X=Fe, Ni and Cu. *J. Chem. Phys*. **1986**, *85*, 354-364.

(24) Bauschlicher, C. W., Jr.; Barnes, L. A.; On the Dissociation Energies and Bonding in $NiC^{0/+}$ and $TiC^{0/+}$. *Chem. Phys. Lett.* **1988**, *124*, 383-394.

(25) Barnes, L. A.; Rosi, M.; Bauschlicher, C. W., Jr. Theoretical Studies of the First- and Second-row Mono- and Di-carbonyl Positive ions. *J. Chem. Phys*. **1990**, *93*, 609-624.

(26) Sodupe, M.; Branchadell, V.; Rosi, M.; Bauschlicher, C. W., Jr. Theoretical Study of M^+-CO_2 and OM^+CO Systems for First Transition Row Metal Atoms. *J. Phys. Chem*. *A* **1997**, *101*, 7854-7859.

(27) Goldman, A. S.; Krogh-Jespersen, K. Why do cationic carbon monoxide complexes have high CO stretching force constants and short CO bonds? Electrostatic effects, not σ bonding. *J. Am. Chem. Soc*. **1996**, *118*, 12159-12166.

(28) Lupinetti, A. J.; Fau, S.; Frenking, G.; Strauss, S. H. Theoretical Analysis of the Bonding Between CO and Positively Charged Atoms. *J. Phys. Chem*. *A* **1997**, *101*, 9551-9559.

(29) Lupinetti, A. J.; Frenking, G.; Strauss, S. H. Nonclassical Metal Carbonyls. *Angew. Chem. Int. Ed.* **1998**, *37*, 2113-2116.

(30) Lupinetti, A. J.; Strauss, S. H.; Frenking, G. Non-classical Metal Carbonyls. *Prog. Inorg. Chem.* **2001**, *49*, 1-112.

(31) Ricks, A. M.; Duncan, M. A. Infrared Spectroscopy of Metal Carbonyl Cations. *J. Mol. Spec.* **2011**, *266*, 63-74.

(32) Huber, K. P.; Herzberg, G. *Molecular Spectra and Molecular Structure IV. Constants of Diatomic Molecules*, Van Nostrand Reinhold Co., 1979.

(33) Liang, B.; Zhou, M.; Andrews, L. Reactions of laser-ablated Ni, Pd, and Pt Atoms with Carbon Monoxide: Matrix Infrared Spectra and Density Functional Calculations on $M(CO)_n$ (n=1-4), $M(CO)^-$ (n=1-3), and $M(CO)^+$ (n=1-2), (M=Ni, Pd, Pt). *J. Phys. Chem. A* **2000**, *104*, 3905-3914.

(34) Gutsev, G. L.; Andrews, L.; Bauschlicher, C. W., Jr. 3d-Metal monocarbonyls MCO, MCO^+ and MCO^- (M=Sc to Cu): Comparative Bond Strengths and Catalytic Ability to Produce CO_2 in Reactions with CO. *Chem. Phys.* **2003**, *290*, 47-58.

(35) Liang, B.; Andrews, L. Reactions of laser-ablated Ag and Au Atoms with Carbon Monoxide: Matrix Infrared Spectra and Density Functional Calculations on $Au(CO)_n$ (n=2,3), $Au(CO)^-$ (n=1,2), and $M(CO)^+$ (n=1-4), (M=Ag, Au). *J. Phys. Chem. A* **2000**, *104*, 9156-9164.

(36) Zhou, M.; Andrews, L. Infrared spectra of $RhCO^+$, RhCO, and $RhCO^-$ in Solid neon: A Scale for Charge Support in Catalyst Systems. *J. Am. Chem. Soc.* **1999**, *121*, 9171-9175.

(37) Zhou, M.; Andrews, L. Matrix Infrared Spectra and Density Functional Calculations of ScCO, $ScCO^-$, and $ScCO^+$. *J. Phys. Chem. A* **1999**, *103*, 2964-2971.

(38) Zhou, M.; Andrews, L. Infrared Spectra and Density Functional Calculations of Small Vanadium and Titanium Carbonyl Molecules and Anions in Solid Neon. *J. Phys. Chem. A* **1999**, *103*, 5259-5268.

(39) Zhou, M.; Andrews, L. Reactions of Zirconium and Hafnium Atoms with CO: Infrared Spectra and Density Functional Calculations of $M(CO)_x$, OMCCO, and $M(CO)_2^-$ (M = Zr, Hf; x = 1-4). *J. Am. Chem. Soc.* **2000**, *122*, 1531-1539.

(40) Fielicke, A.; von Helden, G.; Meijer, G.; Pedersen, D. B.; Simard, B.; Rayner, D. M. Size and Charge Effects on Binding of CO to Small Isolated Rhodium Clusters. *J. Phys. Chem. B.* **2004**, *108*, 14591-14598.

(41) Moore, D. T.; Oomens, J.; Eyler, J. R.; Meijer, G.; von Helden, G.; Ridge, D. P. Gas-Phase IR Spectroscopy of Anionic Iron Carbonyl Clusters. *J. Am. Chem. Soc.* **2004**, *126*, 14726-14727.

(42) a) Fielicke, A.; von Helden, G.; Meijer, G.; Simard, B.; Rayner, D. M. Gold Cluster Carbonyls: Vibrational Spectroscopy of the Anions and the Effects of Cluster Size, Charge, and Coverage on the CO Stretching Frequency. *J. Phys. Chem. B.* **2005**, *109*, 23935-23940.

(43) Fielicke, A.; von Helden, G.; Meijer, G.; Pedersen, D. B.; Simard, B.; Rayner, D. M. Gold Cluster Carbonyls: Saturated Adsorption of CO on Gold Cluster Cations, Vibrational Spectroscopy, and Implications for Their Structures. *J. Am. Chem. Soc.* **2005**, *127*, 8416-8423.

(44) Fielicke, A.; von Helden, G.; Meijer, G.; Pedersen, D. B.; Simard, B.; Rayner, D. M. Size and Charge Effects on the Binding of CO to Late Transition Metal Clusters. *J. Chem. Phys.* **2006**, *124*, 194305-194312.

(45) Velasquez III, J.; Duncan, M. A. IR Photodissociation Spectroscopy of Gas Phase $Pt^{+}(CO)_n$ (n=4-6). *Chem. Phys. Lett.* **2008**, *461*, 28-32.

(46) Velasquez III, J.; Njegic, B.; Gordon, M. S.; Duncan, M. A. IR Photodissociation Spectroscopy and Theory of $Au^{+}(CO)_n$ complexes: Nonclassical Carbonyls in the Gas Phase. *J. Phys. Chem. A* **2008**, *112*, 1907-1913.

(47) Ricks, A. M.; Bakker, J. M.; Douberly, G. E.; Duncan, M. A. Infrared Spectroscopy and Structures of Cobalt Carbonyl Cations. *J. Phys. Chem. A* **2009**, *113*, 4701-4708.

(48) Ricks, A. M.; Reed, Z. D.; Duncan, M. A. Seven-coordinate Homoleptic Metal Carbonyls in the Gas Phase. *J. Am. Chem. Soc*. **2009**, *131*, 9176-9177.

(49) Reed, Z. D.; Duncan, M. A. Infrared Spectroscopy and Structures of Manganese Carbonyl Cations, $Mn(CO)_n^+$ (n=1-9). *J. Am. Soc. Mass Spectrom.* **2010**, *21*, 739-749.

(50) Ricks, A. M.; Gagliardi, L.; Duncan, M. A. Infrared Spectroscopy of Extreme Coordination: The carbonyls of U^+ and UO_2^+. *J. Am. Chem. Soc*. **2010**, *132*, 15905-15907.

(51) Brathwaite, A. D.; Reed, Z. D.; Duncan, M. A. Infrared Photodissociation Spectroscopy of Copper Carbonyl Cations. *J. Phys. Chem. A* **2011**, *115*, 10461-10469.

(52) Ricks, A. M.; Brathwaite, A. D.; Duncan, M. A. Coordination and Spin States in Vanadium Carbonyl Complexes ($V(CO)_n^+$, n = 1–7) Revealed with IR Spectroscopy. *J. Phys Chem. A* **2013**, *117*, 1001-1010.

(53) Brathwaite, A. D.; M. A. Infrared photodissociation spectroscopy of saturated group IV (Ti, Zr, Hf) metal carbonyl cations. *J. Phys. Chem. A* **2013**, **DOI:** 10.1021/jp400793h.

(54) Wang, G.; Chi, C.; Cui, J.; Xing, X.; Zhou, M. Infrared Photodissociation Spectroscopy of Mononuclear Iron Carbonyl Anions. *J. Chem. Phys. A* **2012**, *116*, 2484-2489.

(55) Chi, C.; Cui, J.; Xing, X.; Wang, G.; Liu, Z.; Zhou, M. Infrared Photodissociation Spectroscopy of Trigonal Bipyramidal 19-electron $Ni(CO)_5^+$ cation. *Chem. Phys. Lett.* **2012**, *542*, 33-36.

(56) Chi, C.; Cui, J.; Hua Li, Z.; Xing, X.; Wang, G.; Zhou M. Infrared Photodissociation Spectra of Mass Selected Homoleptic Dinuclear Iron Carbonyl Cluster Anions in the Gas Phase. *Chem. Sci.* **2012**, *3*, 1698-1706.

(57) Cui, J.; Xing, X.; Chi, C.; Wang, G.; Liu, Z.; Zhou M. Infrared Photodissociation Spectra of Mass-Selected Homoleptic Dinuclear Palladium Carbonyl Cluster Cations in the Gas Phase. *Chin. J. Chem.* **2012**, *30*, 2131-2137.

(58) Wechhuysen, B. M.; Keller, D. E. Chemistry, Spectroscopy and the Role of Supported Vanadium Oxides in Heterogenous Catalysis. *Catal. Today.* **2003**, *78*, 25-46.

(59) Asmis, K. R.; Meijer, G.; Brummer, M.; Kaposta, C.; Santambrogio, G.; Woste, L.; Sauer, J. Gas Phase Infrared Spectroscopy of Mono- and Divanadium Oxide Cluster Cations. *J. Chem. Phys*. **2004**, *120*, 6461-6470.

(60) Brummer, M.; Kaposta, C.; Santambrogio, G.; Asmis, K. R. Formation and Photodepletion of Cluster Ion-Messenger Atom Complexes in a Cold Ion Trap: Infrared Spectroscopy of VO^+, VO_2^+, and VO_3^+. *J. Chem. Phys*. **2003**, *119*, 12700-12703.

(61) Zhou, M.; Andrews, L. Infrared Spectra and Density Functional Calculations for OMCO, OM−(η^2-CO), $OMCO^+$, and $OMOC^+$ (M = V, Ti) in Solid Argon. *J. Phys. Chem. A* **1999**, *103*, 2066-2075.

(62) Becke, A. D. 3 Term Correlation Functional. *J. Chem. Phys.* **1993**, *98*, 5648-5652.

(63) Lee, C.; Yang, W.; Parr, R. G. Development of the Coll-Salvetti Correlation Energy Formula into a Functional of the Electron Density. *Phys. Rev B.* **1988**, *37*, 785-789.

(64) Frisch, M. J.; Trucks, G. W.; Schlegel, H. B.; Scuseria, G. E.; Robb, M. A.; Cheeseman, J. R.; Montgomery, J. A. Jr.; Vreven, T.; Kudin, K. N.; Burant, J. C.; Millam, J. M.; Iyengar, S. S.; Tomasi, J.; Barone, V.; Mennucci, B.; Cossi, M.; Scalmani, G.; Rega, N.;

Petersson, G. A.; Nakatsuji, H.; Hada, M.; Ehara, M.; Toyota, K.; Fukuda, R.; Hasegawa, J.; Ishida, M.; Nakajima, T.; Honda, Y.; Kitao, O.; Nakai, H.; Klene, M.; Li, X.; Knox, J. E.; Hratchian, H. P.; Cross, J. B.; Adamo, C.; Jaramillo, J.; Gomperts, R.; Stratmann, R. E.; Yazyev, O.; Austin, A. J.; Cammi, R.; Pomelli, C.; Ochterski, J. W.; Ayala, P. Y.; Morokuma, K.; Voth, G. A.; Salvador, P.; Dannenberg, J. J.; Zakrzewski, V. G.; Dapprich, S.; Daniels, A. D.; Strain, M. C.; Farkas, O.; Malick, D. K.; Rabuck, A. D.; Raghavachari, K.; Foresman, J. B.; Ortiz, J. V.; Cui, Q.; Baboul, A. G.; Clifford, S.; Cioslowski, J.; Stefanov, B. B.; Liu, G.; Liashenko, A.; Piskorz, P. Komaromi, I.; Martin, R. L.; Fox, D. J.; Keith, T.; Al-Laham, M. A.; Peng, C. Y.; Nanayakkara, A.; Challacombe, M.; Gill, P. M. W.; Johnson, B.; Chen, W.; Wong, M. W.; Gonzalez, C. and Pople, J. A. Gaussian 03 (Revision B.02), Gaussian, Inc., Pittsburgh PA, 2003.

(65) Weigend, F.; Ahlrichs, R. Balanced Basis Sets of Split Valence, Triple Zeta Valence and Quadruple Zeta Valence Quality for H To Rn: Design and Assessment of Accuracy. *Phys*. *Chem*. *Chem*. *Phys*. **2005**, *7*, 3297-3305.

(66) Dunning, T. H. Gaussian Basis Functions for Use in Molecular Calculations. I. Contraction of (9*s*5*p*) Atomic Basis Sets for the First-Row Atoms. *J. Chem. Phys.* **1970**, *53*, 2823-2833.

(67) Ricks, A. M.; Gagliardi, L.; Duncan, M. A. Uranium Oxo and Superoxo Cations Revealed Using Infrared Spectroscopy in the Gas Phase. *J. Phys. Chem. Lett.* **2011**, *2*, 1662–1666.

(68) Bauschlicher, C. W., Jr.; Maitre, P. Theoretical-Study of the First Transition Row Metal Oxides and Sulfides. *Theor*. *Chim*. *Acta* **1995**, *90*, 189-203.

CHAPTER 7

CONCLUSION

Due to the importance of metal carbonyl complexes in organometallic and inorganic chemistry, and the ubiquity of carbon monoxide adsorbates in surface science, continued investigation of these systems is worthwhile. The studies presented herein examined the coordination, bonding interactions and electronic structure-dependent frequency shifts, for several transition metal carbonyl complexes. By so doing, we have tested the limits of existing chemical principles and identified fascinating trends in metal carbonyl bonding.

The work presented in Chapter 3 tests the limit of the 18-electron rule. Unfortunately, scandium cation did not form the anticipated eight-coordinate, 18-electron complex. Instead, the seven-coordinate species, $Sc(CO)_7^+$, was found to be the fully coordinated ion. However, yttrium cations did form the desired 18-electron, eight-coordinate structure, confirming the viability of the 18 electron rule, even in cases involving extreme coordination. DFT calculations provide structures and corresponding vibrational spectra in support of the experimental data. $Sc(CO)_7^+$ was found to have a C_{3v} capped octahedral structure, while $Y(CO)_8^+$ has a D_{4d} square antiprism structure. The main infrared bands are observed at 2086 and 2087 cm^{-1} for $Sc(CO)_7^+$ and $Y(CO)_8^+$ respectively. These are among the most red-shifted frequencies measured for a transition metal carbonyl cation in the gas phase.

The carbonyl cations of the group IV metals ($M(CO)_n^+$, M = Ti, Zr, Hf), reveal an interesting trend. The 15 electron, n = 6 complex was found to be the fully coordinated species for each method, and the observed spectra were consistent with octahedral structures, as

predicted by theory. This symmetric structure yielded simple spectra, which facilitated the investigation of trends in the bonding patterns and C-O vibration band positions. These carbonyl frequencies were all significantly red-shifted from the free molecular CO vibration at 2143 cm^{-1}, occurring at 2110, 2094, and 2075 cm^{-1} for titanium, zirconium and hafnium respectively. An increase in the magnitude of the red shift, going from titanium to hafnium, is apparent these complexes. The decrease in the Pauling electronegativity of the metals going down the group is consistent with the increase in the red shift because there is more electron density available for π back-bonding.

Additionally, we investigated the carbonyls of the late transition metal copper. The $Cu(CO)_4^+$ complex was found to be the fully coordinated species for this system. The coordination of the 18-electron ion is analogous to its well-known isoelectronic neutral $Ni(CO)_4$. A single blue-shifted band at 2193 cm^{-1}, indicative of a high symmetry structure, was observed for this complex. DFT calculations confirmed that the lowest energy structure is indeed a 4C tetrahedron, with a d^{10} singlet ground state. This structure is analogous to that of $Ni(CO)_4$. The d^{10} ground state of this complex, as well as the significantly blue-shifted infrared band in its spectrum, allowed us to conclude that these carbonyls are another example of system with non-classical carbonyl bonding.

We expanded our work on pure metal carbonyls to incorporate metal oxide carbonyls. By studying small size-selected ions, we were able to systematically investigate the effect of oxidation on the carbonyl frequencies. Oxidation of the metal atom was found to cause the C-O stretching frequencies to blue shift. All metal oxide complexes were found to have a fully coordinated hexacoordinate structure, analogous to pure vanadium carbonyl. The exceptional agreement between experiment and theory for $VO(CO)_n^+$ and $VO_2(CO)_n^+$ complexes validates

the utility of DFT to model these systems. However, these studies also revealed that the separate vanadyl and superoxide vibrations in $VO_3(CO)_n^+$ complexes, are severely challenging for the level of DFT employed.

The research presented here examines the interaction of carbonyl ligands with singly-charged, monatomic metal cations. These studies can be extended to include dinuclear and trinuclear metal carbonyls. In these metal cluster-ligand species, different carbonyl binding configurations are possible. Examples include bridging, three-fold and "atop" binding sites. These clusters are excellent systems to investigate with IR spectroscopy because the binding sites are expected to have characteristic vibrational frequencies. Preliminary investigation of these clusters has been successful. Figure 7.1 shows the infrared photodissociation spectrum of $Cu_2(CO)_7^+$, along with the spectrum and structure predicted by DFT.

Our group has successfully prepared and investigated several $M^{2+}(H_2O)_n$ complexes. These same conditions and principles can be employed to study $M^{2+}(CO)_n$ ions. The interaction of carbonyl ligands with doubly charged metal cations is interesting. $Fe^{2+}(CO)_6$ would be isoelectronic to $Mn^+(CO)_6$ and $Cr(CO)_6$, $Ni^{2+}(CO)_5$ would be isoelectronic to $Co^+(CO)_5$ and $Fe(CO)_5$, etc. The coordination and electronic states of doubly charged species compared to neutrals and singly charged cations is also worth investigating. Compared to singly charged cations, dications are also expected to have even less electron density available for back-bonding. This can result in unprecedented blue shifts in the C−O stretching frequencies in these complexes.

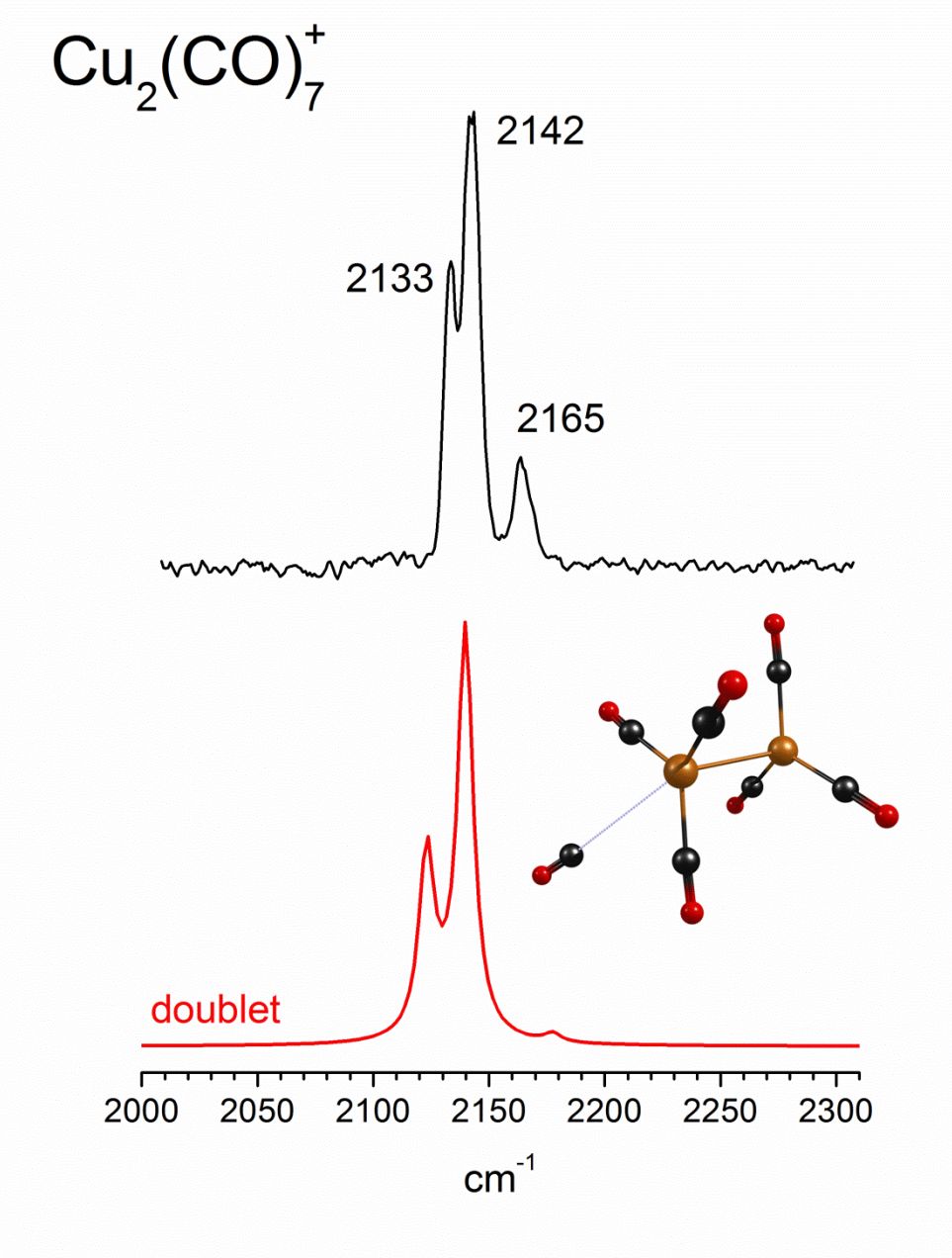

Figure 7.1. Infrared photodissociation spectrum of $Cu_2(CO)_7^+$, along with the spectrum and structure predicted by DFT.